2008

# Dual Bypass Gas Metal Arc Welding Process and Control

Xiaopei Liu
*University of Kentucky*, Xiaopei.Liu@uky.edu

## Recommended Citation

Liu, Xiaopei, "Dual Bypass Gas Metal Arc Welding Process and Control" (2008). *University of Kentucky Doctoral Dissertations*. 664.
https://uknowledge.uky.edu/gradschool_diss/664

# ABSTRACT OF DISSERTATION

Xiaopei Liu

The Graduate School

University of Kentucky

2008

# Dual Bypass Gas Metal Arc Welding Process and Control

---

## ABSTRACT OF DISSERTATION

---

A dissertation submitted in partial fulfillment of the
requirements for the degree of Doctor of Philosophy in the
College of Engineering
at the University of Kentucky

By
Xiaopei Liu

Lexington, Kentucky

Director: Dr. YuMing Zhang, Professor of Electrical Engineering

Lexington, Kentucky

2008

# ABSTRACT OF DISSERTATION

## Dual Bypass Gas Metal Arc Welding Process and Control

GMAW (Gas Metal Arc Welding) is one of the most important arc welding processes being adopted in modern manufacturing industry due to its advantages in productivity, energy efficiency and automation. By monitoring and improving some of the important properties of GMAW such as production rate, metal transfer and base metal heat input, researchers could bring the process efficiency and stability to a new level. In recent years, some innovative modifications of GMAW such as Twins, Tandem and laser-MIG hybrid welding have been adopted into many industrial applications for better productivity.

In this dissertation, a novel GMAW called DB-GMAW (Dual Bypass Gas Metal Arc Welding) using two GTAW torches and one GMAW torch to construct a welding system, is proposed and developed. In DB-GMAW, two GTAW torches perform the bypass system which decouples the total welding current into base metal current and bypass current after the melt down of filler wire. Compared to conventional GMAW, DB-GMAW has many advantages in droplet formation, base metal heat input and penetration achievement due to its unique characteristics in welding arc and current flow. In the first place of the research, experimental system of DB-GMAW is constructed. Then, sufficient experiments under different parameters are performed to provide us a good understanding of the behaviors and characteristics of this novel GMAW process. Observation about metal transfer formation and base metal heat input is studied to verify its theoretical analysis. Full penetration of work piece via DB-GMAW is achieved based on a series of parameter testing experiments. Moreover, image processing techniques are applied to DB-GMAW to monitor the welding process and construct a feedback system for control.

Considering the importance of maintaining stable full penetration during many welding applications, a nonlinear model of DB-GMAW full penetration is developed in this dissertation. To do that, we use machine vision techniques to monitor the welding profile of the work piece. A control algorithm based on the nonlinear model using adaptive control technique is also designed. The achievement of this dissertation provides a fundamental knowledge of a novel welding process: DB-GMAW, and a good guidance for further studies about DB-GMAW.

KEYWORDS: DB-GMAW, metal transfer, base metal heat input, full penetration,
nonlinear control

Xiaopei Liu

09/23/2008

# Dual Bypass Gas Metal Arc Welding Process and Control

By

Xiaopei Liu

YuMing Zhang
Director of Dissertation

YuMing Zhang
Director of Graduate Studies

09/23/2008
Date

# RULES FOR THE USE OF DISSERTATIONS

Unpublished dissertations submitted for the Doctor’s degree and deposited in the University of Kentucky Library are as a rule open for inspection, but are to be used only with due regard to the rights of the authors. Bibliographical references may be noted, but quotations or summaries of parts may be published only with the permission of the author, and with the usual scholarly acknowledgements.

Extensive copying or publication of the dissertation in whole or in part also requires the consent of the Dean of the Graduate School of the University of Kentucky.

A library that borrows this dissertation for use by its patrons is expected to secure the signature of each user.

| Name | Date |
|---|---|
| | |
| | |
| | |
| | |
| | |
| | |
| | |
| | |
| | |

DISSERTATION

Xiaopei Liu

The Graduate School

University of Kentucky

2008

# Dual Bypass Gas Metal Arc Welding Process and Control

---

DISSERTATION

---

A dissertation submitted in partial fulfillment of the
requirements for the degree of Doctor of Philosophy in the
College of Engineering
at the University of Kentucky

By
Xiaopei Liu

Lexington, Kentucky

Director: Dr. YuMing Zhang, Professor of Electrical Engineering

Lexington, Kentucky

2008

*DEDICATED TO MY FAMILY AND CHLOE*

# ACKNOWLEDGEMENT

This work is supported by Los Alamos National Laboratory (Project No. 4431-001-06), the Natural Science Foundation of China (50675093), the National Science Foundation (Grant # CMMI-0355324) and University of Kentucky, Center for Manufacturing.

First of all, I would give sincere thanks and appreciations to my advisor Dr. Yuming Zhang for his profound knowledge, patient guidance, continuous encouragement and trust in me.  I am also grateful to Drs. Bruce L. Walcott, Alan T. Male, Jingshan Li, Larry Holloway and Paul Goodrum for their helpful instructions and advices. It has been a great honor for me to have the opportunity learning from all these professors. Part of my Ph.D research work is collaborated with Dr. Yu Shi from Lanzhou University of Technology. I would like to thank Dr. Shi who shared his experience and knowledge selflessly with me. Moreover, I would like to thank my colleagues of Welding Research Laboratory: Hongsheng Song, Xiangrong Li, Kehai Li, Jinsong Chen, Kun Qian, Xiaodong Na, Yan Shao, Xiaoji Ma, Yi Huang, Zhijiang Wang and Cheng Xue from Lanzhou University of Technology.

Additionally, I give my thanks to my father who loved me with his heart and soul. I thank my mother for her all along support and love. I also want to thank my stepfather for his generosity and confidence in me. I appreciate all the care and encouragement from my family who take good care of my mother while I am absent. Last but not least, I thank my girlfriend, Chloe Hu, for being a part of my life and sharing all the wonderful memories with me.

TABLE OF CONTENTS

Acknowledgments……………………..…………………………………………………iii

List of Tables…………………………………………………………………………vi

List of Figures……………………………………………………………………..…....vii

List of Files………………………………………………………………………………x

CHAPTER 1 INTRODUCTION ........................................................................ 1
  1.1 Background ............................................................................................. 1
  1.2 Objective and approach .......................................................................... 3
  1.3 Dissertation structure .............................................................................. 5

CHAPTER 2 REVIEW OF GMAW, TANDEM AND DE-GMAW........................... 7
  2.1 Review of GMAW…………………………………………………………………...7
    2.1.1 Basic variables of GMAW..................................................................... 8
  2.2 Overview of laser-MIG hybrid and Tandem................................................ 9
    2.2.1 Laser-MIG hybrid welding ..................................................................... 9
    2.2.2 Overview of Tandem ........................................................................... 11
  2.3 Overview of DE-GMAW ........................................................................... 12
  2.4 Advantages of DB-GMAW ....................................................................... 15

CHAPTER 3 SYSTEM CONSTRUCTION AND PARAMETER DESIGN OF DB-GMAW..................................................................................................... 21
  3.1 System construction................................................................................ 21
  3.2 Sensing system........................................................................................ 25
  3.3 Experimental parameters......................................................................... 28
  3.4 Summary.................................................................................................. 32

CHAPTER 4 METAL TRANSFER IN DB-GMAW ............................................... 33
  4.1 Background.............................................................................................. 33
  4.2 Theoretical analysis of forces in the arc.................................................... 36
    4.2.1 Forces of conventional GMAW.............................................................. 36
    4.2.2 Forces of DB-GMAW............................................................................. 39
  4.3 Experimental procedure and results ........................................................ 41
    4.3.1 Experimental procedure ....................................................................... 41
    4.3.2 Experimental results.............................................................................. 41
  4.4 Conclusion ............................................................................................... 46

CHAPTER 5 HEAT INPUT AND PENETRATION ANALYSIS OF DB-GMAW ... 48
  5.1 Thermal process of welding ..................................................................... 48
    5.1.1 Theoretical analysis of heat input.......................................................... 49

5.1.2 Thermal distribution of base metal ..... 50
5.1.3 Welding thermal field ..... 52
5.1.4 Mathematical description of welding heat transfer ..... 54
5.1.5 Theoretical analysis of penetration ..... 55
5.2 Experimental procedure and results ..... 55
5.2.1 Experimental procedure ..... 55
5.2.2 Temperature comparison ..... 57
5.2.3 Penetration comparison ..... 59
5.3 Full penetration achievement on aluminum tube 6061T of DB-GMAW ..... 62
5.4 Theoretical explanation of DB-GMAW penetration ..... 65
5.5 Chapter conclusion ..... 66

CHAPTER 6 IMAGE PROCESSING OF DB-GMAW ..... 67
6.1 Image processing of the front-side profile of the welding pool ..... 67
6.2 Image processing of the droplet transformation in DB-GMAW ..... 73
6.2.1 Image processing of neck shrinking information ..... 73
6.2.2 Image processing of droplet size ..... 85
6.3 Image processing of back-side welding pool profile ..... 90
6.4 Chapter conclusion about three image processing procedures ..... 92

CHAPTER 7 NONLINEAR MODELING OF DB-GMAW ..... 95
7.1 Full penetration of DB-GMAW ..... 95
7.2 Nonlinear system identification ..... 99
7.3 Modeling DB-GMAW full penetration ..... 105
7.3.1 Generation of test signals ..... 106
7.3.2 Model validation ..... 108

CHAPTER 8 ROBUST ADAPTIVE NONLINEAR CONTROL OF FULL PENETRATION ON DB-GMAW ..... 117
8.1 Control of full penetration on DB-GMAW ..... 117
8.2 Control algorithm design ..... 119
8.3 Chapter conslusion ..... 128

CHAPTER 9 CONCLUSION AND FUTURE WORK ..... 126
9.1 Conclusion ..... 126
9.2 Future work ..... 127

REFERENCE ..... 130

VITA ..... 138

# LIST OF TABLES

TABLE 3-1, Parameters of metal transfer research ........................................... 29
TABLE 3-2, Parameters on one foot long work piece for heat input research .... 30
TABLE 3-3, Preset parameters on aluminum ring work piece ............................ 31
TABLE 5-1, Parameters on aluminum cylinder: full penetration comparison...... 62
TABLE 7-1, Constant parameters for modeling experiments ............................. 98

# LIST OF FIGURES

Figure 1-1, System construction (a) and Torch installation (b) of DE-GMAW [4].. 2
Figure 1-2, Geometrical regulation of LANL aluminum cylinder........................... 3
Figure 1-3, (a), DB-GMAW on steel (Base metal -30A), (b), DB-GMAW on steel (Base metal -0A) [6] ........................................................................ 4
Figure 1-4, Organizational structure of dissertation ............................................ 5
Figure 2-1, (a): Conventional GMAW circuit diagram (1) Welding torch (2) Work piece (3) Power source (4) Wire feed unit (5) Electrode source (6) Shielding gas supply; (b): GMAW weld area (1) Direction of travel, (2) Contact tube, (3) Electrode, (4) Shielding gas, (5) Molten weld metal, (6) Solidified weld metal, (7) Work piece. ....................................................................................... 8
Figure 2-2, Torch installation of laser-MIG: (a) Instruction diagram (b) Real torch [11] ........................................................................................................ 10
Figure 2-3, Laser-MIG/MAG welding process [10]............................................ 10
Figure 2-4, Sectional view of tandem torch (a) and operating mode (b) [12]...... 12
Figure 2-5, Non-consumable DE-GMAW system diagram [3] ........................... 13
Figure 2-6, System diagram of consumable DE-GMAW [14] ............................ 15
Figure 2-7, Arc forces acted on droplet in DE-GMAW (Non-consumable).......... 16
Figure 2-8, Droplet travel paths in the arc of DE-GMAW (Non-consumable) ..... 17
Figure 2-9, Experimental verification of arc force influences [4] ........................ 17
Figure 2-10, Arc forces act on the droplet in DB-GMAW ................................... 18
Figure 3-1, Illustration of DB-GMAW ................................................................ 22
Figure 3-2, Geometrical regulation of LANL aluminum cylinder......................... 22
Figure 3-3, Experimental work piece geometry ................................................. 23
Figure 3-4, Torch installation parameters .......................................................... 24
Figure 3-5, Picture of physical torch installation ................................................ 24
Figure 3-6, Olympus i-speed camera ................................................................ 26
Figure 3-7, Thermocouples on the inner surface............................................... 27
Figure 3-8, K-type thermocouple and transmitter .............................................. 27
Figure 3-9, Sketch of experimental system. ...................................................... 28
Figure 4-1, Sketch of three modes of metal transfer.......................................... 35
Figure 4-2, Major forces acting on droplet in GMAW......................................... 37
Figure 4-3, Schematic of forces affecting droplet in DB-GMAW......................... 40
Figure 4-5, Metal transfer without bypass current in experiment 1. The interval between each frame is 1 ms.................................................................... 42
Figure 4-6, Current and voltage in experiment 1. Bypass currents equal to zero. ........................................................................................................ 42
Figure 4-7, Metal transfer with dual 30A bypass current in experiment 2. The interval between each frame is 2.5 ms. ...................................................... 43
Figure 4-8, Currents and voltage in experiment 2. Bypass currents equal to 30A separately. ........................................................................................ 43
Figure 4-9, Metal transfer with dual 40A bypass current in experiment 3. The interval between each frame is 1 ms. ........................................................ 44

Figure 4-10, Currents and voltage in experiment 3. Bypass currents equal to 40A separately. 44
Figure 4-11, Metal transfer with dual 50A bypass current in experiment 4. The interval between each frame is 1.5 ms. 45
Figure 4-12, Currents and voltage in experiment 4. Bypass currents equals to 50A separately. 45
Figure 4-13, Metal transfer with dual 60A bypass current in experiment 5. The interval between each frame is 0.5 ms. 46
Figure 4-14, Currents and voltage in experiment 5. Bypass currents equal to 60A separately. 46
Figure 5-1, Distribution of heat density 50
Figure 5-2, Thermocouples on the inner surface 56
Figure 5-3, Highest temperature distribution via different bypass currents 58
Figure 5-4, Highest temperature comparison on aluminum rings 59
Figure 5-5, Welding cross section of GMAW (left) and DB-GMAW (Right) 59
Figure 5-6-1, Weld bead and cross section view of GMAW 60
Figure 5-6-2, Weld bead and cross section view of DB-GMAW (Bypass current L&R : 30A-30A) 60
Figure 5-6-3, Weld bead and cross section view of DB-GMAW (Bypass current L&R : 40A-40A) 60
Figure 5-6-4, Weld bead and cross section view of DB-GMAW (Bypass current L&R : 45A-45A) 60
Figure 5-6-5, Weld bead and cross section view of DB-GMAW (Bypass current L&R : 50A-50A) 61
Figure 5-6-6, Weld bead and cross section view of DB-GMAW (Bypass current L&R : 55A-55A) 61
Figure 5-7, Weld beads of experiments 1-6 in Table-2 (front, back and cross section view) 64
Figure 5-8, Full penetration comparison of experiments 1-6 in Table-2 64
Figure 5-9, Weld bead of conventional GMAW under 250A welding current 64
Figure 6-1, Original picture of front-side welding pool from DB-GMAW 68
Figure 6-2, Result of wiener filter on our interest region 68
Figure 6-3, Result after histogram image enhancement 69
Figure 6-4, Roberts Operator 70
Figure 6-5, Sobel operator 71
Figure 6-6, Prewitt operator 71
Figure 6-7, Log operator 72
Figure 6-8, Results of different edge detector on interest region image of DB-GMAW 73
Figure 6-9, Composed picture of edge detection and original picture 73
Figure 6-10, Metal transfer image (0.8mm diameter wire), single bypass current 30A 74
Figure 6-11, Metal transfer image (0.8mm diameter wire), single bypass current 50A 74
Figure 6-12, Metal transfer image (0.8mm diameter wire), single bypass current 60A 75

Figure 6-13, Metal transfer image (1.2mm diameter wire), single bypass current 60A .......... 75
Figure 6-14, Comparative results before and after wiener filter .......... 76
Figure 6-15, Comparative results before and after image enhancement .......... 76
Figure 6-16, Edge detection results of Roberts operator .......... 77
Figure 6-17, Edge detection results of Canny operator .......... 78
Figure 6-18, Edge detection results of Log operator .......... 78
Figure 6-19, Edge detection results of Prewitt operator .......... 79
Figure 6-20, Edge detection results of Sobel operator .......... 80
Figure 6-21, Edge detection results of Zero-crossing operator .......... 81
Figure 6-22, Edge detection result of Canny-zero-crossing operator .......... 82
Figure 6-23, Neck shrinking detection from Zero-crossing operator on 0.8mm 30A image .......... 83
Figure 6-24, Neck shrinking detection from Canny-zero-crossing operator on 0.8mm 50A image .......... 83
Figure 6-25, Neck shrinking detection from Sobel operator on 0.8mm 60A image .......... 84
Figure 6-26, Neck shrinking detection from Zero-crossing operator on 1.2mm 60A image .......... 84
Figure 6-27, Droplet size detection, 0.8mm, 30A .......... 87
Figure 6-28, Droplet size detection, 0.8mm, 50A .......... 88
Figure 6-29, Droplet size detection, 1.2mm, 60A .......... 88
Figure 6-31, Comparative results between algorithm and manual on droplet velocity .......... 90
Figure 6-32, Optical system for back-side profile inspection .......... 91
Figure 6-33, Back-side welding profile .......... 91
Figure 6-34, Result image of back-side welding pool profile detection .......... 92
Figure 7-1, Demonstration of different full penetration levels .......... 96
Figure 7-2, Procedure of system identification .......... 100
Figure 7-3, Block oriented models .......... 101
Figure 7-4, Multi-level shift register .......... 103
Figure 7-5, Plot of test signal values .......... 107
Figure 7-6, Bypass current and width waveform (PRTS) .......... 108
Figure 7-7, Simulation and actual output waveforms (Hammerstein) .......... 111
Figure 7-8, Simulation and actual output waveforms (Bilinear) .......... 113
Figure 7-9, Input and output waveforms of system step response .......... 113
Figure 7-10 Simulation and actual output of step response for bilinear model . 114
Figure 7-11, Actual PRTS current and width output .......... 115
Figure 7-12, Actual step response bypass current and width output .......... 115
Figure 8-1, Structure of control experimental system .......... 121
Figure 8-2, Structure of control algorithm .......... 122
Figure 8-3, Simulation result of control algorithm .......... 122
Figure 8-4, On-line control result of DB-GMAW process .......... 123
Figure 8-5, Control result of robustness test .......... 124
Figure 8-6, Open loop penetration of DB-GMAW .......... 124

# LIST OF FILES

Xiaopei Liu’s dissertation…………………………………………………..Size: 11.0M

# CHAPTER 1

# INTRODUCTION

## 1.1 Background

Welding process is one of the most important processes in manufacturing industry such as automotive, aerospace and shipbuilding. Welding is a fabrication process that joins materials, usually metals or thermoplastics, by causing coalescence. This is often done by melting the work pieces and adding a filler material to form a pool of molten material (the *weld puddle*) that cools to become a strong joint, with pressure sometimes used in conjunction with heat, or by itself, to produce the weld. The research about welding methods and welding properties is significantly necessary because every year approximately 45% of finished steel and other material such as aluminum and cooper alloy needs to be welded. The booming development of modern technology and rapid enhancing requirements of more productivity, more efficiency and better quality from manufacturing industry is urging researchers all over the world improving welding techniques [1] [2].

Among all welding methods, arc welding is the most common method adopted industrially which includes stick arc welding, hidden arc welding, GTAW (Gas Tungsten Arc Welding), Plasma arc welding and GMAW (Gas Metal Arc Welding) [2]. In recent years, some novel welding processes such as twins, tandem and laser-MIG hybrid welding are developed for a higher productivity. Although significant progress has been achieved, all these processes have a problem in common: additional base metal heat input. Generally speaking, higher productivity requires more filler metal which demands higher melting current of the process. On the contrast, in most of the cases, the maximum melting current of a certain process is fixed for its work piece due to a fixed geometry of the work piece. The welding current could not go over the maximum limit in order to avoid burn through of the base metal. As a result, the requirements of higher productivity and limitation of maximum melting current form a dilemma for the scholars in this research. To solve this dilemma, a modified GMAW called DE-GMAW system, which is the first bypassed GMAW process, is constructed in University of Kentucky. DE-GMAW (Double Electrode Gas Metal Arc Welding) is a modified GMAW process which decouples the melting current into base metal current and bypass current by adding a bypass torch to a conventional GMAW system to establish a bypass arc. This modification enables the possibility of increasing melting current meanwhile keeping the base metal current at desired level [3]. The system construction and torch installation of DE-GMAW is demonstrated in Figure 1-1. The bypass torch of DE-GMAW could be either a TIG torch (Non-consumable DE-GMAW) or a MIG torch (Consumable DE-GMAW). Generally speaking, MIG torch bypass provides higher productivity but less stability compared to TIG torch bypass.

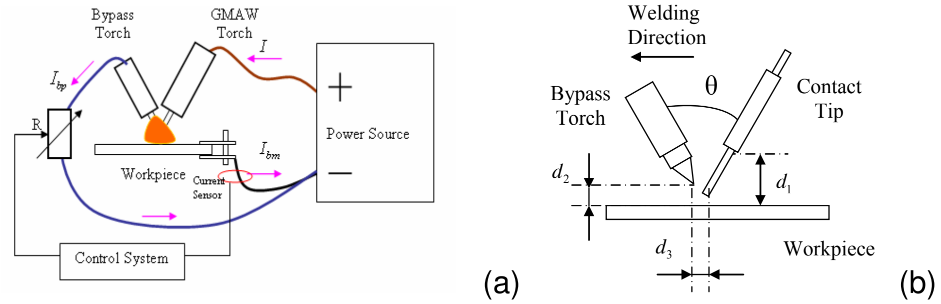

Figure 1-1, System construction (a) and torch installation (b) of DE-GMAW [4]

Based on DE-GMAW, we developed a novel GMAW process called DB-GMAW (Dual Bypass Gas Metal Arc Welding) by adding a dual bypass subsystem to conventional GMAW for a balanced bypass arc. Initially, DB-GMAW is designed to weld aluminum 6061 alloy tube to achieve a minimum base metal heat input, faster travel speed, better metal transfer and minimum spatter. DB-GMAW can also be adopted to weld other base metal such as black metal. DB-GMAW is designed to bring some new advantages, such as welding travel direction, compared to DE-GMAW. DE-GMAW also offers useful experiences in DB-GMAW system design by indicating important parameters such as torch angles which influencing process stability significantly.

## 1.2 Objective and approach

As we mentioned previously, productivity and quality are important concerns through all manufacturing processes. Generally speaking, increasing welding travel speed and increasing deposition rate are two common ways to improve productivity [5]. By increasing deposition rate which is calculated by the volume of melted filler metal in unit time, we need to increase melting current which influences the arc heat input of the process. Considering the influences to welding pool and mechanical properties from base metal heat input [2], we should always keep the base metal heat input under control by restricting it within a desired range.

The research in this dissertation is inspired by Los Alamos National Laboratory (LANL) who is seeking a method to weld aluminum 6061 rings by achieving the minimum melting of work piece while maintaining the welding quality. From previous experimental results of LANL, traditional GMAW cannot provide satisfying results as required. The work piece here is an aluminum ring with a groove on it. The geometrical regulation of LANL aluminum cylinder is showed in Figure 1-2.

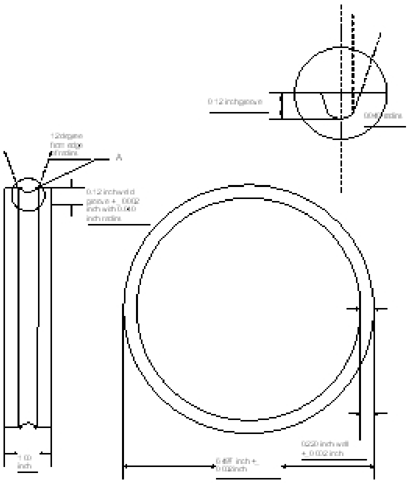

Figure 1-2, Geometrical regulation of LANL aluminum cylinder

Obviously, the objective of LANL is to build a welding system which can reduce base metal heat input meanwhile maintaining or even improving desired welding quality and welding speed. To achieve this proposed objective, we build

DB-GMAW system as a solution. Compared to DE-GMAW, DB-GMAW has several advantages: (1). Offering stronger arc stability by providing a balanced welding arc; (2). Further reducing base metal current by diverse the majority of welding current into bypass system; (3). Offering more possibility in travel direction by balancing the arc column. The theoretical analysis and experimental result demonstrating the reason and fact about DB-GMAW advantages will be discussed in later chapters. Before we reach that far, a series of feasibility testing experiments are performed on to verify that dual TIG bypass GMAW system has the ability to perform a stable welding process. We use both steel and aluminum as base metal in our feasibility testing experiments. It turns out that dual bypass arc can be successfully and stably established on both steel and aluminum [6]. It also indicates us that keeping a certain mount of base metal current is crucial to process stability. Figure 1-3 demonstrates current waveforms both under 250A total welding current whose base metal current is set as 30A and 0A respectively. From Figure 1-3, we can tell that the process with 30A base metal current has a better stability.

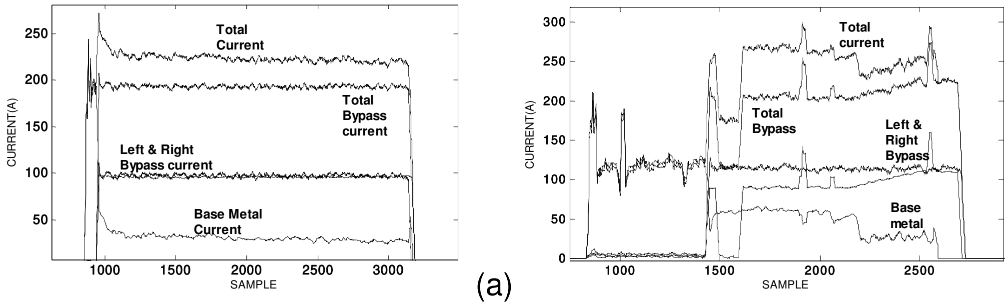

(a) (b)

Figure 1-3, (a). DB-GMAW on steel (Base metal- 30A), (b). DB-GMAW on steel (Base metal- 0A) [6]

As mentioned previously, the research work in this dissertation is also supported by National Science Foundation and China National Science Foundation. DB-GMAW process demonstrates a lot of potentials to become a crucial welding method in manufacturing. It is important for us to understand this process theoretically.

Accordingly, the basic approach to reach our objective includes following steps:

(1). Construct a DB-GMAW experimental system with sensors monitoring the current, voltage and temperature information to help us evaluating whether the system satisfies experimental requirements.

(2). Analyze the characteristics of DB-GMAW in base metal heat input, metal transfer and penetration.

(3). Adopt machine vision technique to analyze the welding process including welding pool profile and metal transfer information.

(4). Design a control algorithm based on nonlinear modeling and adaptive control technique on back-side welding bead profile and penetration.

### 1.3 Dissertation structure

Respecting the approach above, this dissertation has an organizational structure which is showed in Figure 1-4,

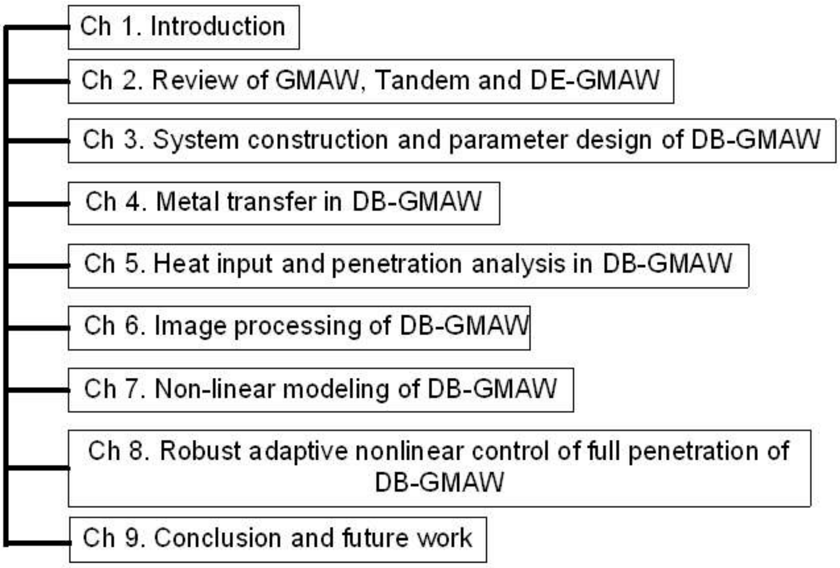

Figure 1-4, Organizational structure of dissertation

In Chapter 1 “Introduction”, background information, objective and approach of the research are discussed.

In Chapter 2 “Review of GMAW, Tandem and DE-GMAW”, introduction of conventional GMAW and high productivity GMAW methods, such as Tandem and DE-GMAW, are presented in detail. The differences between DB-GMAW and DE-GMAW are revealed. The advantages caused by these differences are explained.

Chapter 3 “System construction and parameter design of DB-GMAW” talks about the construction of DB-GMAW and the parameters used on different experiments. Important configuration about DB-GMAW such as torch installation is also introduced in this section.

In Chapter 4 “Metal transfer in DB-GMAW”, background introduction of metal transfer is discussed. Mathematical analysis on arc forces of welding process is studied. The discussion regarding to DB-GMAW and experimental verification through designed experiments is presented.

In Chapter 5 “Heat input and penetration analysis of DB-GMAW”, the base metal heat input calculation is discussed. Theoretical analysis of Lorentz forces acting on the welding pool influencing penetration is discussed and verified by experiments.

Chapter 6 “Image processing of DB-GMAW” develops three different procedures for image processing of DB-GMAW. The advantages and disadvantages among three procedures are discussed and compared.

Chapter 7 “Nonlinear modeling of DB-GMAW” reviews the knowledge and rules of nonlinear modeling. Different model structures and techniques are compared to establish a nonlinear model of DB-GMAW. Validation experiments are performed to verify the model accuracy.

In Chapter 8, “Robust adaptive nonlinear control of full penetration of DB-GMAW”, the theoretical knowledge of adaptive control, predictive control and robust boundedness is introduced. The detail of DB-GMAW back-side profile nonlinear control algorithm is discussed. A series of experiments of simulation and on-line control are performed.

Chapter 9 “Conclusion and future work” concludes our whole project in every academic aspect. The future research objective of this project is also discussed.

# CHAPTER 2

# REVIEW OF GMAW, Tandem and DE-GMAW

## 2.1 Review of GMAW

Gas metal arc welding (GMAW), sometimes referred to by its subtypes metal inert gas (MIG) welding or metal active gas (MAG) welding, is a semi-automatic or automatic arc welding process in which a continuous and consumable wire electrode and a shielding gas are fed through a welding gun. A constant voltage, direct current power source is most commonly used with GMAW, but constant current systems, as well as alternating current, can be used [7].

Originally developed for welding aluminum and other non-ferrous materials in the 1940s, GMAW was soon applied to steels because it allowed for lower welding time compared to other welding processes. The cost of inert gas limited its use in steels until several years later, when the use of semi-inert gases such as carbon dioxide became common. Further developments during the 1950s and 1960s gave the process more versatility and as a result, it became a highly used industrial process. Today, GMAW is the most common industrial welding process, preferred for its versatility, speed and the relative ease of adapting the process to robotic automation. The automobile industry in particular uses GMAW welding almost exclusively. Unlike welding processes that do not employ a shielding gas, such as shielded metal arc welding, it is rarely used outdoors or in other areas of air volatility. A related process, flux cored arc welding, often does not utilize a shielding gas, instead employing a hollow electrode wire that is filled with flux on the inside [8].

Figure 2-1 demonstrates a common GMAW system construction and GMAW torch at work respectively. It gives an image of how traditional GMAW works. Moreover, it helps us to have better understanding of basic parameters of GMAW which will be introduced later.

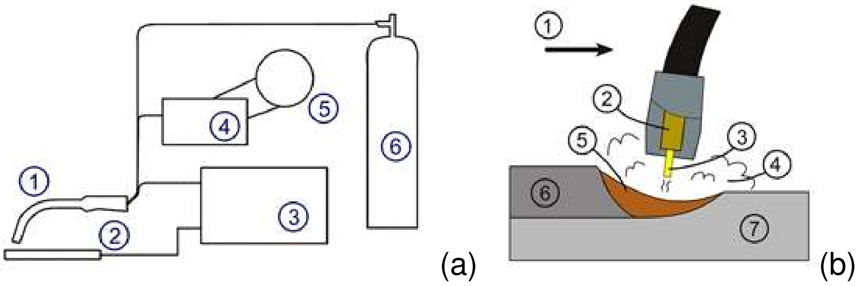

Figure 2-1, (a): Conventional GMAW circuit diagram (1) Welding torch (2) Work piece (3) Power source (4) Wire feed unit (5) Electrode source (6) Shielding gas supply; (b): GMAW weld area (1) Direction of travel, (2) Contact tube, (3) Electrode, (4) Shielding gas, (5) Molten weld metal, (6) Solidified weld metal, (7) Work piece.

GMAW is a huge topic which involves lots of information in many fields. Some aspects such as influences of different shielding gas and different filler material won't be discussed in detail for this dissertation. Some characteristics of GMAW such as Metal transfer mode will be discussed in detail later. In this chapter, we firstly focus on the basic variables of GMAW.

### 2.1.1 Basic variables of GMAW

There are some basic variables of GMAW which will affect weld penetration, bead geometry and overall weld quality [1]. The basic variables of GMAW usually have strong coupling relationship which means that they influence each other significantly.

**Welding Current**: When all other variables are held constant, the welding amperage varies with the electrode feeding speed or melting rate in a nonlinear relation. Generally speaking, for a chosen filler wire, welding current increases itself along with the increment of wire feeding speed. The upper limit of welding current is often regulated by the material and geometry of base metal in order to prevent burn through.

**Polarity**: Polarity is used to describe the electrical connection of the welding gun with relation to the terminals of a direct current power source. When the gun power lead is connected to the positive terminal, the polarity is designated as direct current electrode positive (DCEP), arbitrarily called reverse polarity. When the gun is connected to the negative terminal, the polarity is designated as direct current electrode negative (DCEN), originally called straight polarity [9]. For our situation, we are using DCEP because our base metal material is aluminum.

**Arc Voltage**: arc voltage and arc length are terms that are often used interchangeably. With GMAW, arc length is a critical variable that must be fully controlled [1].

**Travel speed**: travel speed is the linear rate at which the arc is moved along the weld joint. With all other conditions held constant, weld penetration is a maximum at an intermediate travel speed [9].

Besides, other parameters such as wire extension, electrode orientation and shielding gas are also important which influence the process in many ways.

## 2.2 Overview of laser-MIG hybrid and Tandem

Tandem, together with Twins and laser-MIG hybrid welding are innovative methods that oriented to increase GMAW productivity. A brief overview of these methods helps us to understand the advantages and disadvantages of each existing method which eventually benefits our design of experimental system.

### 2.2.1 Laser-MIG hybrid welding

The laser-arc hybrid welding process is a coupling of a traditional arc welding process and a laser welding process. The combination of laser light and an electrical arc into an amalgamated welding process has been known since the 1970's, but has only recently been used in industrial applications. There are three main types of hybrid welding process, depending on the arc used; TIG, Plasma arc or MIG augmented laser welding. While TIG augmented laser welding was the first to be researched, MIG is the first to go into industry and is commonly known as hybrid laser welding. Whereas in the early days that laser sources still had to prove their suitability for industrial use, today they are standard equipment in many manufacturing enterprises. The combination of laser welding with another weld process is called a "hybrid welding process". This means that a laser beam and an electrical arc act simultaneously in one welding zone, influencing and supporting each other. Compared to either of the processes alone, the coupling leads to significant improvements in welding speed and weld quality [10]. Figure 2-2 shows torch installation of laser-MIG.

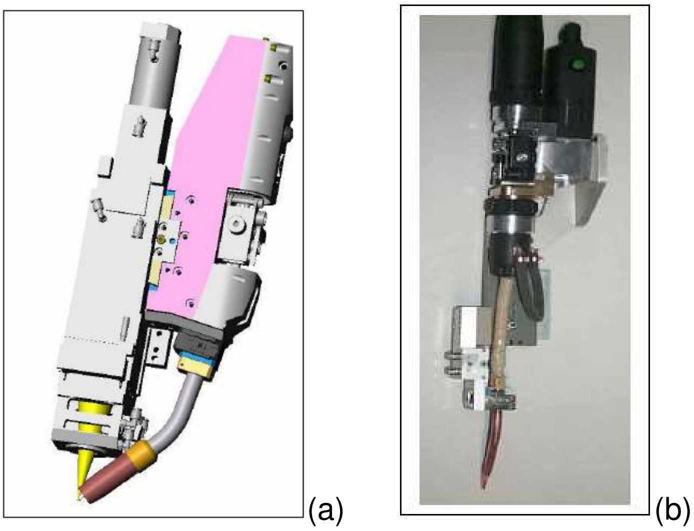

Figure 2-2, Torch installation of laser-MIG: (a) Instruction diagram (b) Real torch [11]

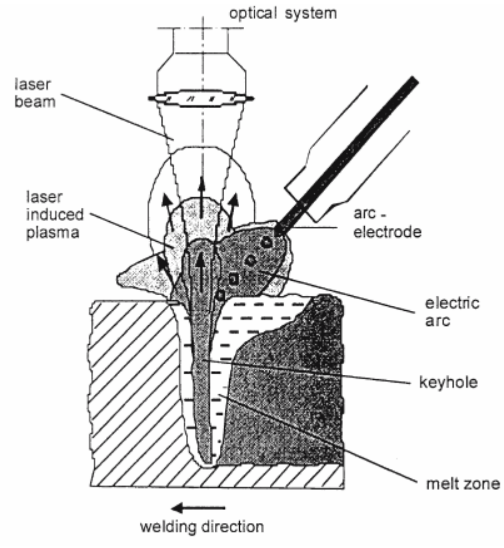

Figure 2-3, Laser-MIG/MAG welding process [10]

The laser-MIG combined advantages from both GMAW and laser welding. The two features of the system influence each other which make parameters difficult to decouple from each other. The laser preheats the work piece to make the droplet transfer easier which also results a deeper penetration. Figure 2-3 shows the working process of laser-MIG welding.

The disadvantage of laser-MIG welding firstly is the cost of equipment. As an expensive device, high power laser generator which could perform functionally in welding process is very luxury to afford. As well, the laser-MIG welding system is not very convenient to install. The travel direction of work piece in laser-MIG welding must follow the direction in Figure 2-3. Moreover, laser-MIG can't reduce base metal heat input because laser is a great heat source.

### 2.2.2 Overview of Tandem

Recent years, reduction of welding construction costs is urgently sought, and therefore, to cope with this demand in the field of arc welding, there has been a noticeable trend of increasing welding efficiency, accompanied by improvements in the quality of welds. Particularly in the field of steel sheet welding, such as in the automobile industry, great efforts to shorten the welding time in production lines have been made [12].

Tandem is actually a GMAW process with two filler metal simultaneously feed to the base metal. Originally, the two filler metal wire is built into a same contact tip which causes many problems to the system stability. Later, a special designed torch for tandem which includes two separate contact tips with good insulation between each other is used to improve the process. Compared to conventional GMAW, tandem has the advantages of higher efficiency, narrower heat effected zone (HAZ), lower spatter and porosity [13]. Tandem is used in both steel welding and aluminum welding. Pulse mode GMAW could also used on tandem welding. As a matter of fact, with appropriate parameters and adjustments, tandem can achieve one pulse one droplet which is a perfect metal transfer formation. Figure 2-4 shows a sectional view of tandem torch and a tandem arc diagram.

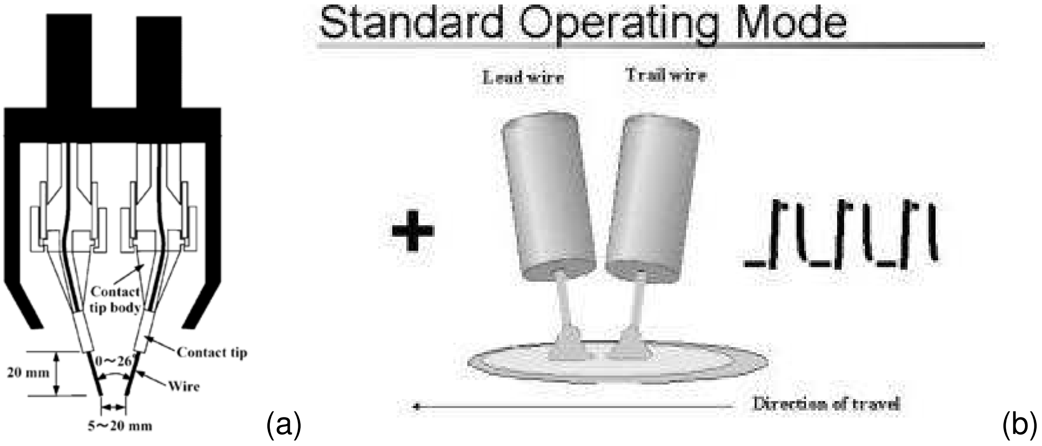

Figure 2-4, Sectional view of tandem torch (a) and operating mode (b) [12]

The inclination angle between two wires of tandem has obvious effect on the welding bead and welding speed. Generally speaking, the angle in Figure 2-4 (a) provides good bead and stable arc. The arc of lead wire and trail wire in tandem doesn't overlap each other. We will talk about this a little bit more when we reach discussion of DE-GMAW.

The disadvantage of tandem firstly is the travel direction of base metal must follow the direction showed in Figure 2-4 (b) to guarantee a good weld bead. The restriction of travel direction is very inconvenient for irregular welding bead which requires seam tracking. Secondly, it still could not reduce base metal heat input because there are two arcs heating the base metal simultaneously.

## 2.3 Overview of DE-GMAW

In early sections, we have already mentioned DE-GMAW system. In chapter 2.3, more details are revealed so the audiences can grasp a better understanding of the differences between tandem and DE-GMAW. The differences between DB-GMAW and DE-GMAW are also presented in detail.

**Motivation**: Originally, Center of Manufacturing, University of Kentucky is seeking a method to double the welding productivity or travel speed meanwhile optimizing other welding properties. As we all know, welding productivity equals the filler metal volume during unit time. It can be calculated by Eq.1-1.

$$Wp = \frac{V_{metal}}{t} = A_{cross} \times \frac{L_{wire}}{t} = A_{cross} \times WFS \qquad \text{Eq.1-1}$$

Where $Wp$ is welding productivity, $V_{metal}$ is metal volume, $A_{cross}$ is the cross area of filler metal, $L_{wire}$ is filler wire length, $WFS$ is wire feeding speed.

From Eq.1-1, it is very clear that greater welding productivity requires faster wire feeding speed. To melt more metal, a larger melting current is necessary in this situation. In conventional GMAW, all melting current flows through base metal which means that melting current equals base metal current. Thus, it is impossible to increase base metal current freely because base metal current is always restricted by the application and material. Otherwise, a burn through of base metal is inevitable and the whole process will fail. In other words, melting current can not be further increased without increasing base metal current.

DE-GMAW is oriented to solve this dilemma by adding a bypass system to conventional GMAW so the melting current has one more path going back to source without compulsorily going through base metal. Figure 1-1 in previous chapter demonstrates a basic system diagram of DE-GMAW. As a matter of fact, that is a non-consumable DE-GMAW system diagram which means the bypass torch is constructed by TIG torch. Figure 2-5 helps us review Figure 1-1.

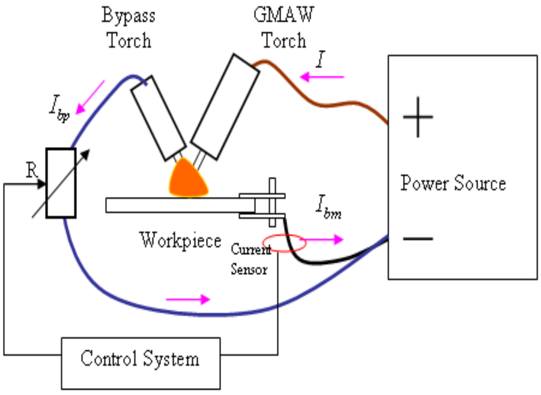

Figure 2-5, Non-consumable DE-GMAW system diagram [3]

In DE-GMAW, the current relationship is represented by Eq.1-2.

$$I_{total} = I_{melting} = I_{basemetal} + I_{bypass} \qquad \text{Eq.1-2}$$

After melting the filler metal, the total current is divided into base metal current and bypass current. The total current of DE-GMAW can be fixed as a constant by fixing the wire feeding speed when the weld power is in constant voltage mode. Therefore, we can adjust base metal current by changing bypass current without changing the melting current. The base metal current is the reason causing work piece burn through. In DE-GMAW, we can have the ability to increasing melting current significantly without increasing base metal current.

Also, we can construct a consumable DE-GMAW by using a MIG torch as bypass system. During the research of non-consumable DE-GMAW, we realized that the bypass current is wasted while it can be used to burn more wire and further increase deposition rate. As a result, we used a MIG torch as bypass system to construct a consumable DE-GMAW.

The current relationship described in Eq.1-2 is still working for consumable DE-GMAW. However, the difference between them is also obvious: non-consumable DE-GMAW has a more stable process than consumable DE-GMAW. In consumable DE-GMAW, the bypass torch wire feeding speed must be controlled at an appropriate rate to ensure the process stability [14].

Consumable DE-GMAW has higher deposition rate compared to non-consumable DE-GMAW because it is burning two wires at the time. Accordingly, consumable DE-GMAW has higher base metal heat input because there are more droplets bringing the heat into the base metal in unit time. Figure 2-6 is system diagram of consumable DE-GMAW.

So far, we spend some time understanding the basic idea of bypass system, non-consumable DE-GMAW and consumable DE-GMAW. It’s time for us to study the benefits and necessity of DB-GMAW.

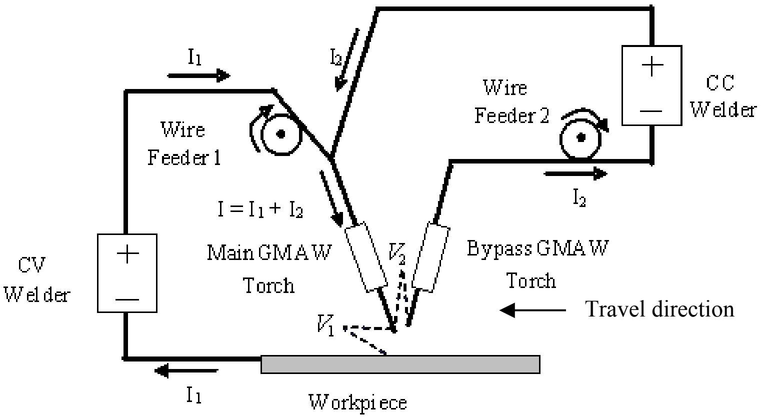

Figure 2-6, System diagram of consumable DE-GMAW [14]

### 2.4 Advantages of DB-GMAW

In previous chapter, we mentioned that DB-GMAW has advantages compared to DE-GMAW: (1). Offering stronger arc stability by providing a balanced welding arc; (2). Further reducing base metal current by diverse the majority of welding current into bypass; (3). Offering more possibility in welding travel direction by balancing the arc column. I will explain the reason of these benefits individually.

(1). **Arc stability**:

In DE-GMAW, during welding, we have one additional arc –bypass arc- compared to conventional GMAW. In conventional GMAW, there is only one arc during welding because there is only one torch. The DE-GMAW arc is composed by two parts: the Main Arc and bypass arc. The main arc is the path that base metal current flows through and the bypass arc is the path that bypass current flows through. An electric arc is an electrical breakdown of a gas which produces an ongoing plasma discharge, resulting from a current flowing through normally nonconductive media such as air. A synonym is arc discharge [15].

Arc is a very complex electrical phenomenon which involves plenty of subjects to talk about. We will theoretical analyze electrical arc and its characteristics in later chapter. Arc force is the Lorentz force generated by arc which is the key factor to help the droplet detaching from the wire tip and accelerating to the base metal.

During the research of DE-GMAW, metal transfer video captured by high speed camera indicates that it is better to keep the difference of bypass current and base metal current close for a stable weld and smooth transfer. If the difference between these two current surpassed a certain level, it is very difficult to maintain a good weld bead. Since the arc force is proportional to the square of current, a significant difference between base metal current and bypass current inevitably results a much bigger difference between main arc force and bypass arc force. The actual arc force is much more complex than the forces showed in Figure 2-7. For simplicity reason, we use $F_{bypass}$ and $F_{mainarc}$ here to represent the Lorentz force acted on the droplet by bypass arc and main arc. Figure 2-7 briefly demonstrates how the main arc force and bypass arc force influence the droplet behavior.

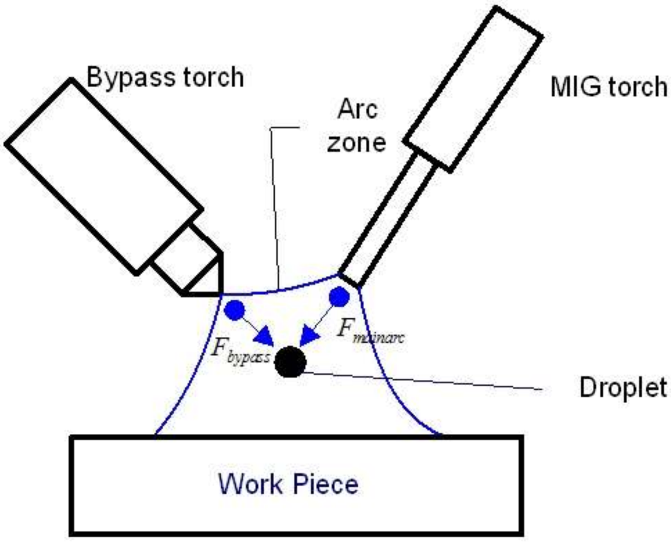

Figure 2-7, Arc forces acted on droplet in DE-GMAW (non-consumable)

From Figure 2-7, it is very obvious to conclude an assumption that these two forces affect the droplet behavior. Figure 2-8 concludes three paths of droplet travel in the arc.

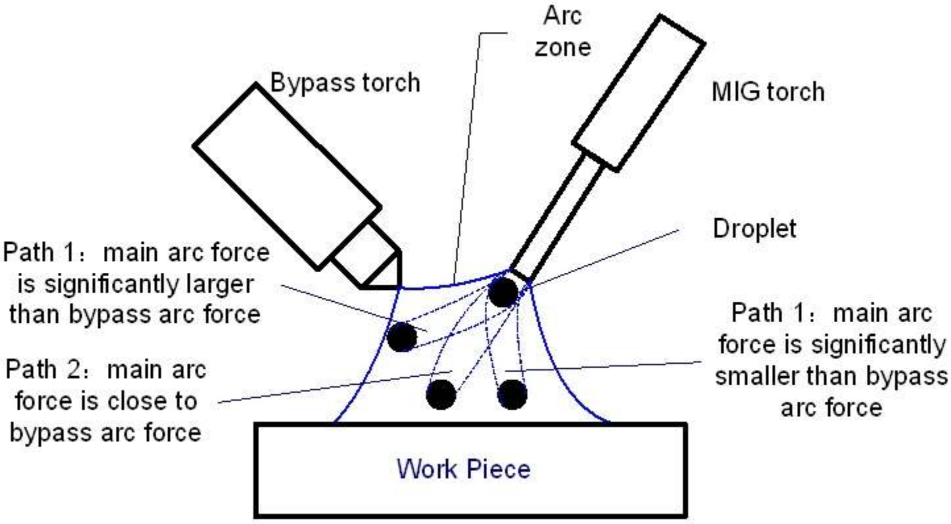

Figure 2-8, Droplet travel paths in the arc of DE-GMAW (non-consumable)

The experimental results also agree with our analysis. Figure 2-9 shows the experimental verification.

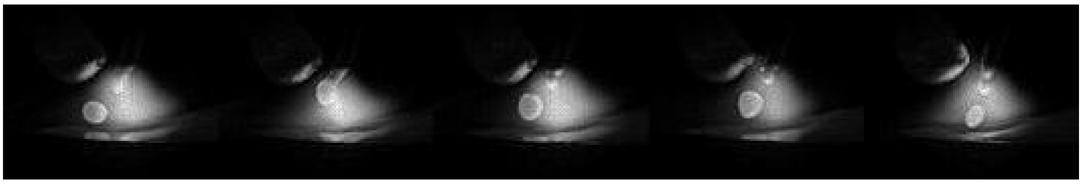

(a): 250A total current, bypass arc doesn’t ignited

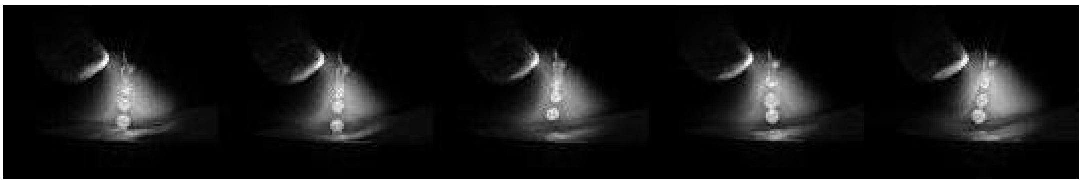

(b): 250A total current with certain bypass current

(c): 250A total current with bigger bypass current than (b)

Figure 2-9, Experimental verification of arc force influences [4]

Actually, Figure 2-9 indicates more things rather than merely demonstrating the droplet behavior.

DE-GMAW satisfies the objective which is to increase weld productivity. However, if the objective is to minimize base metal heat input, the base metal current should be minimized because base metal heat input is proportional to base metal current. When the total current is fixed, we need to maximize the bypass current in order to minimize base metal current.

Figure 2-9 has already proved to us that in DE-GMAW the bypass current shouldn't be significant smaller or significant larger than base metal current to ensure smooth transfer and system stability.

As we mentioned, one of the objectives of DB-GMAW is to reduce base metal heat input which requires the system to decouple as much current as possible after melting the wire. However, it seems very difficult for DE-GMAW to decouple the majority of melting current into bypass loop due to the unbalanced arc force. To solve this problem, another bypass torch is introduced into DE-GMAW and the basic idea of DB-GMAW is proposed.

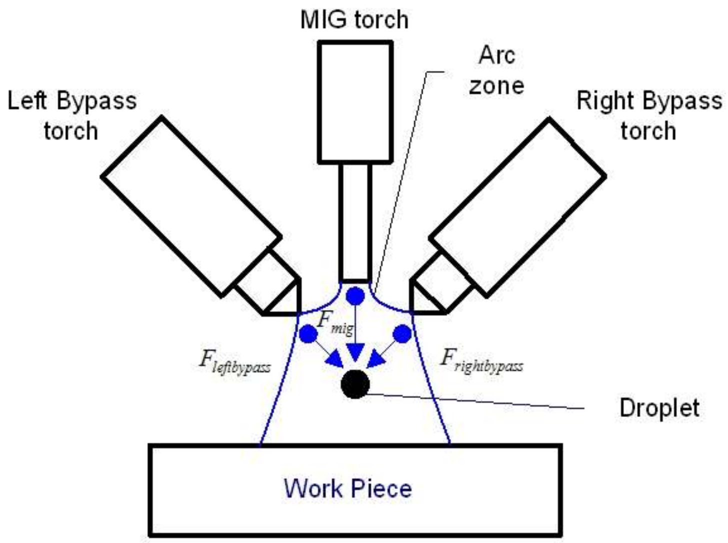

Figure 2-10, Arc forces act on the droplet in DB-GMAW

Figure 2-10 indicates the arc forces acting on the droplet in DB-GMAW. From Figure 2-10, it is clear to tell that the droplet will hit the base metal vertically if we can keep $F_{leftbypass}$ equals $F_{rightbypass}$. In other words, we can obtain a stable arc and transfer by keeping left bypass current equal to right bypass current. It is not necessary any more to keep the value of base metal current and bypass current close to each other. In DB-GMAW, the bypass current has the ability to be much greater than base metal current and decouples the majority of melting current into bypass loops without disturbing arc stability.

Please note that the actual arc forces in DB-GMAW are much more complicated than the situation demonstrated in Figure 2-10. The theoretical analysis of Lorentz force in DB-GMAW arc will be discussed in later chapter. Figure 2-10 is the simplified version used to explain why DB-GMAW has the ability to balance the arc.

(2). **Further reducing base metal current**:

Providing another bypass loop also helps us to further reduce base metal current. In DB-GMAW, the majority of melting current can go back to source through bypass loop. For instance, if the melting current is approximately 200 Amps, in DE-GMAW process, the base metal current is usually around 120A while the bypass current is usually around 80A. Experimental results verify that such current distribution performs a good weld. Identically, if the melting current is still approximately 200 Amps, in DB-GMAW process, the bypass can decouple around 140A away while the base metal current is just around 50-60A.

Base metal current affects base metal heat input proportionally. The ability of further reducing base metal current means the ability to further reduce base metal heat input.

Technically, we can also construct two MIG bypasses to develop a consumable DB-GMAW. A consumable DB-GMAW definitely has the ability to further increase deposition rate and weld productivity. The reason that we develop a non-consumable DB-GMAW system is because increasing welding productivity is not our priority objective in this research. Consumable DB-GMAW cannot help reducing heat input because the number of droplets bringing heat to the base metal will nearly tripled in consumable DB-GMAW. In our further work, we can develop a consumable DB-GMAW system to further increase deposition rate and welding productivity.

(3). **Travel direction**:

The base metal travel direction of DE-GMAW must follow the direction demonstrated in Figure 2-6. In welding process, the disturbance of current is a common noise which could not be prevented completely. Figure 2-7 shows us the arc forces act on the droplet in DE-GMAW. The disturbance of current leads to the disturbance of arc forces which leads the droplet into difference paths demonstrate in Figure 2-8. If the base metal is traveling through the direction showed in Figure 2-6, the welding bead won't be influenced too much by the disturbance of current. However, if the base metal is traveling not through the direction showed in Figure 2-6 but towards the audience or far from the audience, the welding bead can be asymmetrical or even non-continuous.

Generally speaking, we can assume the disturbance of current follows Gaussian distribution. Since there are two bypass torches installing opposite to each other in DB-GMAW, the disturbance of left bypass current and right bypass current could statistically counteract each other. Moreover, the disturbance of base metal current practically doesn't influence the landing position of droplet because the MIG torch is vertically installed. As a result, DB-GMAW has more dimensions of travel direction which is essential for seam tracking.

# CHAPTER 3

## System construction and parameter design of DB-GMAW

System construction is basically composed by two key modules: construction of experimental system and construction of sensing system. Experimental system includes power sources, torch installation and rotation station for work piece. Sensing system includes voltage and current sensors, temperature sensors and high speed video camera.

### 3.1 System construction

**Principles of DB-GMAW**:

A Dual Bypass GMAW process showed in Figure 3-1 has been developed at Center of Manufacturing, University of Kentucky. As illustrated, the system includes a constant voltage (CV) power supply to provide the base metal current $I_{cv}$, and two constant current (CC) power supplies to provide the left and right bypass currents: $I_{left}$ and $I_{right}$. The positive terminals of all three power supplies are connected together to the GMAW torch (which provides the bypass tungsten electrodes), respectively. In DB-GMAW, the total melting current which melts the wire is the sum of three currents, i.e., $I = I_{basemetal} + I_{left} + I_{right}$. Thus, the base metal current that controls the base metal heat input and arc pressure imposed on the work piece can be much less than the total melting current. It has been verified by experiments that the total melting current is determined by the preset wire feed speed (WFS) and the welding voltage for the CV power supply. Hence, the base metal current can be decreased by increasing the bypass currents since their sum is a constant. Since the bypass currents are provided by two CC power supplies and can be adjusted freely, the DB-GMAW can provide a large range of base metal current for each set of wire feed speed and welding voltage to meet the requirements from different applications.

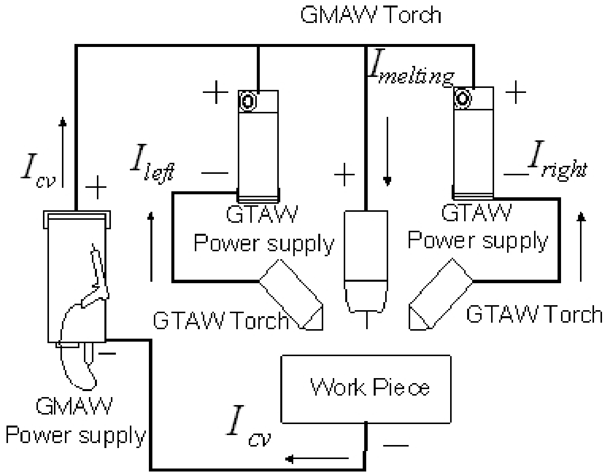

Figure 3-1, Illustration of DB-GMAW

**<u>Base metal and Rotation station</u>:**

As our project supporter, Los Alamos National Laboratory (LANL) is looking for a method to weld aluminum rings which could achieve a minimum melting of work piece while maintaining weld quality. The work piece is an aluminum ring with a groove on it. The geometrical regulation of LANL aluminum cylinder is showed in Figure 3-2.

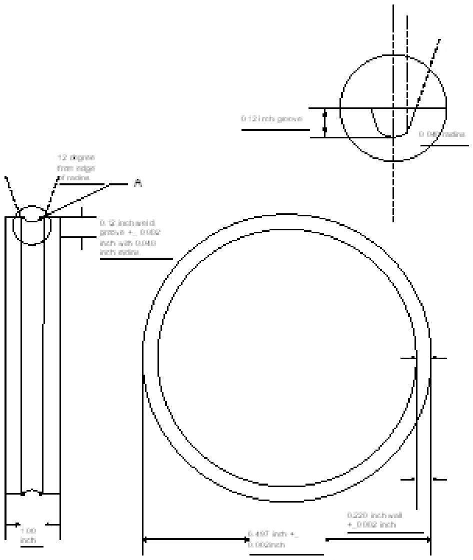

Figure 3-2, Geometrical regulation of LANL aluminum cylinder

Considering the complexity of machining a U-shape groove on the aluminum tube, we also adopt work piece demonstrated in Figure 3-3 which is more common in manufacturing in our research. The geometrical parameter is similar with the work piece in Figure 3-2 but approximately 15%-20% thicker in dimension.

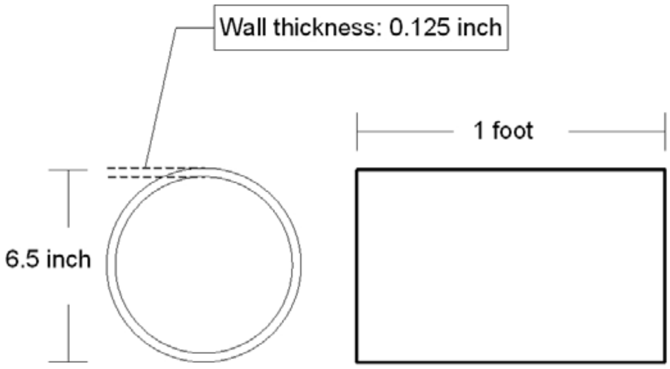

Figure 3-3, Experimental work piece geometry

Aluminum is the most commonly used nonferrous metal in manufacturing industry for its excellent physical and mechanical properties such as low density, high strength density ratio and high thermal and electrical conductivity. Base metal material in our research is aluminum 6061 T6. The filler metal is aluminum 4043 alloy with 0.8mm and 1.2mm diameter. Aluminum 6061 T6 is Alu-Mg-Si alloy. Aluminum 4043 belongs to Alu-Si alloy [16].

The rotation system is a bidirectional (clockwise & anticlockwise) spiral chuck with a DC control board which controls the rotational direction and speed.

**Torch Installation**:

In DB-GMAW, the welding arc contains three components: the main arc between the filler wire and the work piece, the left bypass arc between the filler wire and the left bypass electrode, and the right bypass arc between the filler wire and the right bypass electrode. Here, the filler wire serves as the common anode. The three cathodes in DB-GMAW are: the work piece and the two tungsten electrodes. While the main arc is assured by the continuous wire feeding, the bypass arcs are assured by an appropriate setting of the bypass torches.

In order to obtain stable bypass arc and process, the torch setting must be able to ignite and maintain the bypass arcs easily. The DB-GMAW torch setting illustrated in Figure 3-4 has been developed. In DB-GMAW, there are two GTAW torches symmetrically mounted to the GMAW torch, which is perpendicular to the surface of the work piece. The two GTAW torches act as the bypass electrodes to deliver the bypass currents. All these three torches are in the same plane perpendicular to the welding direction. Figure 3-5 is a picture of the physical torches.

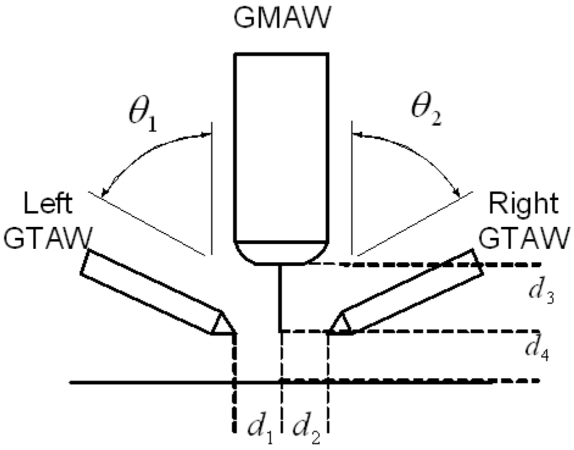

Figure 3-4, Torch installation parameters

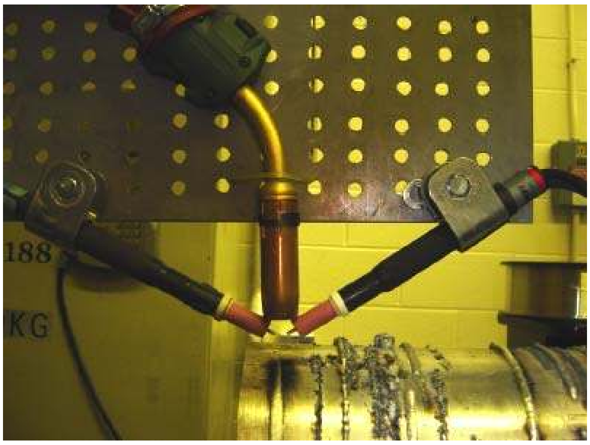

Figure 3-5, Picture of physical torches installation

The tungsten in the bypass GTAW torch can easily emit electrons to assure the ignition of the bypass arc due to its low electron work function (eV). At the same time, the bypass tungsten electrodes must be close enough to the wire to establish the bypass arcs after the main arc's ignition. The following geometrical parameters illustrated in Figure 3-5 must be set appropriately:

$d_1$ – Distance from the tip of the left bypass electrode to the wire.

$d_2$ – Distance from the tip of the right bypass electrode to the wire.

$d_3$ – Vertical distance from the axis of the GMAW contact-tube to the tips of the bypass electrodes.

$d_4$ – Vertical distance from the tips of the bypass electrodes to the work piece.

$\theta_1$, $\theta_2$ – Angles between left or right bypass torch and GMAW torch, usually 60-70 degree. $\theta_1$ always equals to $\theta_2$.

Among these parameters, $d_1$, $d_2$, $\theta_1$ and $\theta_2$ should be pre-set, while $d_3$ and $d_4$ will be determined by wire feed speed, welding voltage and electrode extension in welding process. In our experiments, the $d_1$ and $d_2$, $\theta_1$ and $\theta_2$ were set to 1.5mm-1.7mm and 60 degree respectively.

### 3.2 Sensing system

All the data of our experiment is collected through sensing system via particular sensors to data acquisition board. The data to be collected includes welding currents, welding voltage, base metal temperature and metal transfer image.

**Welding currents**:

The welding currents to be monitored are base metal current, left bypass current and right bypass current. Three CLN-500 closed loop hall effect current sensors are used to monitored the current value. CLN-500 current sensor has a nominal current of 500A rms with a measuring range of 0 to ±1200A. The accuracy at $25^{\circ}$C is ±0.5% of the nominal current and response time is less than $1\mu s$.

**Welding Voltage**:

According to the fact that welding voltage signal is companied with significant high frequency noise signal, isolation board is adopted for noise elimination. During experiments, main arc voltage and bypass arc voltage are monitored.

**Metal transfer video and image**:

The metal transfer process is monitored through Olympus i-speed camera. A narrow band filter of 685nm is applied for clear images of metal transfer. The recording frame rate is preset as 4000 frame per second. The image can also be collected into computer via NI PCI-1410 video acquisition card.

Figure 3-6, Olympus i-speed high speed camera

**Base metal temperature monitoring system**:

We use fast-response K-type thermocouples (120ms for 0-63% of full scale) as sensors to monitor the work piece temperature during experiments. Thermocouples are attached compactly to the work piece inner surface. Figure 3-7 shows geographic placement of thermocouples, torches and work piece. Figure 3-8 shows the thermocouples and transmitters adopted in our experiment. Signals are amplified by thermocouple transmitters before being read by data acquisition board. After DB-GMAW process achieves stability, the thermocouples go through the arc column meanwhile the highest temperature of process is recorded.

As the reflection of base metal heat input, the highest temperature captured by thermocouples is proportional to base metal heat input. The comparison of highest temperature between traditional GMAW process and DB-GMAW process indicates which process has greater base metal heat input. The position of thermocouples is approximately quarter circle advanced the welding torch at the beginning of experiment which means the thermocouples travel through the arc column after a quarter of the whole experimental time. Such arrangement guarantees the weld process to achieve stability before the thermocouples meet the arc column. The highest temperature is captured at the moment that the thermocouples are right under the arc column.

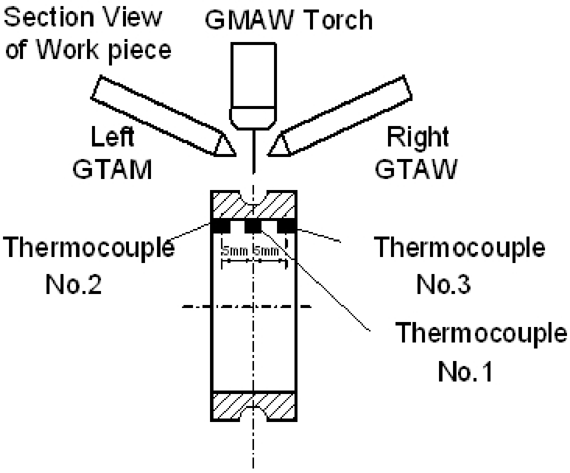

Figure 3-7, Thermocouples on the inner surface

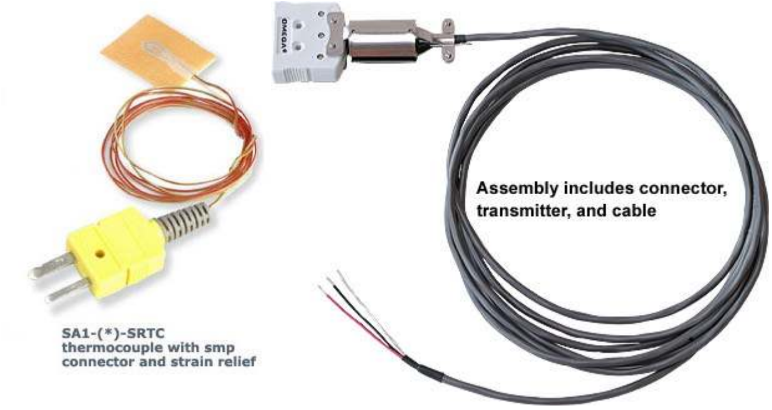

Figure 3-8, K-type thermocouple and transmitter

We cannot measure the temperature of the melt welding pool directly due to its extremely high temperature and liquid metal. As a result, we use the base metal temperature as a reflection of base metal heat input. In most of the situation, base metal temperature is a good parameter to reflect heat input. However, there are still other parameters influencing the results of thermocouples which will be discussed in later chapter.

All experimental system components introduced above work together under the coordination of the computer. The software platform of our station is LabView real-time system. The data acquisition board adopted is NI PCI-6221. The sampling rate of this system is approximately 1K (963 samples per second). The operation system is window XP professional.

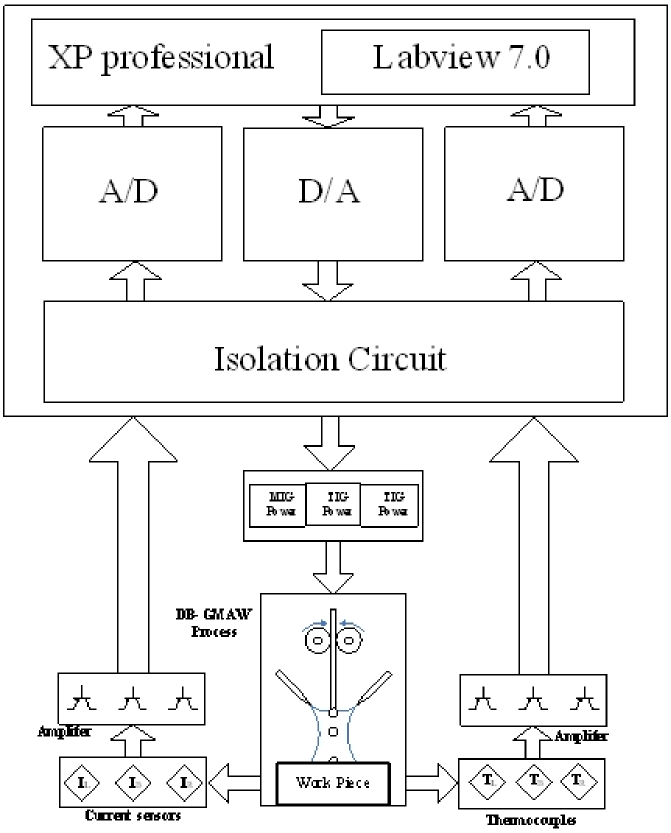

Figure 3-9, Sketch of experimental system.

### 3.3 Experimental parameters

During our research, the experiments are designed for four phases of research: feasibility test, test on the one foot long work piece, test on the grooved aluminum ring work piece and penetration control research. Due to the differences of objectives from different phases of research, the parameter of experiments varies slightly according to different requirements. The experimental procedure also changes slightly. Detail data recording the information of each experiment will be revealed and discussed in related chapter. The parameter and procedure discussed here are basic preset parameters and general designed procedure for each experiment.

**Parameters on 1 foot long work piece for metal transfer research**:

The research work about metal transfer is based on experiments performed on Figure 3-3 showed work piece. The preset parameter on this section follows Table 3-1.

Table 3-1, Parameters of metal transfer research

| Bypass current (Left and Right) | |
|---|---|
| 0 A | Experiment 1 |
| 30 A | Experiment 2 |
| 40 A | Experiment 3 |
| 50 A | Experiment 4 |
| 60 A | Experiment 5 |
| Constant parameters | |
| Wire | 0.8mm<br>ER 4047 |
| Base metal | Al6061 T6<br>thickness: 3.2mm |
| Shielding gas | Pure Argon |
| Gas flow | 12 L/min |
| Welding speed | 240 cm/min |
| Wire feeding speed | 18.6m/min |
| Preset welding voltage | 21.5 V |
| Total welding current | 160 A |

Experiment 1-5 in Table 3-1 refers to experiments with different bypass current. The preset bypass current varies from 0 to 60 A. The current value is the current goes through one bypass torch. Here, the preset left bypass current equals the preset right bypass current.

Experiments on different bypass current help us understand the influence of bypass arc, bypass current and bypass Lorentz force on the arc stability, wire extension, metal transfer and droplet formation.

**<u>Parameters on 1 foot long work piece for heat input research</u>**:

Preset Parameters for heat input research is slightly different from parameters in Table 3-1.

Table 3-2, Parameters on one foot long work piece for heat input research

| | |
|---|---|
| GMAW base metal current 1 | 200A |
| Bypass current (L & R) 2 | 30A |
| Bypass current (L & R) 3 | 40A |
| Bypass current (L & R) 4 | 45A |
| Bypass current (L & R) 5 | 50A |
| Bypass current (L & R) 6 | 55A |
| Constant parameters | |
| Wire type | 1.2 mm<br>ER 4047 |
| Base material | Al6061 T6<br>thickness: 3.2mm |
| Shielding Gas (MIG torch) | Argon |
| Shielding Gas (bypass torch) | Argon |
| Gas flow | 12 L/min |

Table 3-2, cont.

| | |
|---|---|
| Welding speed | 240 cm/min |
| Wire feeding speed | 18.6m/min |
| Preset welding voltage | 21.5 V |
| Total welding current | 200A |

Parameters above in Table 3-2 help us understand the influence of bypass current to the base metal heat input and penetration.

**Parameters on Aluminum Ring**:

The aluminum ring work piece demonstrated in Figure 3-2 is precisely designed by LANL for particular reason. Specific parameters are required for welding on this work piece. The preset parameters in Table 3-3 satisfy the requirements and help us to compare traditional GMAW and DB-GMAW. Moreover, it helps us understand the influences of shielding gas.

Table 3-3, Preset parameters on aluminum ring work piece

| **Experiments:** | |
|---|---|
| Type 1: GMAW base metal current | 50A |
| Type 2: GMAW base metal current | 50A |
| Type 3:DB-GMAW Bypass current (L & R) | 50A |
| Type 4:DB-GMAW Bypass current (L & R) | 50A |
| Constant parameters | |
| Wire type | 0.8mm<br>ER 4047 |
| Base material | Al6061 T6<br>thickness: 3.2mm |

Table 3-3, cont.

| | |
|---|---|
| Shielding Gas for experiment type 1 & 3 | Shielding Gas (MIG torch): 85%Helium+15%Argon<br>Shielding Gas (bypass torch): 100% Argon |
| Shielding Gas for experiment type 2 & 4 | Shielding Gas (MIG torch): 100% Argon<br>Shielding Gas (bypass torch): 100% Argon |
| Gas flow | 12 L/min |
| Welding speed | 240 cm/min |
| Wire feeding speed | 18.6m/min |
| Preset welding voltage | 21.5 V |
| Total welding current | 160 A |

### 3.4 Summary

The system designed above is a non-consumable DB-GMAW with monitoring modules which feedbacks all necessary information back to computer for control and reference.

This experimental platform is capable of performing smooth conventional GMAW and non-consumable DB-GMAW on cylindrical work piece. Necessary information such as welding current and welding voltage is collected to computer for further control and reference. High speed camera is adopted to record metal transfer process. The platform is suitable to research the characteristics of DB-GMAW.

# CHAPTER 4

# Metal transfer in DB-GMAW

## 4.1 Background

Metal transfer refers to the modes that the droplet detaches from wire tip and transfers to the base metal. Metal transfer is one of the most important properties of GMAW which affects the welding bead and process magnificently. The metal transfer of the GMAW process is best described in terms of the three basic means by which metal is transferred from the electrode to the work piece:

(1). Globular transfer:

GMAW with globular metal transfer is often considered the most undesirable of the three major GMAW variations, due to its tendency to produce high heat, a poor weld surface, and spatter. The method was originally developed as a cost efficient way to weld steel using GMAW, because this variation uses carbon dioxide, a less expensive shielding gas than argon. Adding to its economic advantage was its high deposition rate, allowing welding speeds of up to 110 mm/s (250 in/min) [7]. As the weld is made, a ball of molten metal from the electrode tends to build up on the end of the electrode, often in irregular shapes with a larger diameter than the electrode itself. When the droplet finally detaches either by gravity or short circuiting, it falls to the work piece, leaving an uneven surface and often causing spatter [17]. As a result of the large molten droplet, the process is generally limited to flat and horizontal welding positions. The high amount of heat generated also is a downside, because it forces the welder to use a larger electrode wire, increases the size of the weld pool, and causes greater residual stresses and distortion in the weld area.

(2). Short-circuiting transfer:

Further developments in welding steel with GMAW led to a variation known as short-circuiting or short-arc GMAW, in which carbon dioxide shields the weld, the electrode wire is smaller, and the current is lower than for the globular method. As a result of the lower current, the heat input for the short-arc variation is reduced, making it possible to weld thinner materials while decreasing the amount of distortion and residual stress in the weld area. As in globular welding, molten droplets form on the tip of the electrode, but instead of dropping to the weld pool, they bridge the gap between the electrode and the weld pool as a result of the greater wire feed rate. This causes a short circuit and extinguishes the arc, but it is quickly reignited after the surface tension of the weld pool pulls the molten metal bead off the electrode tip. This process is repeated about 100 times per second, making the arc appear constant to the human eye. This type of metal transfer provides better weld quality and less spatters than the globular variation, and allows for welding in all positions, albeit with slower deposition of weld material. Setting the weld process parameters (volts, amps and wire feed rate) within a relatively narrow band is critical to maintaining a stable arc: generally less than 200 amps and 22 volts for most applications [19].

(3). Spray transfer.

Spray transfer GMAW was the first metal transfer method used in GMAW, and well-suited to welding aluminum and stainless steel while employing an inert shielding gas. In this GMAW process, the weld electrode metal is rapidly passed along the stable electric arc from the electrode to the work piece, essentially eliminating spatter and resulting in a high-quality weld finish. As the current and voltage increases beyond the range of short circuit transfer the weld electrode metal transfer transitions from larger globules through small droplets to a vaporized stream at the highest energies [18]. Since this vaporized spray transfer variation of the GMAW weld process requires higher voltage and current than short circuit transfer, and as a result of the higher heat input and larger weld pool area (for a given weld electrode diameter), it is generally used on work pieces of thicknesses above about 6.4 mm (0.25 in) [18]. Also, because of the large weld pool, it is often limited to flat and horizontal welding positions and sometimes also used for vertical-down welds.

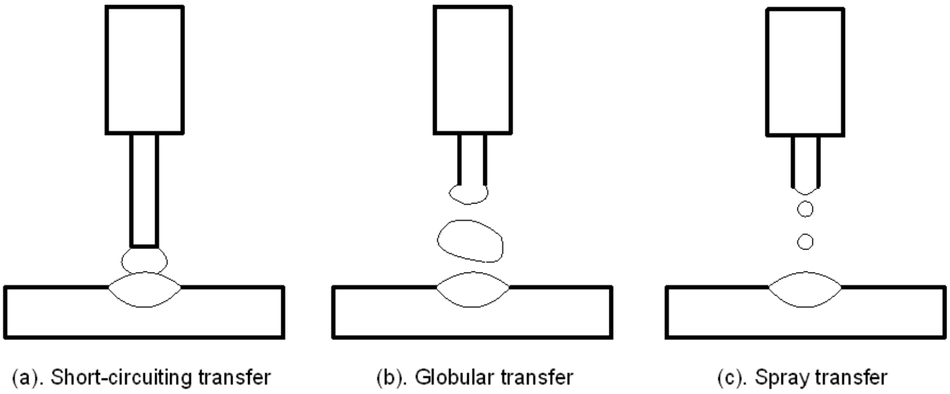

Figure 4-1, Sketch of three modes of metal transfer

Each of these modes has a characteristic arc length, weld penetration and weld pool shape. The spray transfer region can be further divided into three sub-classifications: Projected drop spray, streaming spray and rotating spray. Project drop spray transfer is characterized by roughly spherical droplets of molten metal and is the sub-classification most often referred by welding professionals. With further increases in wire feed rate and voltage, individual droplets become less distinct, and an almost continuous column of molten metal extends from the electrode to the base plate. In rotating spray transfer, the electromagnetic forces have become so large that the metal in the arc column experiences forces with non-axial components which cause the molten column to have an initial velocity that is at an angle to the electrode axis. The liquid metal follows a helical course from the electrode to the base metal [19].

Generally speaking, by increasing the welding current, the short-circuiting transfer can change to globular transfer then to spray transfer. The globular transfer will become spray transfer once the welding current surpasses the transient current. For different sets of parameters and material, the transient current is different from each other. Once the filler metal, material and welding parameters are fixed, the transient current will be fixed under that condition.

## 4.2 Theoretical analysis of forces in the arc

The formation of the metal droplets is governed by a combination of factors, including the balance of forces acting on the droplet, thermal phenomena in the wire, heat transfer from the arc, and the current density distribution in the droplet [20]. Two major models developed to describe the droplet formation are the static-force balance theory (SFBT) [21] and the magnetic pinch instability theory (PIT) [22-23]. The SFBT considers the balance between gravity, electromagnetic forces, plasma drag force, and surface tension acting on the pendant drop. The PIT considers perturbation due to the magnetic pinch force acting on an infinite cylindrical column of liquid metal. Among all the forces mentioned, the electromagnetic force plays an important role in droplet detachment [20].

After detachment, the droplet is accelerated in the arc by the Lorentz force acting on it. The acceleration of the droplet is often calculated by applying an arc plasma drag force on the droplet [24].

### 4.2.1 Forces of conventional GMAW

Low base metal heat input and arc pressure are often critical in meeting specified requirements in aluminum welding [25]. In traditional GMAW process, GMAW operates in the globular metal transfer mode at relatively low continuous waveform currents. However, this transfer mode is characterized by periodic formation of large droplets which detach from the electrode primarily by the gravitational force and are typically associated with arc instability [26]. At higher currents, the transfer mode changes to the desirable spray mode which offers high deposition rate and desirable arc stability but at the expense of high heat inputs which may be too high for many aluminum welding applications. In order to solve this problem, pulsed gas metal arc welding (P-GMAW) has been developed. In P-GMAW, the pulse parameters can be adjusted to control the droplet transfer mode, heat input, droplet size or droplet velocities for different applications. However, to achieve the spray transfer, the peak current has to be greater than the transition current which is relatively high. This relatively high peak current produces a large arc pressure which can easily generate burn-through in full penetration applications especially during aluminum welding. Furthermore, the parameters for the pulse waveform need to be determined according to material, shield gas, and wire diameter.

In conventional GMAW, the major forces acting the droplet include the gravity, electromagnetic force, aerodynamic drag force, surface tension, and vapor jet force [27]. According to the static-force balance theory (SFBT) [21], the balance of these forces determines the metal transfer process, i.e., droplet formation, size and frequency. Figure 4-2 demonstrates the major forces acting on a droplet in conventional GMAW.

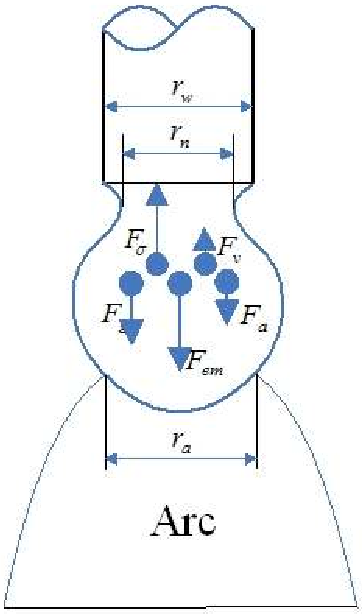

Figure 4-2, Major forces acting on droplet in GMAW

In Figure 4-2, there are five major forces acting on the droplet which are: the force due to gravity, $F_g$; surface tension, $F_\delta$; the aerodynamic drag force, $F_a$; the vapor jet force, $F_v$ and the electromagnetic force, $F_{em}$, respectively.

The force due to gravity can be expressed as:

$$F_g = mg = \frac{4}{3}\pi r_d^{\ 3}\rho g \qquad \text{Eq.4-1}$$

where $r_d$ is the droplet radius, $\rho$ is the droplet density, and $g$ is the acceleration of the gravity.

The surface tension is given as [27]

$$F_\sigma = 2\pi R\sigma \qquad \text{Eq.4-2}$$

where $R$ is the electrode radius, while $\sigma$ is the surface tension coefficient.

The aerodynamic drag force can be expressed as [27]

$$F_a = 0.5\pi v_f{}^2 \rho_f r_d{}^2 C_d \qquad \text{Eq.4-3}$$

where $C_d$ is the aerodynamic drag coefficient, $\rho_f$ and $v_f$ are the density and fluid velocity of the plasma. This force is higher with higher droplet radius and plasma velocity.

The vapor jet force is given as [27]

$$F_v = \frac{m_0}{d_f} IJ \qquad \text{Eq.4-4}$$

where $m_0$ is the total mass vaporized per second per ampere, $I$ is the welding current, and $J$ is the vapor density.

The electromagnetic force, $F_{em}$, is given as [21]

$$F_{em} = \frac{\mu_0 I^2}{4\pi}(1/2 + \ln\frac{r_i}{r_u}) \qquad \text{Eq.4-5}$$

where $\mu_0$ is the magnetic permittivity, $I$ is the welding current, $r_i$ is the *exit* radius of the current path and $r_u$ is the *entry* radius of the current path. At the time the droplet is initially formed, the radius of droplet is smaller than the arc radius. At this particular time, $r_i = r_w$ ($r_w$ the radius of filler wire), $r_u = r_a$ （$r_a$ the radius of anode area）. After the appearance of droplet neck, $r_i = r_n$, （$r_n$ the droplet neck radius） and $r_u = r_a$.

The balance of the forces on a droplet is given by：

$$F_g + F_a + F_{em} = F_\sigma + F_v \qquad \text{Eq.4-6}$$

For spray transfer, Ref. 21 calculated $F_g$, $F_{em}$, $F_\sigma$ and $F_a$ when the welding current is 300A and the droplet mass is 30mg. Calculation indicated that the influence from $F_g$ and $F_a$ to droplet is relatively smaller; $F_v$ obviously influences the droplet only under large welding currents [27]. Therefore, the electromagnetic force is the dominant force facilitating the droplet transfer and the surface tension is the dominant force retaining the droplet from being transferred. The value of electromagnetic force is exceptionally sensitive to the variation in $r_a$ [21]. The electromagnetic force only facilitates the spray when $r_a$ is larger than $r_w$.

### 4.2.2 Forces of DB-GMAW

The forces in DB-GMAW change significantly from conventional GMAW due to the existence of bypass arcs/currents and the resultant changes in the electromagnetic forces. The two bypass currents generate $F_{eml}$ and $F_{emr}$ which are also governed by Eq.4-5. Assume the bypass currents/arcs are symmetric and the two bypass currents are equal, then we have:

$$F_{eml} = F_{emr} = \frac{u_0 I_{by}^2}{4\pi}(1/2 + \ln\frac{r_i}{r_u}) \qquad \text{Eq.4-7}$$

Where $I_{by}$ is the amperage of left and right bypass current, $r_i = r_{byl}$ ($r_{by1}$ the bypass arc root radius), $r_u = r_{by2}$ ($r_{by2}$ the bypass arc tip radius). However, due to the change in the direction of the current flow, the direction of the electromagnetic forces generated by the bypass currents changes from that of the electromagnetic force in conventional GMAW as showed in Figure 4-3.

Due to the direction change, the bypass currents generated electromagnetic forces can be projected into two directions: along the axis of the electrode and perpendicular to the axis. The components along the electrode axis balance out part of the surface tension. In addition, the perpendicular components of $F_{eml}$ and $F_{emr}$ will try to shrink the neck of the droplet so that $r_u$ should be reduced. As a result, both $F_{eml}$ and $F_{emr}$ would tend to increase to accelerate the separation of the droplet from the wire.

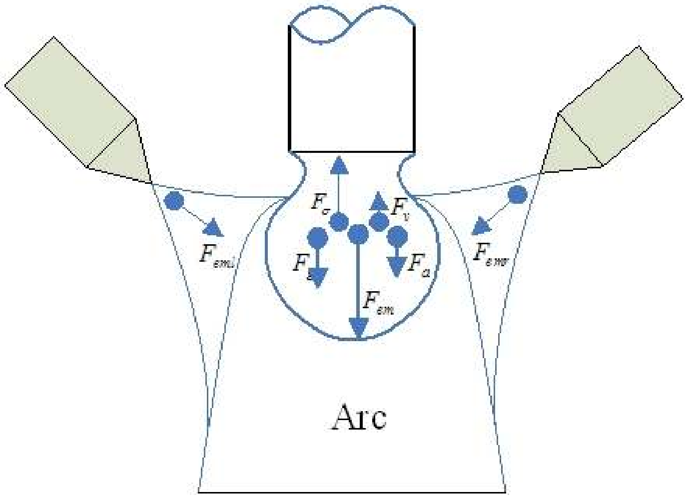

Figure 4-3, Schematic of forces affecting droplet in DB-GMAW

In addition, bypass arcs would increase the anode area so that the arc root now covers the majority or entire droplet surface (see the differences between Figure 4-5 and Figure 4-13). Hence, DB-GMAW increases $r_a$, $F_{emr}$ and $F_{eml}$. As a result, the droplet is easier to transfer in DB-GMAW than in conventional GMAW.

Bypass arc will facilitate the air flowing from the upper of the droplet to the lower so that the plasma fluid velocity $V_f$ is increased. According to Eq.4-3, an increase in $V_f$ will causes an increase in the aerodynamic drag force $F_a$. Although not as dominant as electromagnetic forces, $F_a$ as well enhances the detachment of the droplet.

The distribution of the forces acting on the droplet in DB-GMAW is showed in Figure 4-3. The introduction of the bypass arcs facilitate an easier transfer of droplets in various ways leading to the consequence that the critical current for the spray transfer is decreased from that in conventional GMAW.

## 4.3 Experimental procedure and results

### 4.3.1 Experimental procedure

The experimental system has been introduced in previous chapter. The preset parameters here follow Table 3-1. Figure 4-4 shows the sketch of system.

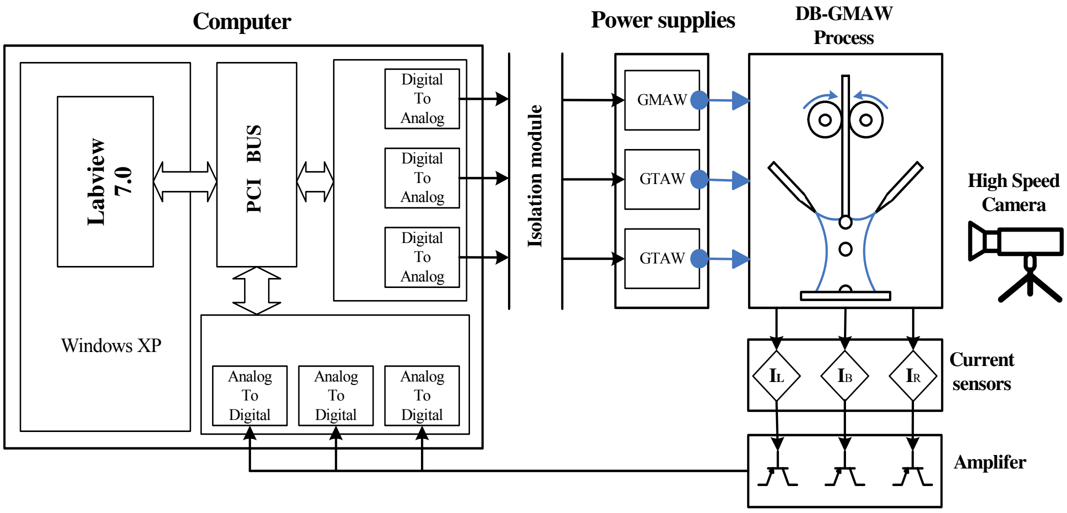

Figure 4-4, Sketch of system only involves metal transfer

Due to the constraint of total current value, the sum of the bypass could not overstep 140A to ensure the minimum base metal current for cathode pulverization effect which is the key factor to maintain aluminum GMAW stability.

### 4.3.2 Experimental results

Different experiments have been performed using the DB-GMAW under the parameters showed in Table 3-1.

Figures 4-5 and 4-6 illustrate the droplet transfer process captured by the high speed camera and the welding current waveform for experiment 1 in Table 3-1 where the bypass current is zero. (The process is thus the conventional GMAW). In this case, as can be seen from Figure 4-5, the metal transfer is obviously of short circuit transfer. The droplet grows during the process and transfers itself from the wire tip into the weld pool when it touches the weld pool surface. Spatters are observed.

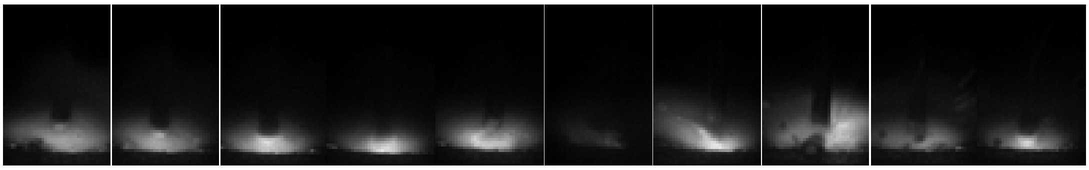

Figure 4-5, Metal transfer without bypass current in experiment 1. The interval between each frame is 1ms.

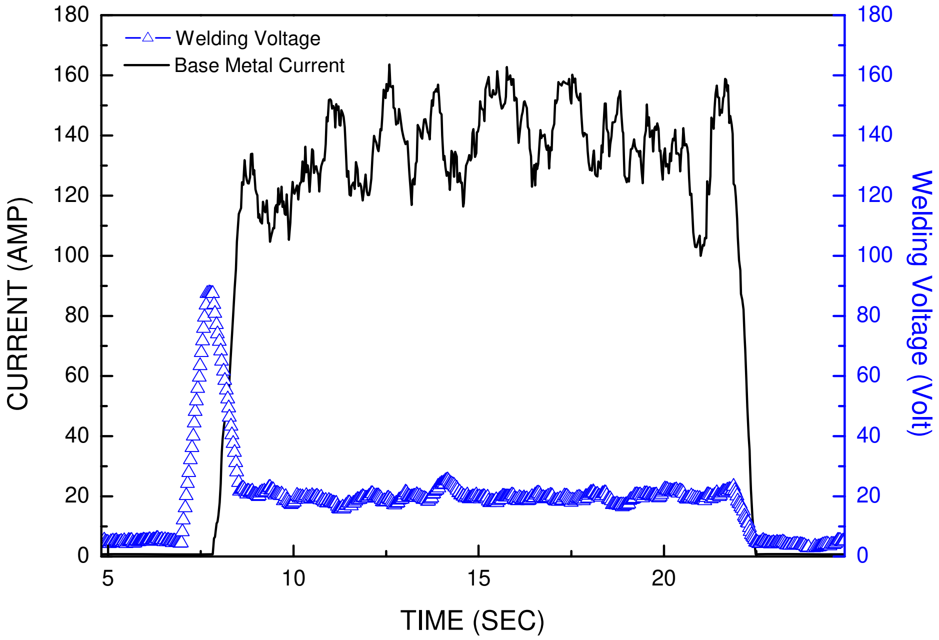

Figure 4-6, Current and voltage in experiment 1. Bypass currents equal to zero.

In experiment 2, the bypass current increased from zero to 30A and the process is truly DB-GMAW. Figure 4-7 and 4-8 are the droplet transfer images and welding current waveform respectively. In this case, the arc length increased but the transfer is still short circuit. As can be seen in the images, the droplet keeps increasing before it is transferred into the weld pool; however, it is difficult for the cathode spot to climb from the bottom of the droplet to the wire tip because of the puniness of bypass arc. In this case, cathode spot force and $F_{em}$ would become a resistance which blocks the droplet from transferring. As long as the droplet keeps growing, the transfer sometimes becomes repelled transfer because of the existence of such resistance. The whole process lacks stability and can lead to undesirable bead shapes.

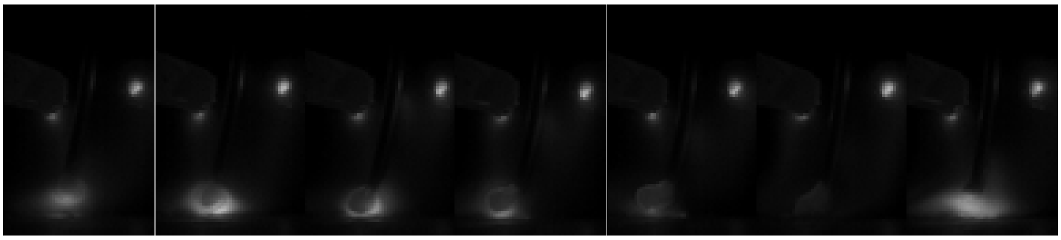

Figure 4-7, Metal transfer with dual 30A bypass current in experiment 2. The interval between each frame is 2.5 ms.

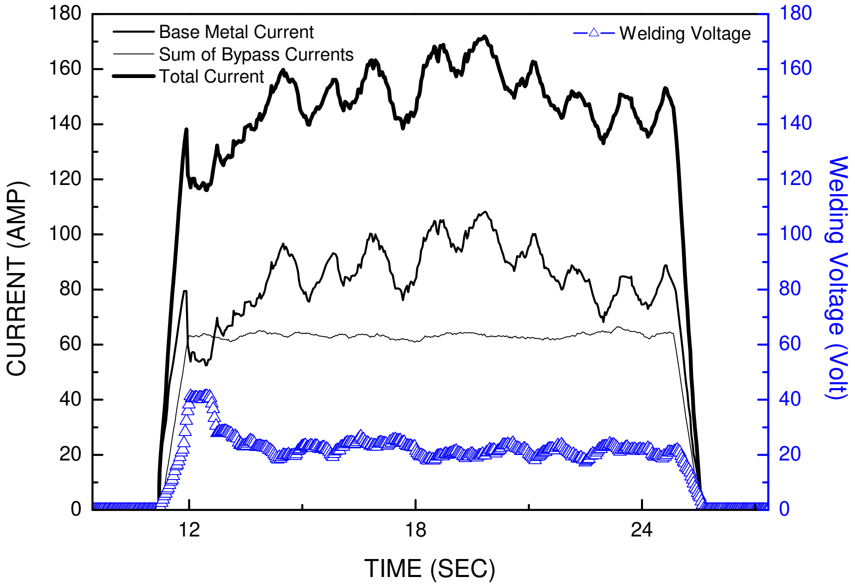

Figure 4-8, Currents and voltage in experiment 2. Bypass currents equal to 30A separately.

Figure 4-9 is the droplet transfer images in experiment 3 where the bypass current is 40 A. Figure 4-10 is the current and voltage waveforms. Observation shows that the droplet size under this parameter is smaller although the droplet transfer is still in a short circuit. In this case, short circuit duration in each period has become much shorter. This suggests that the metal transfer under this set of parameters is a combination of spray transfer and short circuit transfer. Such behavior is a lot similar with the meso-spray transfer obtained in aluminum GMAW process. When performing as a combination of spray transfer and short circuit transfer, the droplet neck pinching and transfer would be accomplished within a very short time beginning with the moment that the droplet touches the weld pool surface. The process is more stable and leads to better weld beads.

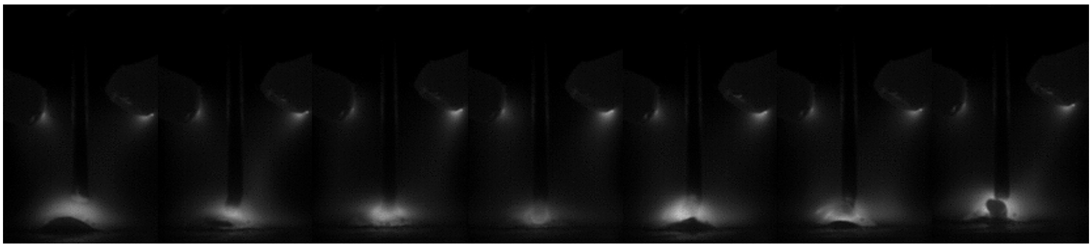

Figure 4-9, Metal transfer with dual 40A bypass current in experiment 3. The interval between each frame is 1 ms.

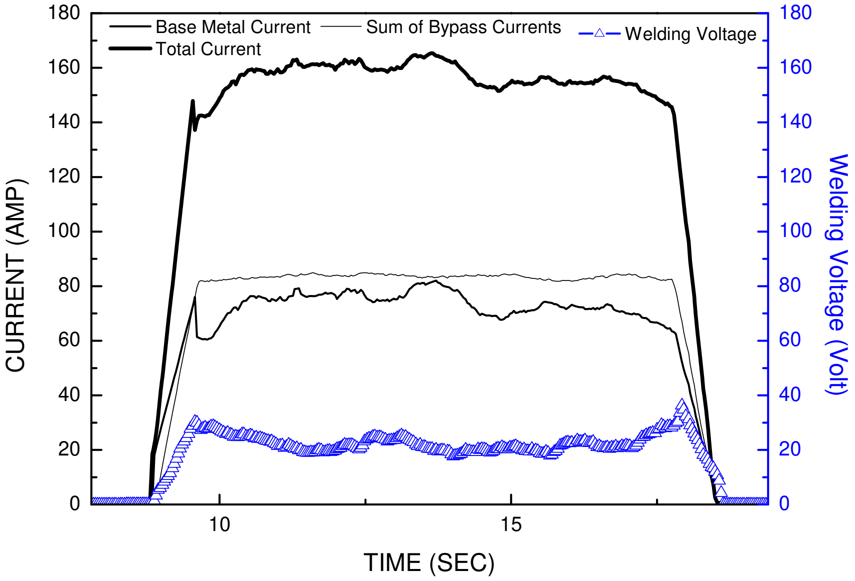

Figure 4-10, Currents and voltage in experiment 3. Bypass currents equal to 40A separately.

Figure 4-11 is the droplet transfer images captured when the bypass current is 50A (Experiment 4). Figure 4-12 is its current and voltage waveforms. After the bypass current reached 50A, the droplet transfer becomes globular free transfer with a very stable process and well shaped weld beads produced. The arc could climb itself from the bottom of the droplet to the upper during the droplet growing. This makes the droplet transfer resistance forces decrease rapidly. The transfer frequency becomes 150~250 drop/sec under such set of parameters. Hence, 50A of bypass current can be considered as a “critical” current for the transfer changes from short circuiting to a free transfer in aluminum DB-GMAW when the total current is approximately 160A.

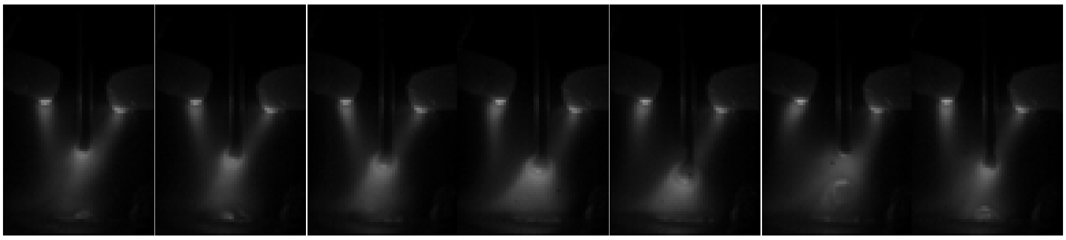

Figure 4-11, Metal transfer with dual 50A bypass current in experiment 4. The interval between each frame is 1.5ms.

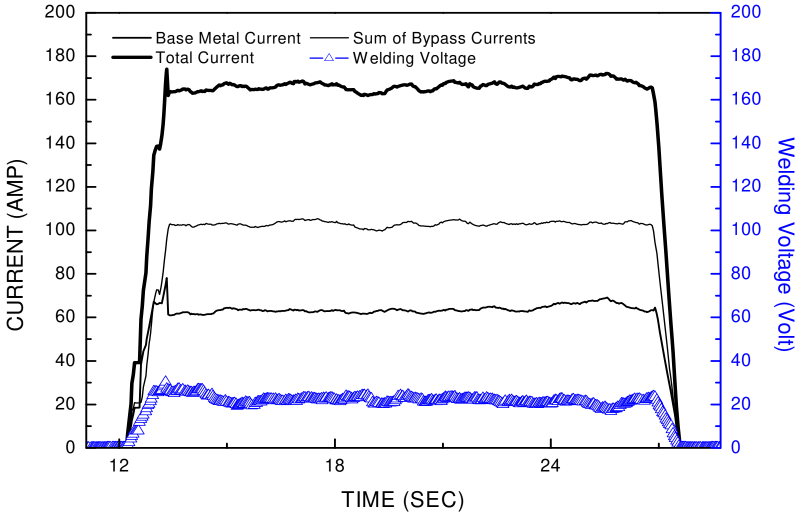

Figure 4-12, Currents and voltage in experiment 4. Bypass currents equals to 50A separately.

In experiment 5, the bypass is further increased to 60A. The transfer becomes a stable spray transfer as showed in Figure 4-13. The current and voltage waveforms in this case are showed in Figure 4-14. Observation confirmed that the whole process of droplet growing, neck shrinking and droplet detaching from the wire tip is quite stable. The frequency of transfer is approximately 400~600 drop/sec with uniform droplet size and desirable weld beads produced with no spatters.

All experimental results thus have demonstrated that the droplet transfer mode varies with the parameters. This is caused by the changed forces acting on the droplet and the change in the bypass current under the same total current is responsible for the force changes. Such results agree with the theoretical analysis in previous section.

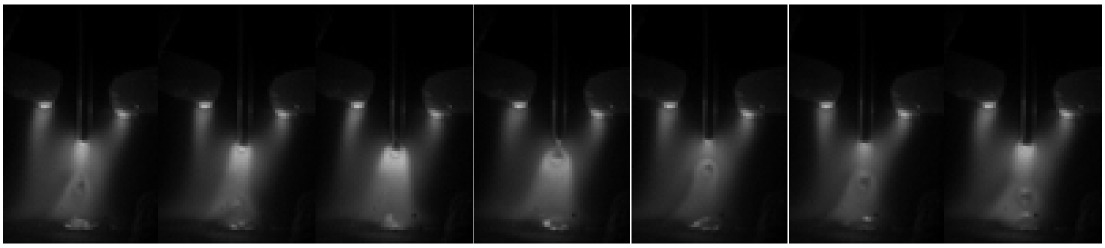

Figure 4-13, Metal transfer with dual 60A bypass current in experiment 5. The interval between each frame is 0.5ms.

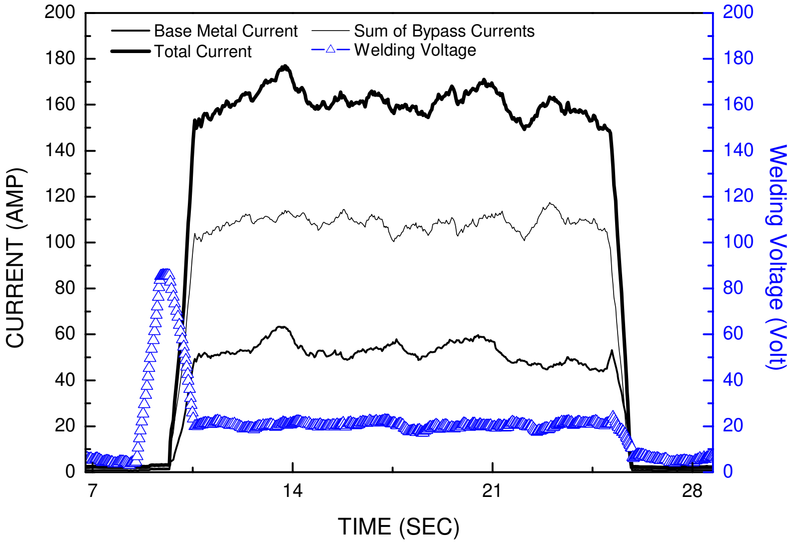

Figure 4-14, Currents and voltage in experiment 5. Bypass currents equal to 60A separately.

### 4.4 Conclusion

1. DB-GMAW decouples the total welding current into bypass currents and base metal current and then controls them separately. This mechanism provides an advantage to reduce the base metal heat input without compromising the wire melting speed and efficiency. As a result, the Heat Affected Zone (HAZ) and distortion can be reduced in certain application without affecting the productivity.
2. The bypass arcs significantly affect the forces acting on the droplet which determine the droplet transfer mode:
   - The electromagnetic forces generated by the bypass arcs enhance the shrinking of the droplet neck and enlarge anode area on the bottom of

the droplet. The net effect of the neck shrinkage and anode enlargement is to increase the detaching forces.

- The bypass arcs increase the aerodynamic drag force by changing the arc size and plasma flow speed to accelerate the droplet detachment from the wire tip.

The combination of these effects is that the critical current needed to generate the desirable spray transfer is reduced.

A series of experiments have been performed to confirm that DB-GMAW indeed has the ability to achieve spray transfer at a lower current than that in conventional GMAW. In addition, it has also been experimentally demonstrated that the metal transfer in DB-GMAW possesses four different modes: short circuiting, globular, meso-spray, and spray transfer. When the total current is given, the transfer mode is determined by the bypass currents or the distribution of the current in three directions: left bypass, base mental and right bypass.

# CHAPTER 5

## Heat input and penetration analysis of DB-GMAW

### 5.1 Thermal process of welding

During welding, the whole process of pyrogenation, meltdown, solidification and cooling off of the base metal is called thermal process of welding [16]. The thermal process exits and takes effects all through the welding process and becomes a dominant factor that influences welding quality and productivity due to following reasons:

(1). Amount and distribution of base metal heat input determines welding pool shape and geometry.

(2). Coefficients of thermal process influences the process of solidification which also involves with the micro-structure of base metal.

(3). Asymmetrical heat input results asymmetrical stress status which brings different stress deformation.

(4). Different thermal process may result crack or fracture of the base metal.

(5). Heat input determines the melt rate of filler metal which influences welding productivity. [16]

The heat source of our experiment is welding arc: the most common heat source in welding. There are other heat source such as plasma arc, laser and friction heat. Each heat source has particular characteristics such as max power density or minimum heating area.

As we mentioned before, during the past decade, some innovative methods such as Twins, Tandem and Laser-MIG hybrid welding have been successfully applied into manufacturing applications and have been making good progress in increasing productivity to meet the higher requirements from the industry [28-31].

The motivation of so many different technologies is that, as one of widely used aluminum welding methods, GMAW process needs improvements in order to achieve higher weld quality and higher productivity. Since the characteristic of metal transfer in GMAW significantly affects the weld quality especially with respect to its microstructure, porosity formation, strength, and fatigue properties etc, researchers have made great efforts to study the metal transfer in GMAW [32-35].

Also, although based on different solutions, all these methods have one common disadvantage to be improved which is the increment of Base Metal Current. Exorbitant Base metal heat input always leads to the weakness of mechanical property [36] (i.e. toughness) and the burn through of base metal. DB-GMAW has the ability to overcome this disadvantage. Chapter 4 has explained how DB-GMAW benefits the metal transfer. In this chapter, thermal advantages of DB-GMAW will be discussed.

### 5.1.1 Theoretical analysis of heat input

The first concept to get familiar is thermal efficiency of arc welding process. During the welding process, the power of arc is calculated by:

$$Q = UI \qquad \text{Eq.5-1}$$

Where $U$ is the arc voltage and $I$ is welding current,

Since part of the heat is lost in surrounding media, base metal receives less heat than the source provides. The effective power of arc is calculated by:

$$q = \eta q_0 \qquad \text{Eq.5-2}$$

Where $q$ is the effective power of arc and $\eta$ is welding thermal efficiency coefficient.

We can divide $q$ into two parts following the relationship of $q = q_1 + q_2$, where $q_1$ is the heat for melting metal in unit time and $q_2$ is the heat transferred into surrounded metal and environment by the overheated melt metal. By doing that, the effective usage coefficient $\eta_m$ is defined by:

$$\eta_m = \frac{q_1}{q_1 + q_2} \qquad \text{Eq.5-3}$$

In conventional GMAW process with base metal material as aluminum, $\eta_m$ is usually from 0.70-0.85.

### 5.1.2 Thermal distribution of base metal

The heat source transfers the heat to base metal via a certain heating area which mostly depends on welding method. For arc welding, the area is called heating spot. If we assume the radius of the heating spot is $r_H$, the definition of $r_H$ is that during the heat transfer process, 95% of the heat is distributed within the spot with $r_H$ as radius. The heat transferred to the base metal via heating spot in unit time is usually called heating density which can be approximately described by Gaussian distribution as demonstrated in Figure 5-1.

The heat density at point $A$ can be expressed as:

$$q_{(r)} = q_m e^{(-Kr^2)} \qquad \text{Eq.5-4}$$

$q_{(r)}$ - The heat density at $A$ ($W/m^2$);

$q_m$ - Max heat density at the center of heating spot;

$K$ - Coefficient of heat efficiency;

$r$ - The distance between $A$ and the center of heating spot;

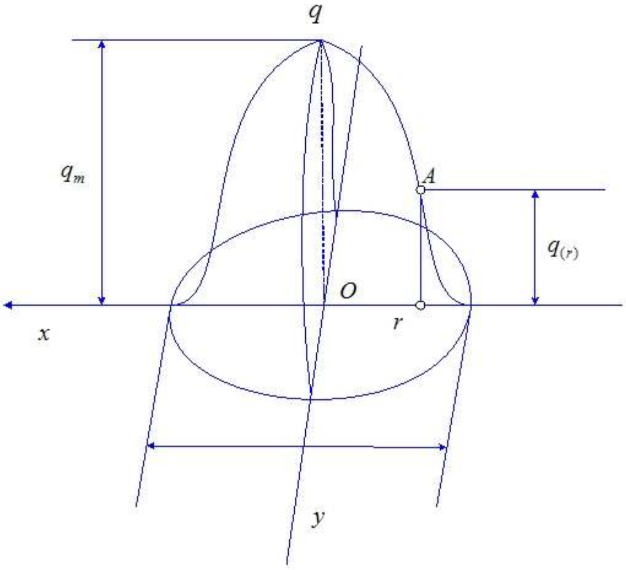

Figure 5-1, Distribution of heat density

The total heat power under this Gaussian distribution can be expressed as:

$$q = \int_0^{\infty} q_{(r)} 2\pi r dr = \frac{\pi}{K} q_m \qquad \text{Eq.5-5}$$

As a result:

$$q_m = \frac{K}{\pi} q = \frac{K}{\pi} \eta UI \qquad \text{Eq.5-6}$$

According to the definition of $r_H$ and Eq.5-4, we know that:

$$95\%q = \int_0^{r_h} \frac{Kq}{\pi} \exp(-Kr^2) 2\pi r dr = q[1 - \exp(-Kr^2)]$$

$$\text{Thus } 0.05 = \exp(-Kr^2) \qquad [16]$$

$$\text{Where } K = \frac{3}{r_H{}^2}$$

Generally speaking, arc heat includes anode heat, cathode heat and arc column heat. According to previous research [37], arc column heat will radiate itself rapidly which means it does not actually affect base metal heat input. When calculating conventional GMAW base metal heat input, we ignore arc column heat and the base metal heat input will approximately equal to:

$$Q = \frac{\eta * I}{u} * (U_{anode} + U_{cathode}) \qquad \text{Eq.5-7}$$

Where $Q$ is the base metal heat input, $\eta$ is thermo-efficiency coefficient, $I$ is total welding current, $u$ is welding travel speed and $U$ is welding voltage. $U$ equals $U_{anode}$ plus $U_{cathode}$ which are anode voltage drop and cathode voltage drop respectively. In GMAW case, the current flow through anode equals the current flow through cathode.

In DB-GMAW process, base metal heat input is divided into three parts, one anode heat input and two cathode heat input:

$$Q_{heatinput} = \frac{\eta}{u} * (I_{total} * U_{anode} + I_{basemetal} * U_{cathode}) \qquad \text{Eq.5-8}$$

In our particular process, we know that:

$$I_{basemetal} = I_{total} - I_{leftbypass} - I_{rightbypass} \qquad \text{Eq.5-9}$$

During present experiments, $I_{leftbypass}$ and $I_{rightbypass}$ are usually kept equaling to each other for the sake of process stability. We use $I_{bypass}$ instead of $I_{leftbypass}$ and $I_{rightbypass}$. So we have:

$$Q_{DB-GMAWheatinput} = \frac{\eta}{u} * I_{total} * (U_{anode} + U_{cathode}) - \frac{\eta}{u} * 2 * I_{bypass} * U_{cathode} \qquad \text{Eq.5-10}$$

For a stable DB-GMAW process, we consider $\eta, u, I_{total}, U_{cathode}, U_{anode}$ as constants. If we compare Eq.5-10 and Eq.5-7, we can notice that Eq.5-10 is actually formed by Eq.5-7 added by a negative part. Eq.5-10 theoretically supports the consumption that DB-GMAW has lower base metal heat input than conventional GMAW.

### 5.1.3 Welding thermal field

To understand the welding thermal field, we need to be familiar with several rules.

(1) Fourier heat transfer equation:

Fourier heat transfer equation is one of the most basic equations to describe the heat transfer in an objective:

$$q_c = -\lambda \frac{\partial T}{\partial n} \qquad \text{Eq.5-11}$$

$\lambda$ - Thermal conductivity coefficient ($W / m \bullet K$)

$\frac{\partial T}{\partial n}$ - Gradient of temperature

Eq.5-11 shows us that the heat density of a certain point in an object is directly proportional to the temperature gradient which perpendicular to this point.

(2) Convective heat transfer equation:

Convective heat transfer is a mechanism of heat transfer occurring because of bulk motion (observable movement) of fluids. This can be contrasted with conductive heat transfer, which is the transfer of energy by vibrations at a molecular level through a solid or fluid, and radiative heat transfer, the transfer of energy through electromagnetic waves. The basic equation to describe this is Newton's law of cooling:

$$q_r = \alpha_k \Delta T \qquad \text{Eq.5-12}$$

$\Delta T$ - Temperature difference between the fluid and solid ($K$)

$\alpha_k$ - Convective heat transfer coefficient ($W/m^2 \bullet K$)

(3) Radiative heat transfer equation:

In radiative heat transfer, heat is transferred between bodies by electromagnetic radiation. In natural radiative heat transfer (that which happens when the electromagnetic radiation is generated naturally by heat), the spectrum of this radiation is that of a black body, and its power depends on the fourth power of the absolute temperature of the body.

According to Stefan-Boltzmann law, the heat density of radiation from a heated object is proportional to the quad square of its surface temperature:

$$q_r = \varepsilon C_0 T^4 \qquad \text{Eq.5-13}$$

$\varepsilon$ - Black-body degree coefficient

$T$ - Surface temperature ($K$)

$C_0$ - Black-body radiation rate: 5.67 ($W/m^2 \bullet K^4$)

As a matter of fact, there is no absolute black-body which means a no real object could absorb all radiation energy reaches it ($\varepsilon = 1$). So for a grey-body, $0 < \varepsilon < 1$.

In welding, we can assume the temperature of the work piece is $T$ and the surrounding environment is $T_f$, the heat transfer from work piece to surrounding environment via radiation can be calculated by: [16]

$$q_r = \varepsilon C_0 (T^4 - T_f^4) \qquad \text{Eq.5-14}$$

We can assume $\alpha_r$ as radiative heat transfer coefficient:

$$\alpha_r = \varepsilon C_0 (\frac{T^4 - T_f^4}{T - T_f}) \qquad \text{Eq.5-15}$$

Then we can describe $q_r$ by the temperature difference directly,

$$q_r = \alpha_r (T - T_f) \qquad \text{Eq.5-15}$$

### 5.1.4 Mathematical description of welding heat transfer

The mathematical description of welding heat transfer is based on finite element analysis. To use Fourier heat equation and conservation of energy, we can develop a differential equation of general heat transfer for a three-dimensional situation:

$$\rho C_p \frac{\partial T}{\partial t} = \frac{\partial}{\partial x}(\lambda \frac{\partial T}{\partial x}) + \frac{\partial}{\partial y}(\lambda \frac{\partial T}{\partial y}) + \frac{\partial}{\partial z}(\lambda \frac{\partial T}{\partial z}) \qquad \text{Eq.5-16}$$

$\rho$ - Density ($kg / m^3$)

$C_p$ - Heat capacity at constant pressure ($J / kg \bullet K$)

$T$ - Temperature ($K$)

$t$ - Time ($s$)

$\lambda$ - Heat conductive rate ($W / m \bullet K$)

$x, y, z$ - coordinate ($m$)

For accurate calculation, there are many parameters needing to be considered such as the moving speed of the heat source, initial condition and boundary condition.

In actual welding process, the complexity of the problem makes the equation and boundary condition extremely complicated. Numerical analysis is applied to simulate the actual situation. However, numerical analysis leads to different results basing on different initial condition and boundary condition. Since there is no way to exactly measure initial condition and boundary condition, numerical analysis usually requires experimental verification correctness inspection. Due to this reason, in our research, we use indirect measurement to exam our assumption.

### 5.1.5 Theoretical analysis of penetration

The electromagnetic force $F_{em}$ acting on welding pool is a crucial parameter influencing penetration which is given by [27].

$$F_{em} = \frac{\mu_0 I^2}{4\pi} \log(\frac{r_{bottom}}{r_{top}}) \qquad \text{Eq.5-17}$$

Where $\mu_0$ is the magnetic permittivity, $I$ is the welding current, $r_{bottom}$ is the radius of arc where it contacts with base metal and $r_{top}$ is the radius of arc where it contacts with welding electrode. Eq.5-17 indicates that electromagnetic force acting on the welding pool is proportional to the square of welding current.

For conventional GMAW, electromagnetic force $F_{em-GMAW}$ :

$$F_{em-GMAW} = \frac{\mu_0 I_{total}^2}{4\pi} \log(\frac{r_{bottom}}{r_{top}}) \qquad \text{Eq.5-18}$$

In DB-GMAW, electromagnetic force $F_{em-DBGMAW}$ becomes:

$$F_{em-DBGMAW} = \frac{\mu_0 I_{basemetal}^2}{4\pi} \log(\frac{r_{bottom}}{r_{top}}) \qquad \text{Eq.5-19}$$

We know that $I_{basemetal}$ is obviously smaller than $I_{total}$ which indicates that $F_{em-DBGMAW}$ is obviously smaller than $F_{em-GMAW}$ . Hence, penetration of DB-GMAW should be smaller than penetration of GMAW.

This is our initial theoretical analysis about the influences of DB-GMAW on penetration. More comprehensive analysis about the influences from DB-GMAW on weld penetration will be discussed in later chapter.

## 5.2 Experimental procedure and results

### 5.2.1 Experimental procedure

As we mentioned previously, the whole system is designed to weld aluminum 6061T tube work piece with GMAW and DB-GMAW process while collecting welding current, welding voltage and base metal temperature. All information collected by appropriate sensors is recorded by data acquisition board. The welding platform is constructed by two GTAW torches and one GMAW torch connecting to their own power sources which are two TIG welders and one MIG welder. The computer outputs control signal which keeps base metal and bypass current at desired level while collects data from current sensors and thermocouples.

We use fast-response K-type thermocouples (120ms for 0-63% of full scale) as sensors to monitor the work piece temperature during experiments. Thermocouples are attached compactly to the work piece inner surface. Figure 5-2 shows geographic placement of thermocouples, torches and work piece. Signals are amplified by thermocouple transmitters to data acquisition board. The whole experiment is one rotation of the work piece which takes approximate 15 seconds. After DB-GMAW process achieves stability, the thermocouples go through Arc column meanwhile the highest temperature of process can be recorded.

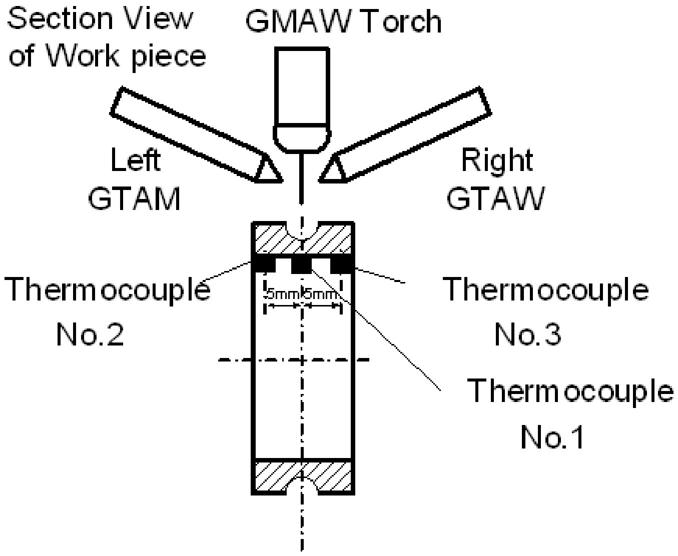

Figure 5-2, Thermocouples on the inner surface

As the reflection of base metal heat input, the highest temperature captured by thermocouples is proportional to base metal heat input. The comparison of highest temperature between traditional GMAW process and DB-GMAW process indicates which process has greater base metal heat input.

In all DB-GMAW experiments, left bypass current is set to equal to right bypass current all the time. So we will use the value of one bypass current to represent both of them. Please keep in mind that if the expression is bypass 30A experiment, it represents that both left bypass and right bypass current equals to 30A which makes the total bypass current 60A. The preset parameters here follow Table 3-2 and Table 3-3.

### 5.2.2 Temperature comparison

After series of experiments, we collected highest temperature information from different experiments and they are indicated in Figure 5-3. The weld bead and penetration of these experiments are indicated in Figure 5-4-1 though Figure 5-4-6. Theoretical analysis illustrates us that the GMAW have greater base metal heat input while DB-GMAW has relative smaller heat input since part of the melting current flows into bypass torch instead of into base metal. In Figure 5-2, GMAW has a higher base metal temperature than any other DB-GMAW process which agrees with theoretical analysis. Another interesting fact is that the highest temperature of bypass 40-45A is lower than other bypass experiments which indicates that bypass 40-45A experiment has lowest base metal heat input among all bypass experiments. Before bypass 40-45A, the base metal heat input decreases itself along with the increment of bypass current. After bypass 40-45A, the base metal heat input stopped decreasing and begin to claim up.

Verification on aluminum ring experiment is oriented to weld the work piece in good quality and minimize the base metal heat input at the same time. We choose bypass current 50A due to its stability. Different types of experiments are designed in this section because we also want to test the influences of different shielding gas.

In Figure 5-3, all highest temperature data is presented in the same chart for the convenience of comparison. To ensure the accuracy of this comparison, other parameters which can affect base metal heat input are kept constant between different experiments. Before every experiment, enough cooling down time is counted in the preparation to make sure that the initial temperature of work piece equals to room temperature.

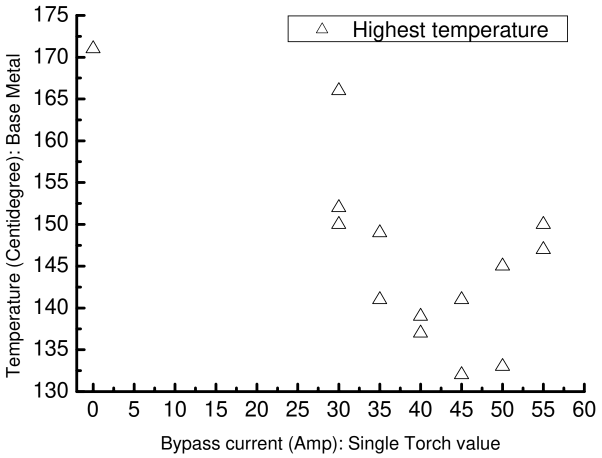

Figure 5-3, Highest temperature distribution via different bypass currents

We compared highest temperature curves of all 4 types of experiment included by Table 3-3 in Figure 5-4. From Figure 5-4, we can tell that GMAW has higher temperature curve than DB-GMAW process. Moreover, under same welding parameters and conditions, 85% Helium + 15% Argon shielded experiments temperature curves are lower than 100% Argon shielded experiments.

According to Figure 5-3, DB-GMAW always has a smaller base metal heat input compared to traditional GMAW method as we predicted. However, the theoretical analysis about base metal heat input suggests us that the base metal heat input should decrease along with the decrement of base metal current while fixing total welding current. In Figure 5-3, the highest temperature data stop decreasing but to increase after bypass current surpassed 40-45A. This experimental fact does not agree with our initial theoretical analysis. In our previous theoretical analysis, a lower base metal current results a lower base metal heat input. And a lower base metal heat input results a lower highest temperature value. So the highest temperature value of a bypass 50A experiment should be smaller than the value of a bypass 45A experiment. Thus, the highest temperature value should be descending along with the increment of bypass current.

As the experiments continue, we found the reason of this problem. The explanation for this phenomenon will be revealed later in this chapter.

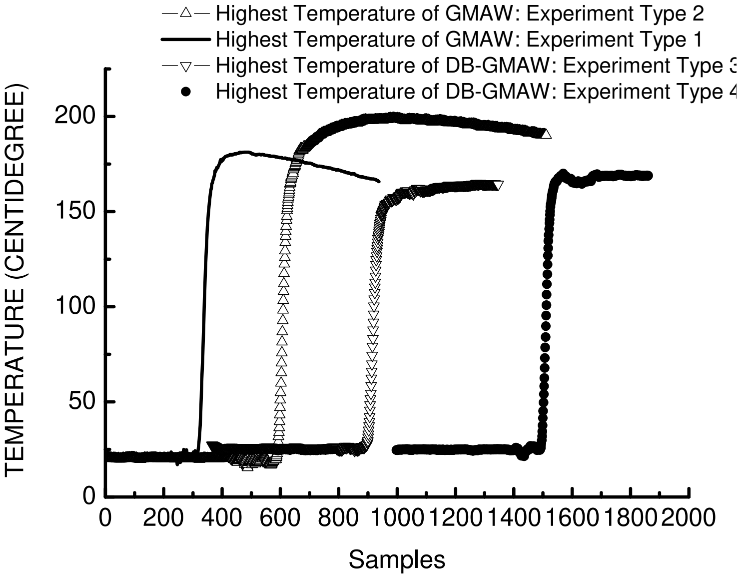

Figure 5-4, Highest temperature comparison on aluminum rings

### 5.2.3 Penetration comparison

Figure 5-5 shows the cross section view of DB-GMAW and GMAW process on aluminum ring work piece.

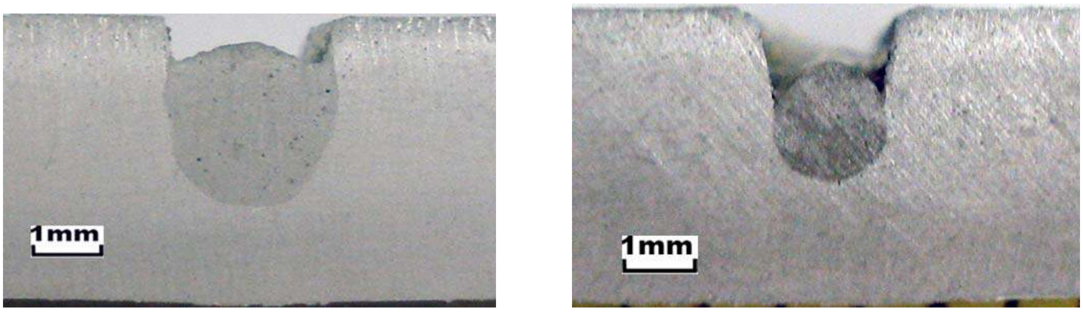

Figure 5-5, Welding cross section of GMAW (left) and DB-GMAW (Right)

Figure 5-5 indicates that GMAW has deeper penetration compared with DB-GMAW process due to its higher arc forces acted on the welding pool and bigger base metal current.

Figure 5-6-1 to Figure 5-6-6 show the weld beads and cross section views of all DB-GMAW process with different bypass current values.

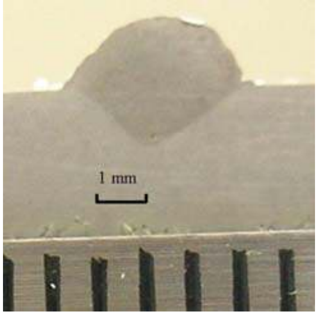

Figure 5-6-1, Weld bead and cross section view of GMAW

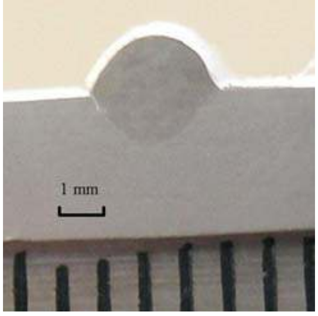

Figure 5-6-2, Weld bead and cross section view of DB-GMAW (Bypass current L&R : 30A-30A)

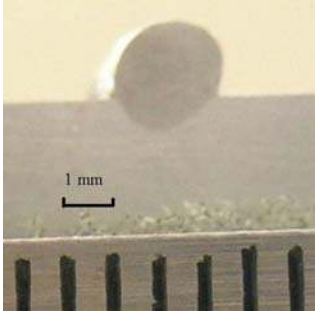

Figure 5-6-3, Weld bead and cross section view of DB-GMAW (Bypass current L&R : 40A-40A)

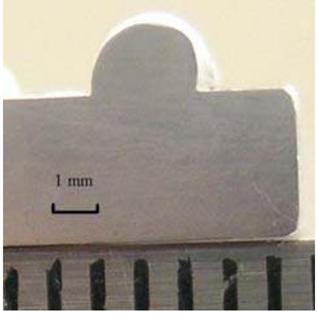

Figure 5-6-4, Weld bead and cross section view of DB-GMAW (Bypass current L&R : 45A-45A)

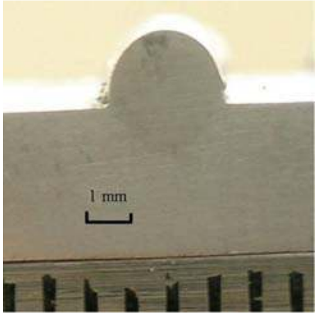

Figure 5-6-5, Weld bead and cross section view of DB-GMAW (Bypass current L&R : 50A-50A)

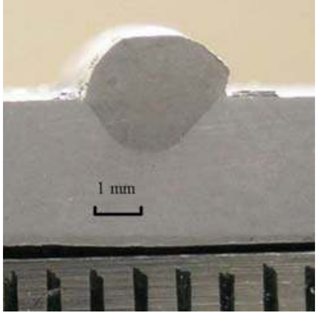

Figure 5-6-6, Weld bead and cross section view of DB-GMAW (Bypass current L&R : 55A-55A)

Theoretical analysis indicates that GMAW has bigger penetration than DB-GMAW because of the difference between electromagnetic force acting on the welding pool. By looking through Figure 5-6-1 to 5-6-6, we can tell that GMAW does have a bigger penetration comparing to all DB-GMAW. Moreover, among all DB-GMAW experimental penetrations, bypass 40-45A experiment has a smaller penetration than any other bypass experiments. This fact agrees with the highest temperature distribution and explains why bypass 40-45A experiment has lower highest temperature than other bypass experiments. Before bypass 40-45A, the penetration decreases along with the increment of bypass current. After bypass 40-45A, the penetration begins to get greater.

The observation of penetration of DB-GMAW basically agrees with temperature observation of Figure 5-3. Since we are using K-type thermocouple as temperature sensors, with similar base metal heat input, the penetration of base metal inevitably affect the temperature reading of thermocouples because the alternation of penetration varies the distance from the thermocouple to the heating source.

### 5.3 Full penetration achievement on aluminum tube 6061T of DB-GMAW

The preset parameters of full penetration experiments are showed in Table-2. Figure 5-7 shows the weld beads of experiments 1-6 in Table-2 by indicating the front, back and cross section views of each bead. Figure 5-8 compares the penetration of experiments 1-6 in Table-2. When the bypass current increases from 65A to 90A, the full penetration level which can be represented by the back bead height first decreases itself from bypass 65A to bypass 70A then increases itself from bypass 70A to bypass 75A. From bypass 75A to bypass 80A, the penetration level doesn't appear significant difference. From bypass 80A to bypass 90A, the penetration level decreases again along with the increment of bypass current. This explains the highest temperature curve showed in Figure 5-3. We also performed a conventional GMAW on the work piece with the parameters in Table-2 which means the base metal current is 250A. Experimental data indicates that a conventional GMAW under such preset parameters leads to definite burn through of the base metal which is showed in Figure 5-9. Therefore, when the total welding current is same, DB-GMAW could always provide a smaller penetration than GMAW due to its smaller electromagnetic force acting on the welding pool.

Table 5-1，Parameters on aluminum cylinder: full penetration comparison

| | |
|---|---|
| Ex.1-DB-GMAW, Bypass current (L & R) | 65A |
| Ex.2-DB-GMAW, Bypass current (L & R) | 70A |
| Ex.3-DB-GMAW, Bypass current (L & R) | 75A |
| Ex.4-DB-GMAW, Bypass current (L & R) | 80A |
| Ex.5-DB-GMAW, Bypass current (L & R) | 85A |
| Ex.6-DB-GMAW, Bypass current (L & R) | 90A |
| Constant parameters | |

Table 5-1, cont.

| | |
|---|---|
| Wire type | 1.2 mm ER 4047 |
| Base material | Al6061 T6 thickness: 3.2mm |
| Shielding Gas (MIG torch) | Argon |
| Shielding Gas (bypass torch) | Argon |
| Gas flow | 12 L/min |
| Welding speed | 112.5 cm/min |
| Wire feeding speed | 11.5m/min |
| Preset welding voltage | 21.5 V |
| Total welding current | 250A |

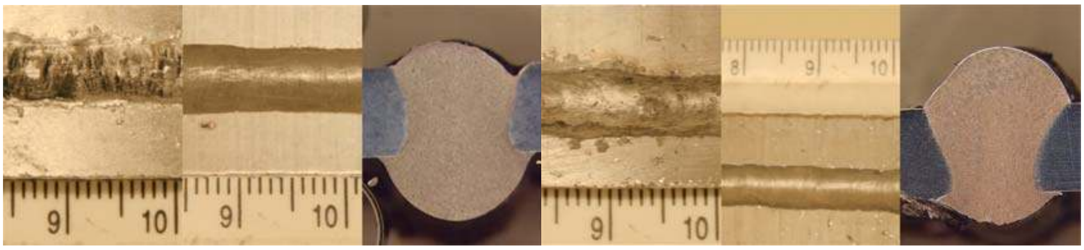

Ex.1 Ex.2

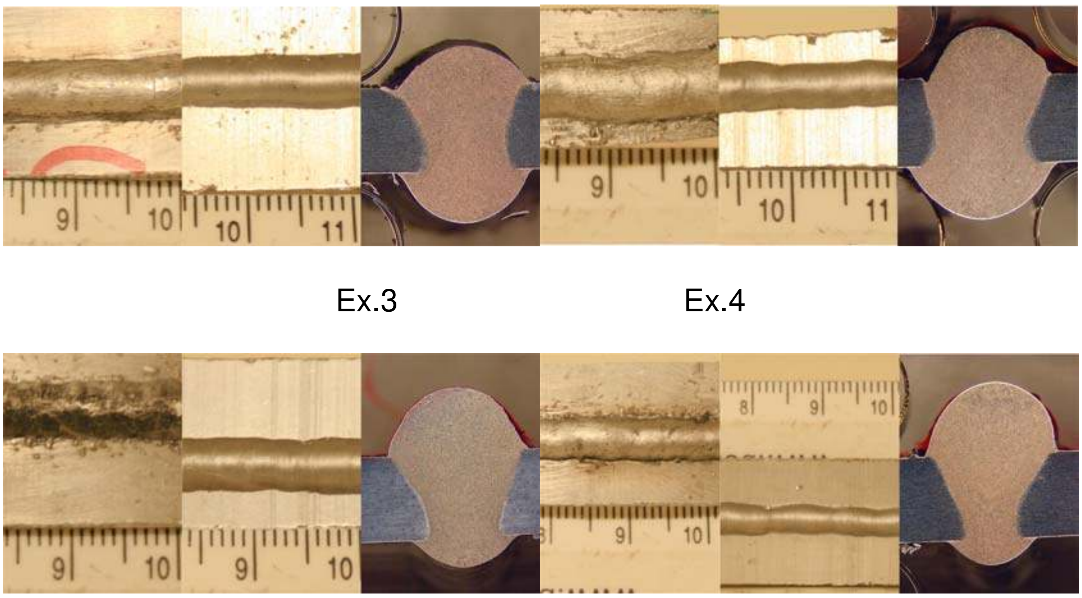

Ex.3 Ex.4

Ex.5 Ex.6

Figure 5-7, Weld beads of experiments 1-6 in Table-2 (front, back and cross section view)

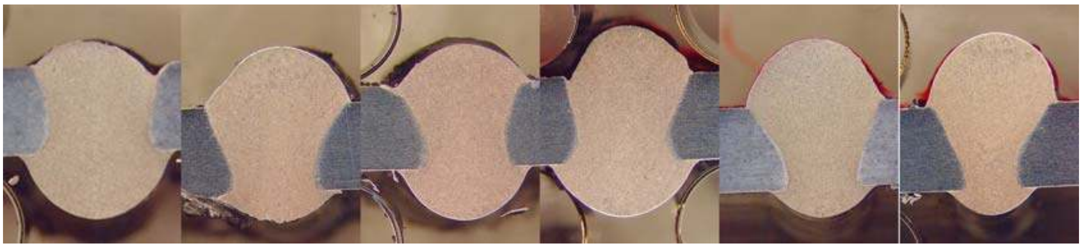

Ex.1 Ex.2 Ex.3 Ex.4 Ex.5 Ex.6

Figure 5-8, Full penetration comparison of experiments 1-6 in Table-2

Figure 5-9, Weld bead of conventional GMAW under 250A welding current

### 5.4 Theoretical explanation of DB-GMAW penetration

There are two important parameters influencing the penetration: electromagnetic force acting on the welding pool [38-41] and the impulse force $F_{droplet}$ from the droplet to the welding pool [20, 42]. If we suppose the impulse force from the droplet to the welding pool is a constant, we can achieve a conclusion that the base metal heat input should decrease along with the increment of bypass current, which means bypass 40A experiment should have bigger penetration than bypass 50A and 55A experiments. The fact that bypass 50A and 55A experiments have bigger penetration indicates that $F_{droplet}$ is not a constant. The bypass arc will act a force $F_{bypass}$ on the droplet which accelerates the droplet to detach the wire tip and land on the base metal. If $F_{bypass}$ on the droplet gets bigger, the droplet detaches the wire tip easier and land faster on the base metal which also means the impulse force from the droplet to the base metal is bigger. Also, bigger impulse force results deeper penetration which is reflected by a higher base metal temperature captured by the thermocouple.

We use high speed camera to verify our analysis by recording the metal transfer of DB-GMAW. The frame rate of the high speed camera was set as 4000 frame per second which means the interval between two frames is 0.25ms. The high speed camera data indicates that it takes approximately 10-11 frames for a droplet to transfer from the wire tip to land on the base metal in bypass 55A experiment. However, it takes approximately 24-26 frames to complete the same process in bypass 30A experiment. Moreover, the arc length of bypass 55A experiment is also longer than bypass 30A experiment which means that droplet travels longer in bypass 55A before landing on the base metal. To conclude, droplet in bypass 55A experiment travels longer distance in a shorter period than bypass 30A experiment. Hence, droplet in bypass 55A experiment brings bigger impulse force to the welding pool which deepens the penetration. The rising impulse force acting on the welding pool overcomes some influences of decreasing electromagnetic force and makes the penetration grow again after a certain limit which seems to be between 40-45A bypass current.

### 5.5 Chapter Conclusion

Basing on the previous analysis and data, the conclusion of this chapter can be given as follow:

1. DB-GMAW has the ability to provide a lower base metal heat input than conventional GMAW. The theoretical analysis supports this prediction and it is also verified by experiments.
2. DB-GMAW has a smaller penetration than conventional GMAW when the total welding current of the two processes is set to same value. The theoretical analysis supports this prediction and it is also verified by experiments.
3. The penetration of DB-GMAW does not decrease proportional to the increment of bypass current value when the total welding current is fixed. The penetration of DB-GMAW bead is a combined influenced by the electromagnetic force from the main arc and bypass arc.

# CHAPTER 6

# Image Processing of DB-GMAW

In all previous chapters, we have discussed and demonstrated how DB-GMAW could benefit and improve traditional GMAW aluminum welding by giving theoretical analysis and experimental verification of the physical properties such as metal transfer and base metal heat input. In this chapter, image processing algorithm of DB-GMAW is developed aiming to establish an effective way of monitoring the welding pool profile of full penetration.

Usually, we can use a laser back-lighting system to collect information of droplet and welding pool profile [20], or we can use high speed camera to record the welding process and collect the information through appropriate image processing technique. Due to the high expense of optical equipment in laser back-lighting system and its confinement in industrial circumstance, we would like to use high speed camera and image processing technique in DB-GMAW process.

Initially, there are three approaches to obtain DB-GMAW welding pool profile:

1. Monitoring the front-side profile of the welding pool.
2. Monitoring the metal transfer of the process.
3. Monitoring the back-side profile of the welding pool.

To bring out the optimum solution, all these three approaches are attempted. Both their advantages and disadvantages are compared to conclude the best solution for our system.

## 6.1 Image processing of the front-side profile of the welding pool

Considering the strong arc light and reflection from the base metal, there is always significant noise in high speed video of aluminum GMAW process. A pre-processing which usually includes grey-scale transformation, filtering, image enhancement, interest region cutting and binarization is necessary for further processing.

Figure 6-1, Original picture of front-side welding pool from DB-GMAW

There are many filters such as averaging filter, mean filter, linear filter, high-pass or low-pass filters that can be useful to filter the noise in the image. Since the high reflection rate of aluminum, image from aluminum GMAW process usually doesn't have significant boundaries and blur details. Finally, wiener filter is employed in our procedure.

The basic idea of wiener filter is trying to find the minimum square error between original and estimations. In frequency domain, wiener filter can be presented by Eq.6-1:

$$F(u,v) = \left[ \frac{1}{H(u,v)} \bullet \frac{|H(u,v)|^2}{|H(u,v)|^2 + 1/\lambda \left[ S_n(u,v)/S_f(u,v) \right]} \right] G(u,v) \qquad \text{Eq.6-1}$$

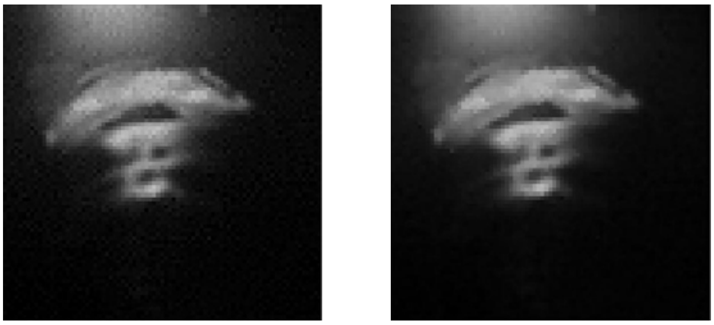

a) interest region b) after wiener filter

Figure 6-2, Result of wiener filter on our interest region

The next step is to give image enhancement for a better result of edge detection. Histogram algorithm is a common method in image enhancement usually with good results.

If we use $f(x,y)$ and $g(x,y)$ to represent the grey level value before and after image enhancement at pixel (x, y), histogram algorithm can be expressed as:

$$G[f(x,y)] = |f(x,y) - f(x+1,y)| + |f(x,y) - f(x,y+1)|$$

$$g(x,y) = \begin{cases} G[f(x,y)] & G[f(x,y)] \geq T \\ f(x,y) & \text{else} \end{cases} \qquad \text{Eq.6-2}$$

In Eq.6-2, $T$ is non-negative threshold value. The grey level value of any pixel which is larger than $T$ would be forced equaling to $T$ after Image enhancement.

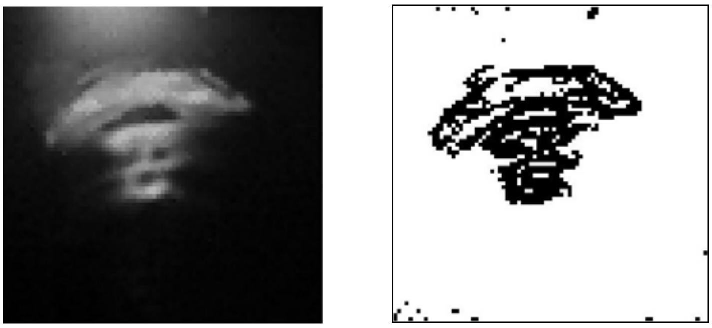

a) After wiener filter b) After image enhancement

Figure 6-3, Result after histogram image enhancement

After filtering and image enhancement, the interest region image is ready for edge detection and welding pool profile information extraction. Traditional edge detection is basing on the calculation of the gradient of every pixel since the edge is usually companied with significant grey-scale change. Eq.6-3 is commonly used in edge detection of digital image:

$$G[F(j,k)] = [(\frac{\partial F}{\partial j})^2 + (\frac{\partial F}{\partial k})^2]^{\frac{1}{2}} \qquad \text{Eq.6-3}$$

Where $F(j,k)$ is the function of image grey level

In Matlab, such job is completed by convolution between image grey level function and different operators. Operator such as Roberts, Sobel, Prewitt, Log, Canny and Zero-crossing are very common in edge detection. Their results on our process image are compared in this chapter.

**Roberts Operator [45]:**

For digital image, Eq.6-3 can be expressed as:

$$G[F(j,k)] = \{[F(j,k) - F(j-1,k)]^2 + [F(j,k) - F(j,k-1)]^2\}^{\frac{1}{2}} \qquad \text{Eq.6-4}$$

Eq.6-4 can be simplified into:

$$G[F(j,k)] = |F(j,k) - F(j-1,k)| + |F(j,k) - F(j,k-1)| \qquad \text{Eq.6-5}$$

Considering the fact that:

$$\Delta_x F(j,k) = F(j,k) - F(j-1,k)$$
$$\Delta_y F(j,k) = F(j,k) - F(j,k-1)$$

Roberts operator algorithm can be express as:

$$G[j,k] = |F(j,k) - F(j+1,k+1)| + |F(j+1,k) - F(j,k+1)| \qquad \text{Eq.6-6}$$

To match Eq.6-6, Roberts Operator is often in following forms:

| | |
|---|---|
| 1 | 0 |
| 0 | −1 |

| | |
|---|---|
| 0 | 1 |
| −1 | 0 |

Figure 6-4, Roberts Operator

**Prewitt and Sobel Operator [45]:**

Suppose the grey-level of the digital image satisfies following equation:

$$M_{x,y} = \alpha x + \beta y + \gamma \qquad \text{Eq.6-7}$$

Where $(\alpha, \beta)$ is the gradient

Thus, the 3 by 3 neighborhood grey matrix will be:

$$\begin{bmatrix} -\alpha-\beta+\gamma & -\alpha+\gamma & -\alpha+\beta+\gamma \\ -\beta+\gamma & \gamma & \beta+\gamma \\ \alpha-\beta+\gamma & \alpha+\gamma & \alpha+\beta+\gamma \end{bmatrix}$$

By defining horizontal and vertical operator as:

$$\begin{bmatrix} -a & -b & -a \\ 0 & 0 & 0 \\ a & b & a \end{bmatrix} \quad \begin{bmatrix} -a & 0 & a \\ -b & 0 & b \\ -a & 0 & a \end{bmatrix}$$

We can get derivative in $x$ and $y$ direction as:

$$g_x = 2\beta(2a+b)$$
$$g_y = 2\alpha(2a+b)$$

And the gradient at current pixel is:

$$G = 2(2a+b)\sqrt{\alpha^2+\beta^2}$$

Which means $2(2a+b)=1$.

A 1/6 Prewitt operator is to let a=b=1/6. A 1/8 Sobel operator is to let a=1/8 and b=1/4.

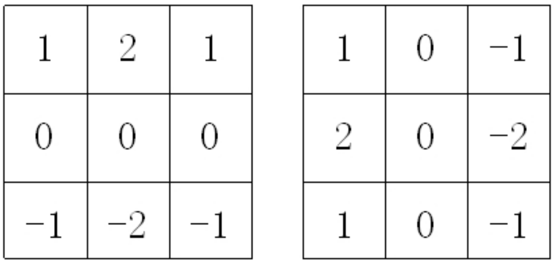

| | | |
|---|---|---|
| 1 | 2 | 1 |
| 0 | 0 | 0 |
| −1 | −2 | −1 |

| | | |
|---|---|---|
| 1 | 0 | −1 |
| 2 | 0 | −2 |
| 1 | 0 | −1 |

Figure 6-5, Sobel operator

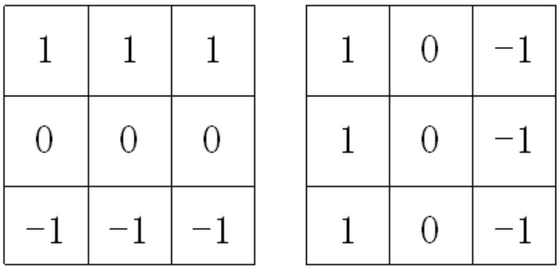

| | | |
|---|---|---|
| 1 | 1 | 1 |
| 0 | 0 | 0 |
| −1 | −1 | −1 |

| | | |
|---|---|---|
| 1 | 0 | −1 |
| 1 | 0 | −1 |
| 1 | 0 | −1 |

Figure 6-6, Prewitt operator

**Log operator [45]**:

Log operator is a combination of Gaussian smoothing filter and Laplace operator.

| | | | | |
|---|---|---|---|---|
| −2 | −4 | −4 | −4 | −2 |
| −4 | 0 | 8 | 0 | −4 |
| −4 | 8 | 24 | 8 | −4 |
| −4 | 0 | 8 | 0 | −4 |
| −2 | −4 | −4 | −4 | −2 |

Figure 6-7, Log operator

**Canny operator [45]:**

Canny operator use two threshold values to identify significant edge and insignificant edge which is very helpful in avoiding noise influences.

**Zero-crossing operator [45]:**

Zero-crossing operator searches zero-crossing point after specific filter.

a) Sobel

b) Robert

c) Log

d) Prewitt

e) Canny f) Zero-crossing

Figure 6-8, Results of different edge detector on interest region image of DB-GMAW

Basing on the results in Figure 6-8, canny operator gives the best result among all six operators by providing a continuous and smoothing front-side welding pool profile.

Figure 6-9, Composed picture of edge detection and original picture

### 6.2 Image processing of the droplet transformation in DB-GMAW

#### 6.2.1 Image processing of neck shrinking information

Droplet transformation contains much information reflecting almost every aspect of the process. By analyzing the brightness of arc, transfer frequency, droplet velocity and size, we can estimate welding parameters and welding pool profile.

**<u>Pre-processing</u>:**

The first step of pre-processing is cutting out the interest region from original picture. Since we are focusing on the metal transfer, we cut out the wire tip and droplet part from the original picture to avoid noise and accelerate calculation speed.

a) Original picture b) Interest region

Figure 6-10, Metal transfer image (0.8mm diameter wire), single bypass current 30A

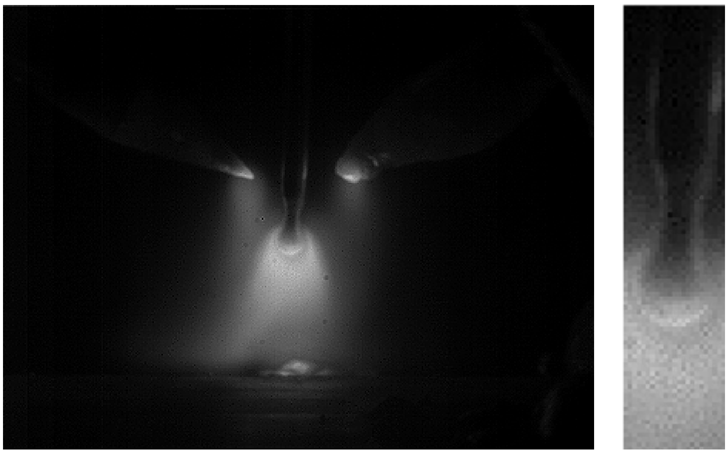

a) Original picture b) Interest region

Figure 6-11, Metal transfer image (0.8mm diameter wire), single bypass current 50A

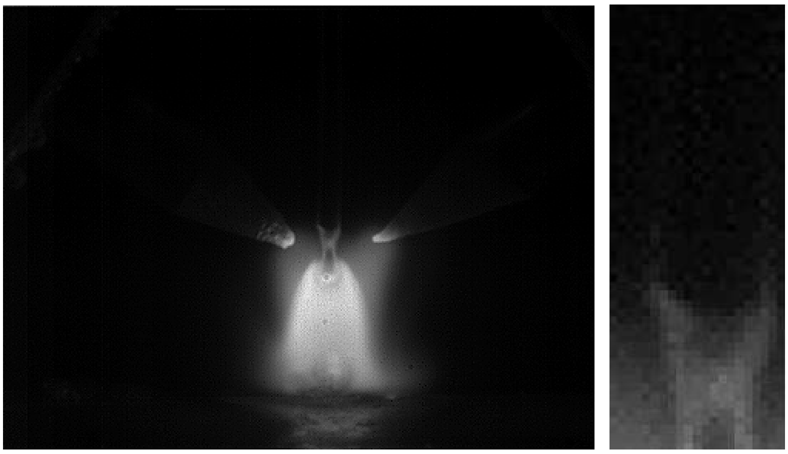

a) Original picture b) Interest region

Figure 6-12, Metal transfer image (0.8mm diameter wire), single bypass current 60A

a) Original picture b) Interest region

Figure 6-13, Metal transfer image (1.2mm diameter wire), single bypass current 60A

As we mentioned earlier, noise filtering is necessary for these pictures due to all the noise from arc, signal processing and electromagnetic environment. By applying wiener filter to all interest region images, a comparative result of before and after wiener filter is showed in Figure 6-14.

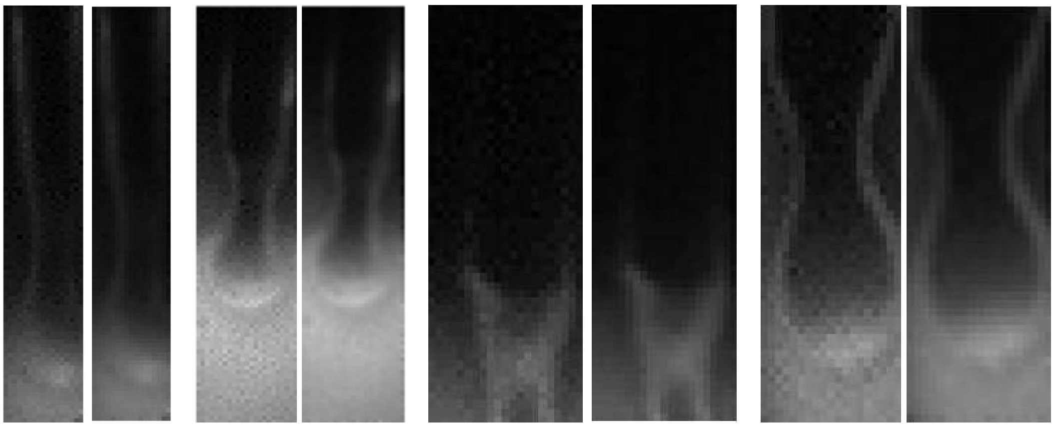

a) 0.8mm, 30A b)0.8mm, 50A c) 0.8mm, 60A d)1.2mm, 60A

Figure 6-14, Comparative results before and after wiener filter

Apparently, interest region images look much smoother and less noise after noise filtering.

Histogram algorithm is still applied for image enhancement. The result of four images in Figure 6-14 is showed in Figure 6-15.

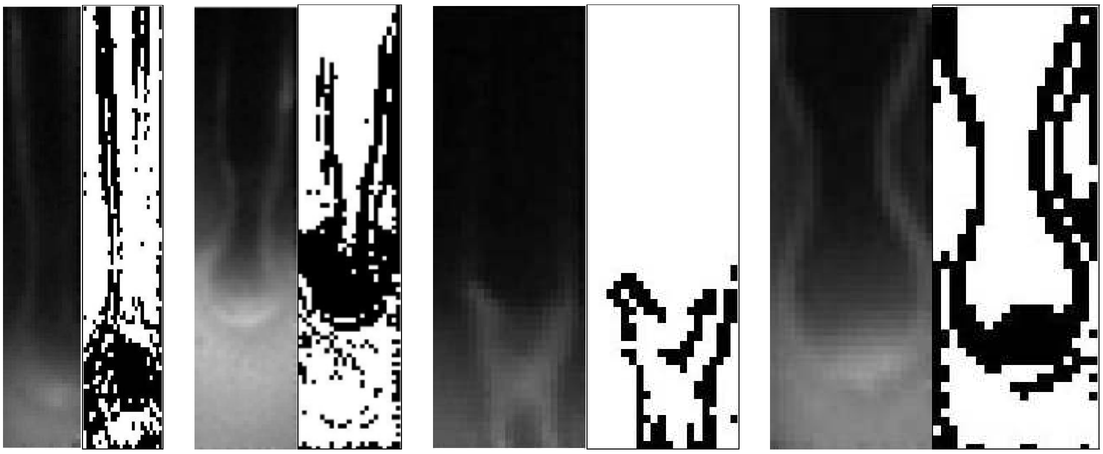

a) 0.8mm, 30A b) 0.8mm, 50A c) 0.8mm, 60A d) 1.2mm, 60A

Figure 6-15, Comparative results before and after image enhancement

There is some important information that we would like to obtain from these images:

1. Neck shrinking of droplet
2. droplet size
3. droplet trajectory

Neck shrinking is the first step to form a droplet from the wire tip and is essential for droplet transfer frequency calculation. Droplet size reveals a lot of information about metal transfer mode and welding current. Finally, droplet trajectory is a very important parameter for welding pool profile.

**Edge detection of droplet neck shrinking:**

Edge detectors introduced previously are applied for all four different images in Figure 6-15.

Roberts Operator:

Edge detection results of Roberts operator for all these four images are showed in Figure 6-16:

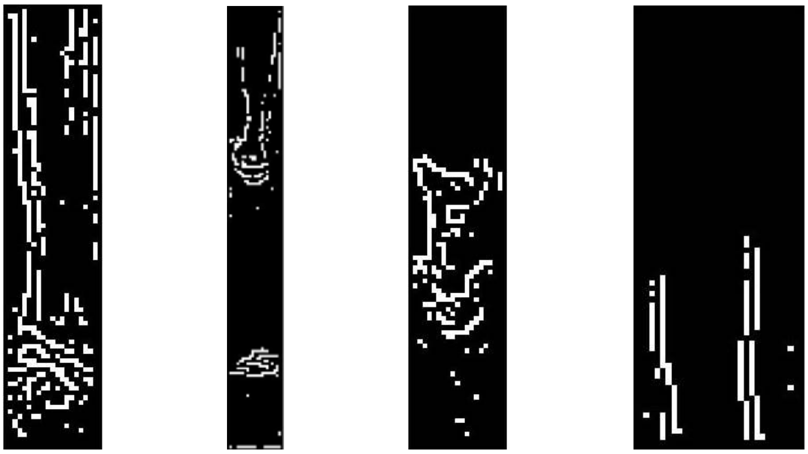

a) 0.8mm, 30A b) 0.8mm, 50A c)0.8mm, 60A d) 1.2mm, 60A

Figure 6-16, Edge detection results of Roberts operator

Basing on the results in above figure, Roberts operator doesn't have the ability to extract continuous profile of droplet neck shrinking. Therefore, it will not be used in this detection.

Canny operator:

Edge detection results of canny operator for all these four images are showed in Figure 6-17:

a) 0.8mm, 30A b) 0.8mm, 50A c)0.8mm, 60A d) 1.2mm, 60A

Figure 6-17, Edge detection results of Canny operator

Based on the results of canny edge detection, canny operator has difficulty in distinguishing droplet neck shrinking and noise. Even though canny operator does extract the edge information of neck shrinking in (b) and (d), it is also obvious that canny operator produces more noise with a more continuous edge information extraction. As a result, canny operator will not be used in this detection.

Log operator:

Edge detection results of canny operator for all these four images are showed in Figure 6-18:

a) 0.8mm, 30A b) 0.8mm, 50A c)0.8mm, 60A d) 1.2mm, 60A

Figure 6-18, Edge detection results of Log operator

Basing on the results in Figure 6-18, Log operator has failed to extract complete neck shrinking information from images (a) (b) (c). Although Log operator is able to extract basic information of neck shrinking, we still have difficulty to calculate neck shrinking because of discontinuity. Therefore, log operator is not suggested in this detection.

Prewitt operator:

Edge detection results of Prewitt operator for all these four images are showed in Figure 6-19:

Based on the results of Prewitt operator, it can extract a relative complete profile of image (a) and (c). However, due to the significant discontinuity and double layer, Prewitt operator could cause obvious calculation error which makes the calculation meaningless. Thus, Prewitt operator will not be adopted in this detection.

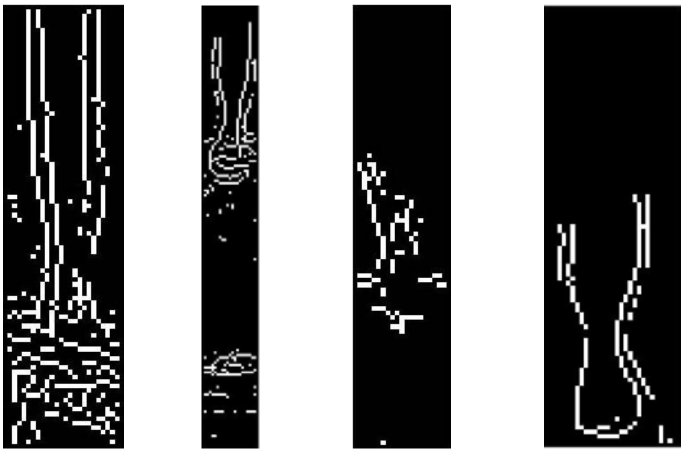

a) 0.8mm, 30A b) 0.8mm, 50A c)0.8mm, 60A d) 1.2mm, 60A

Figure 6-19, Edge detection results of Prewitt operator

Sobel operator:

Edge detection results of canny operator for all these four images are showed in Figure 6-20:

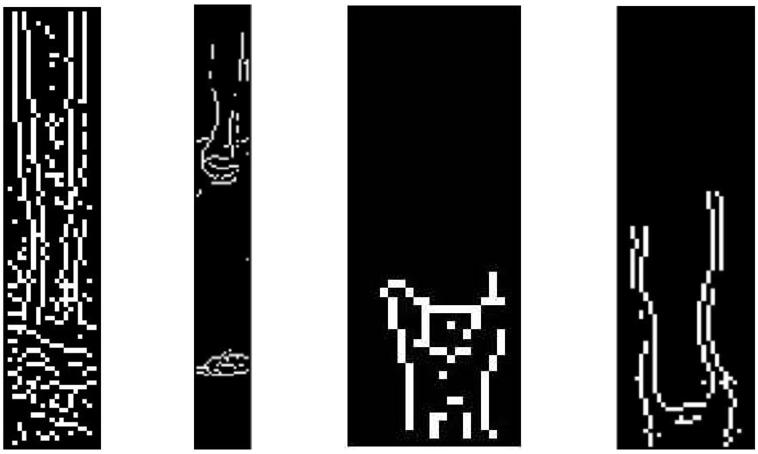

a) 0.8mm, 30A b) 0.8mm, 50A c)0.8mm, 60A d) 1.2mm, 60A

Figure 6-20, Edge detection results of Sobel operator

Based on the result of Sobel operator, it can not separate the noise from desired information on image (a). It can not extract a continuous neck shrinking profile from image (b). Even through it could extract a continuous neck shrinking profile from image (d), the double layer edge causes huge calculation error. However, Sobel operator does have the ability to extract a noise-free continuous neck shrinking image from image (c). Thus, Sobel operator will be used for edge detection of regulation (c).

Zero-crossing:

Edge detection results of canny operator for all these four images are showed in Figure 6-21:

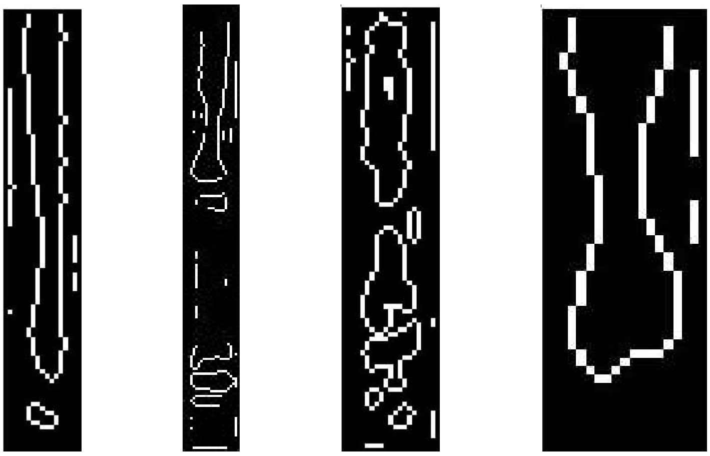

a) 0.8mm, 30A b) 0.8mm, 50A c)0.8mm, 60A d) 1.2mm, 60A

Figure 6-21, Edge detection results of Zero-crossing operator

Basing on the results of Zero-crossing operator, it can extract complete and continuous neck shrinking information from regulation (a) and (d) which can be used for neck shrinking size calculation. For regulation (b) and (c), zero-crossing is not able to extract satisfying results of profile.

To conclude all the results of six operators, images from 0.8mm 30A, 0.8mm 60A and 1.2mm 60A regulation can be processed. Yet, image from 0.8mm 50A regulation still waits for its solution.

Further observation through the results of canny operator and Zero-crossing operator gives us a clue of solving the problem of 0.8mm 50A regulation. Canny operator is able to extract almost 95% of the profile continuously but performs very poor in noise isolation. On the other hand, the result on 0.8mm 50A regulation of Zero-crossing operator is not very dependable. Zero-crossing operator seems to like giving various results depends on the illumination. However, we could combine these two operators together to form a canny-zero-crossing operator which can low the odds of profile discontinuity with appropriate algorithm.

Canny-zero-crossing operator:

Edge detection results of canny-zero-crossing operator for all these four images are showed in Figure 6-22:

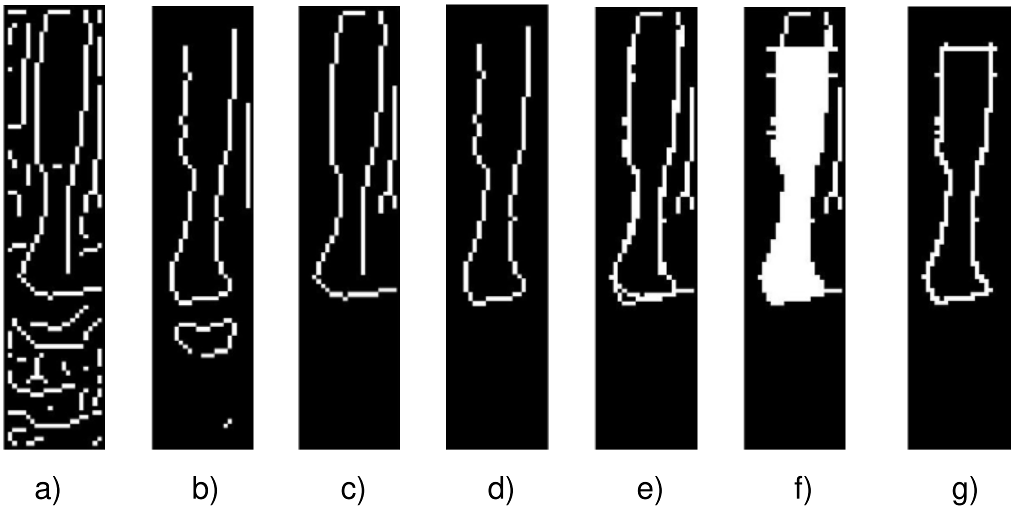

a) b) c) d) e) f) g)

a) canny operator edge detection b) zero-crossing edge detection c) edge elimination for canny edge detection d) edge elimination for zero-crossing edge detection e) overlapping of result ‘c’ and result ‘d’ f) morphology dilation and corruption operation g) final result

Figure 6-22, Edge detection result of Canny-zero-crossing operator

Step 1, wiener filtering and image enhancement for interest region image of 0.8mm 50A

Step 2, use Canny operator and Zero-crossing operator for edge detection on the image

Step 3, edge elimination algorithm on both detection results. The spirit of edge elimination is to calculate the number of any continuous group of pixels and compare this number with a preset threshold. The group of pixels with a smaller amount than the threshold will be eliminated from the image. This is a very practical technique to avoid discrete noise signal in digital image.

Step 4, overlapping the results of both operators after edge elimination.

Step 5, use the dilation algorithm in morphological image processing technique (MIP for short) to further connect all discontinuous pixels and then correct the profile back to original shape by applying Erosion algorithm in MIP. Manually enclose the profile and fill the area with region filling algorithm in MIP.

The word morphology commonly denotes a branch of biology that deals with the form and structure of animals and plants. We use the same word here in the context of mathematical morphology as a tool for extracting image components that are useful in the representation and description of region shape, such as boundaries, skeletons, and the convex hull. [45]

Operators in MIP including dilation and erosion can be briefly mathematically expressed as follows:

Let $A$ be a set in $R^n$, point set $B \in R^n$, vectors $a \in A$ and $b \in B$, the reflection of set $B$, denoted $\hat{B}$, is defined as

$$\hat{B} = \{\omega \mid \omega = -b, b \in B\}$$

The translation of set $A$ by point $z = (z_1, z_2)$, denoted $(A)_z$, is defined as

$$(A)_z = \{c \mid c = a + z, a \in A\}$$

Dilation of $A$ by $B$, denoted $A \oplus B$, is defined as

$$A \oplus B = \{z \mid (\hat{B})_z \cap A \neq \phi\}$$

Erosion of $A$ by $B$, denoted $A \Theta B$, is defined as

$$A \Theta B = \{z \mid (B)_z \subseteq A\}$$

Step 6, final detection result achievement

Therefore, we have found out suitable algorithm for each image: Sobel operator for 0.8mm 60A image, Zero-crossing for 0.8mm 30A and 1.2mm 60A image, Canny-zero-crossing for 0.8mm 50A image. The results of neck shrinking information are showed in following figures:

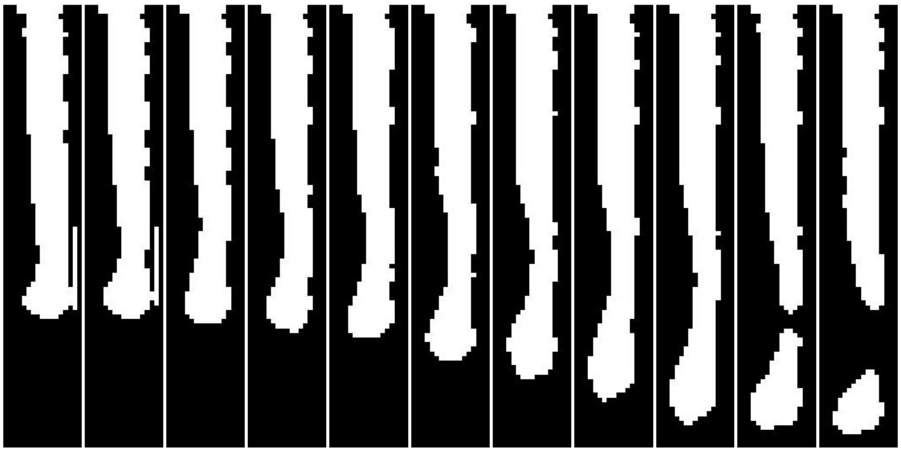

Figure 6-23, Neck shrinking detection from Zero-crossing operator on 0.8mm 30A image

Figure 6-24, Neck shrinking detection from Canny-zero-crossing operator on 0.8mm 50A image

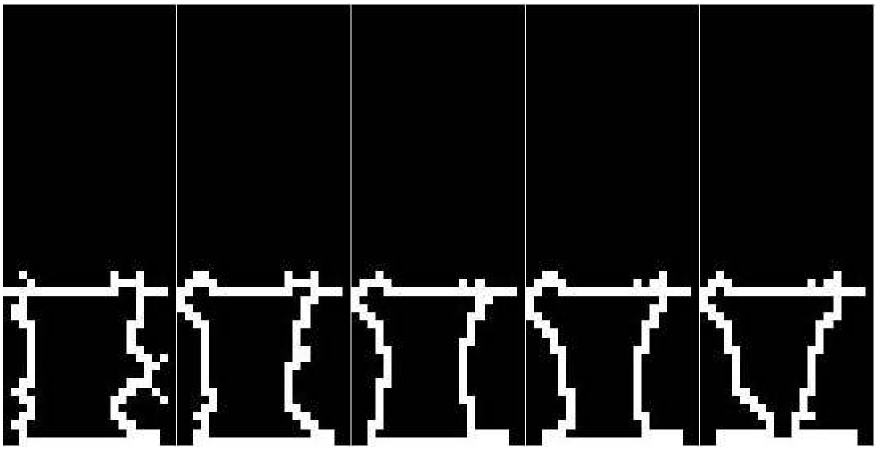

Figure 6-25, Neck shrinking detection from Sobel operator on 0.8mm 60A image

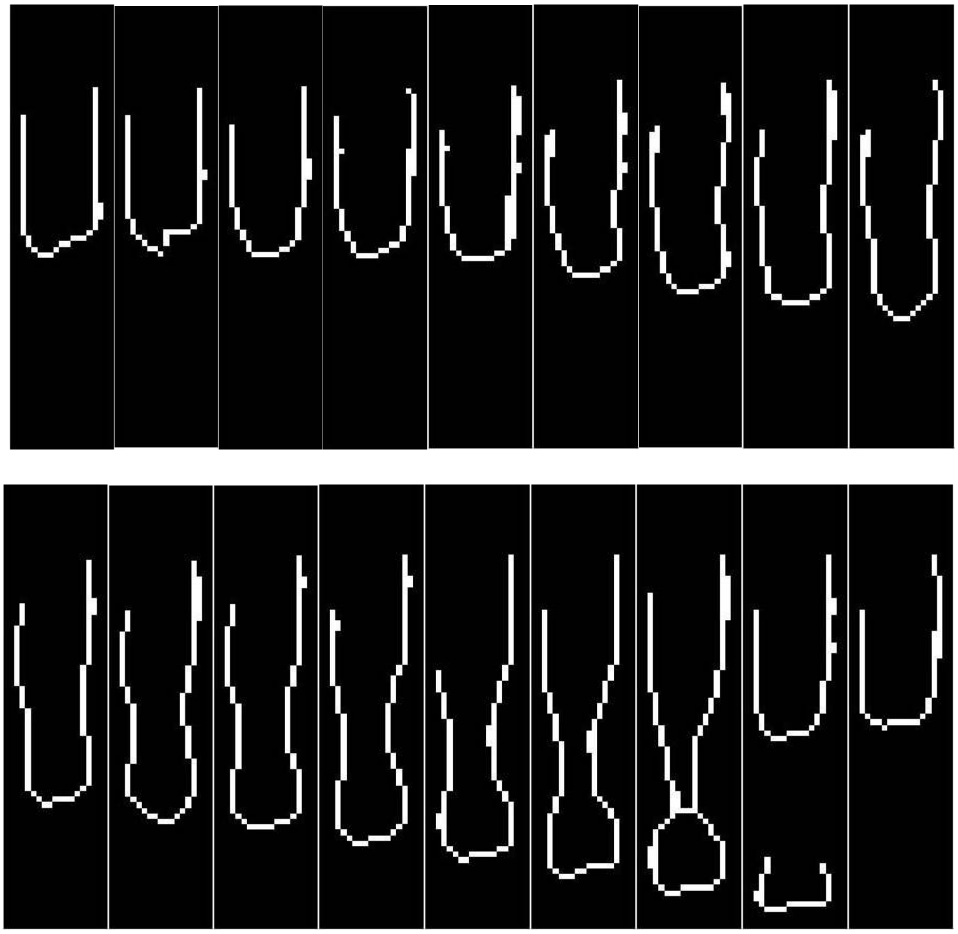

Figure 6-26, Neck shrinking detection from Zero-crossing operator on 1.2mm 60A image

Figures 6-23~26 show that selected operator gives a good performance on neck shrinking detection.

### 6.2.2 Image processing of droplet size

Droplet size information is directly related to the droplet weight, both of which reflect the stability of the process. Droplet size also strongly correlates with the welding pool profile. Additionally, together with the droplet trajectory analysis later, it can provide information of droplet acceleration and droplet velocity which are direct indication of arc force. A practical procedure of droplet size analysis is a strong support for DB-GMAW full penetration research.

The image processing of droplet size is more challenging than the front-side profile extraction or the neck shrinking detection. The intensity of arc at welding pool and wire tip is usually very constant without obvious or sudden oscillation. Moreover, the contrast rate at these two positions is relatively higher which means a set of appropriate parameter of operators are good enough to extract desired information. On the contrast, a droplet moves long distance during welding process with huge noise and influences from almost every aspect. A droplet causes obvious grey value change at the moment of detachment from wire tip and then travels along arc column which contains complicated brightness change and noise.

To step over this obstacle, a brightness based subtraction between target image and a reference image took at the beginning of the process [46] is necessary. The first image from the process will be taken as reference image. Every image to be analyzed later will perform a subtraction operation with the reference to avoid similar but useless noise in the image. The only moving objective between images is the droplet which means that the droplet information will be left after the subtraction.

The procedure of droplet size detection is discussed as follows:

Step 1, reserve the reference image, select interest region and reverse the grey value of the image. The reference image should be taken as the first image captured by the high-speed camera. Cutting out interest region is still helpful to avoid noise and accelerate the calculation speed. Since the droplet always holds a lower grey value compared to arc column. Reversing the grey value of the image is helpful to highlight the droplet.

Step 2, continue to load more images for analyzing and repeat step 1 operation to all these images. The coordinate and size of interest region of these images should be kept exact same with reference image for calculation accuracy.

Step 3, subtraction operation between target images and reference images which could be mathematically expressed as Eq.6-8

Step 4, binarization operation for highlighting droplet information in the image.

Step 5, erosion operation for the droplet.

Step 6, dilation operation for the droplet.

$$G_i(x,y) = f_i(x,y) - f_R(x,y)$$

Where $f_i(x,y)$ is the $l^{th}$ frame of the target image, Eq.6-8

$f_R(x,y)$ is the reference image

Detection results of droplet size are showed in following Figures assorted by its procedure. The images are grey-value-reversed for clearer demonstration.

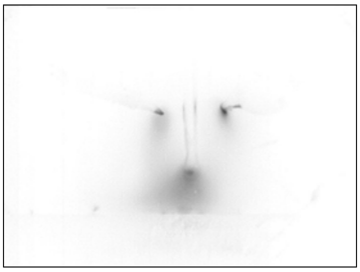

a) reversed Reference image

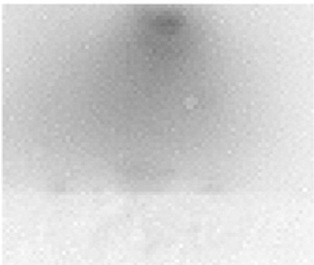

b) interest region

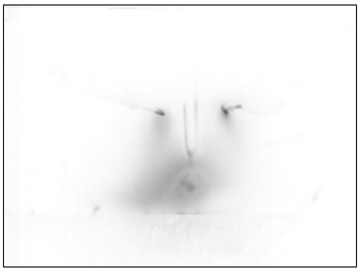

c) reversed target image

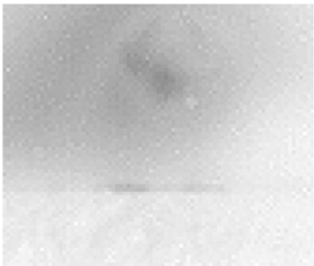

d) interest region

e) subtraction f) filtering after subtraction g) binarization

h) edge elimination i) erosion j) dilation

Figure 6-27, Droplet size detection, 0.8mm, 30A

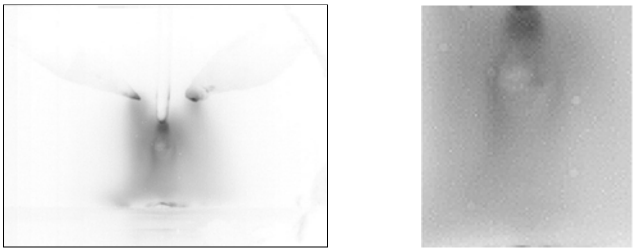

a) reversed reference image b) interest region

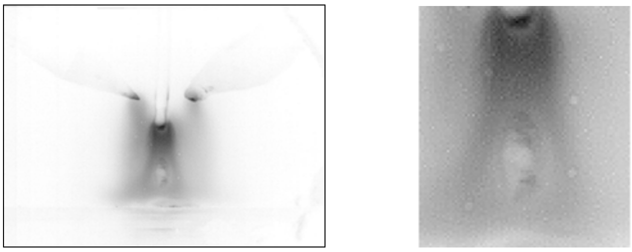

c) reversed target image d) interest region

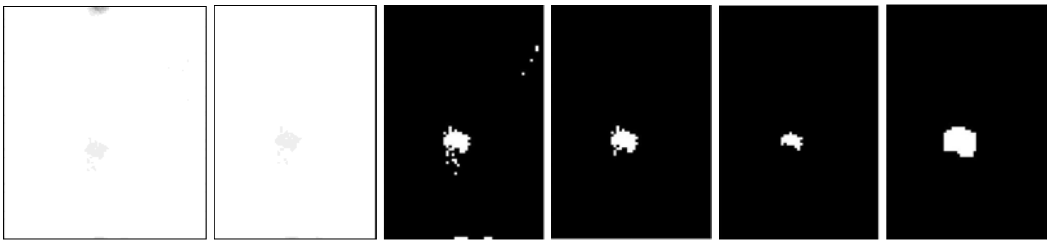

e) subtraction f) filtering g) binarization h)elimination i) erosion j) dilation

Figure 6-28, Droplet size detection, 0.8mm, 50A

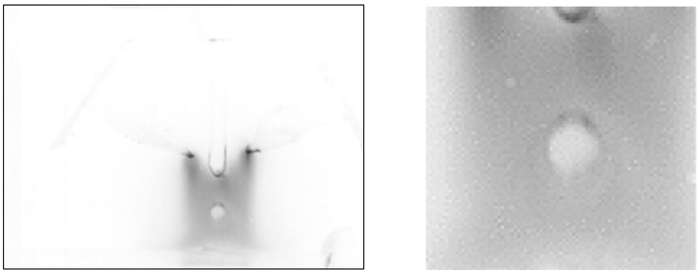

a) reversed reference image b) interest region

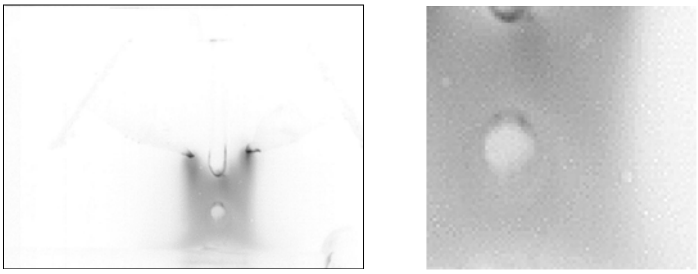

c) reversed target image d) interest region

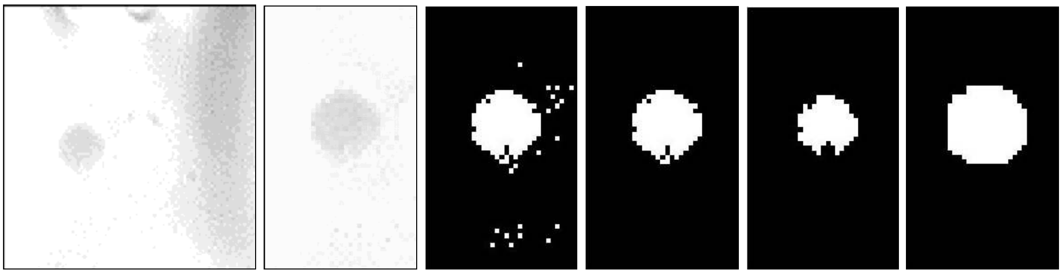

e) subtraction f) filtering g) binarization h) elimination i) erosion j) dilation

Figure 6-29, Droplet size detection, 1.2mm, 60A

The droplet trajectory is relatively easy after achievement of droplet size detection algorithm. After droplet size detection, we use Eq.6-9 to calculation the approximate center of the droplet.

$$X = \frac{X_{Max} + X_{Min}}{2}$$
$$Y = \frac{Y_{Max} + Y_{Min}}{2} \quad \text{Eq.6-9}$$

To verify the practicability and accuracy of our algorithm, we manually measured the droplet size and velocity to compare with the results from our detection algorithm. The comparative result showed in figure 6-30~31 indicates that the algorithm is practical for this propose.

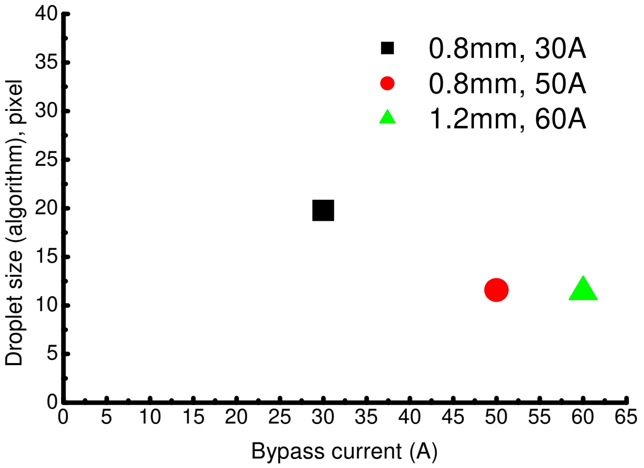

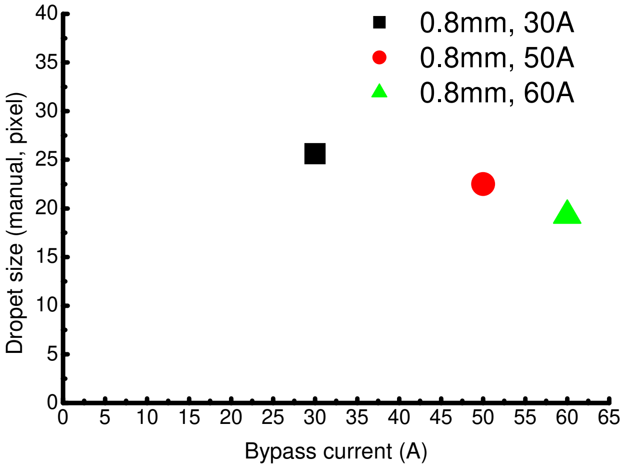

Figure 6-30, Comparative results between algorithm and manual on droplet size

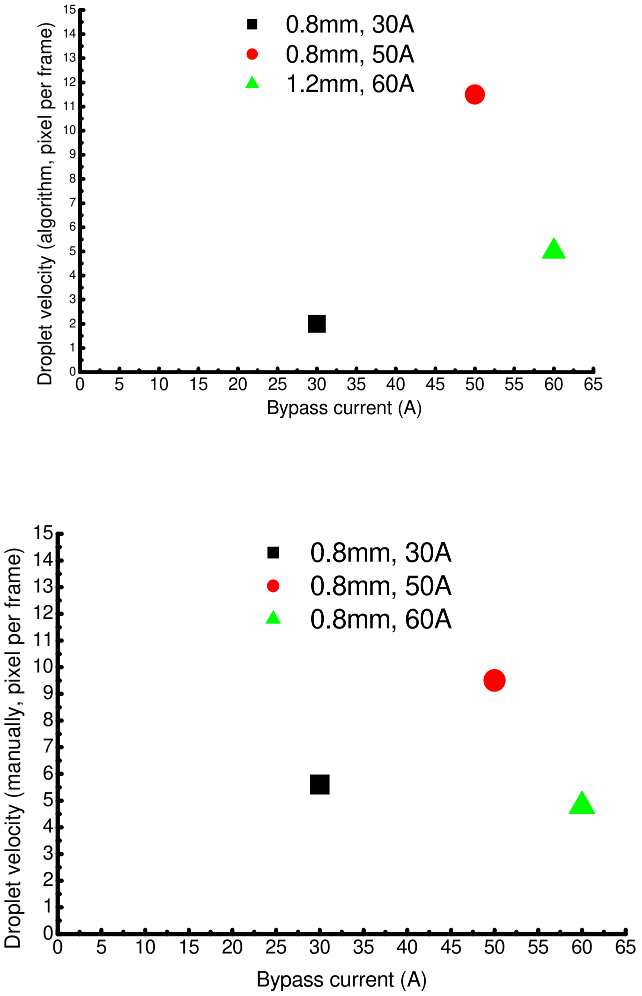

Figure 6-31, Comparative results between algorithm and manual on droplet velocity

## 6.3 Image processing of back-side welding pool profile

Under full penetration condition, the welding pool has profiles both on the front-side and back-side of the work piece. Compared with front-side welding pool profile and droplet information, back-side welding pool profile is relatively easier to obtain. A reflection optical system is established to assist getting the back-side welding pool profile which is showed in Figure 6-32:

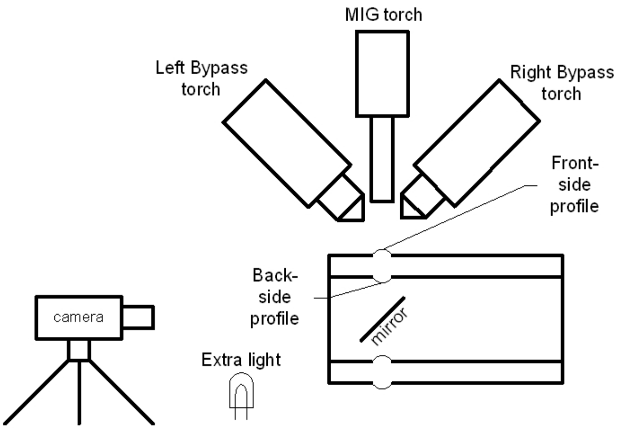

Figure 6-32, Optical system for back-side profile inspection

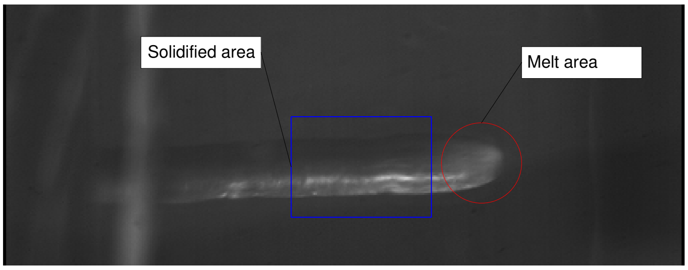

Figure 6-33, Back-side welding profile

The objective is to exam the width in pixel of the back-side welding pool. Compared with previous tasks, this is relative easier to accomplish. We use square root grey-value transformation for image enhancement in this procedure since the original image is a little dark. After image enhancement, we could use directional edge detection technique to determine the width. Firstly, we choose our interest region. In Figure 6-33, the melt area is the welding pool underneath the arc column and solidified area is the actual back-side welding pool profile. We choose our interest region as the solidified area right next to melt area for calculation accuracy. Vertical straight lines across the interest region are set as directions of edge detection. Any grey-value change which is greater than the preset threshold is recorded and compared with other results from other vertical straight lines to determine the width of profile. The result image of back-side welding pool profile detection is showed in Figure 6-34. The green box in the figure is our interest region. The image enhancement in this procedure follows

Eq.6-10:

$$G_{(i,j)} = (f_{(i,j)})^{\frac{1}{2}}$$

Where $G_{(i,j)}$ and $f_{(i,j)}$ is the grey-value function of the image after and before image enhancement respectively Eq.6-10

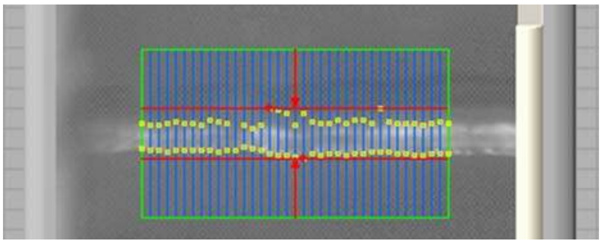

Figure 6-34, Result image of back-side welding pool profile detection

### 6.4 Chapter conclusion about three image processing procedures

In this chapter, we have discussed three image processing procedures including their theory, algorithm and processing results. Each of these procedures has its advantages and disadvantages. Ultimately, we want to determine the best method to be the monitoring and feedback system in full penetration DB-GMAW control design.

**Front-side welding pool profile detection:**

The front-side welding pool profile detection is the first procedure we established and it gives good detection results on the profile. We compared results between six operators and find out that canny operator gives the best result on detection. The result of canny operator is continuous and most completed. The algorithm is not very complicated for this detection. Traditionally, this is really a good procedure to monitor front-side welding pool which gives plenty of information about arc stability. It is known that arc voltage signal could be used to monitor the penetration in TIG welding [47]. In conventional GMAW, good front-side profile detection is also valid to estimate back-side profile once major welding parameter is fixed such as welding voltage and welding speed.

That is because once the welding voltage and welding speed is fixed, for the same work piece, the front-side profile has a strong bounding with the back-side profile both of which are directly related with welding current. In other words, in conventional GMAW, we can inspect back-side welding pool profile by inspecting front-side welding pool profile. However, the front and back side welding pool profile of DB-GMAW doesn't have this strong bounding anymore due to the existence of bypass arc. The bypass arc changed the distribution of arc forces which are the key factors influencing welding pool profile and penetration. Under the same totally welding current, the penetration level between bypass GMAW and conventional GMAW varies obviously [48]. Thus, in DB-GMAW, several weld beads with very similar front-side welding pool profiles may have totally different back-side welding pool profiles.

**Metal transfer information detection - neck shrinking, droplet size and droplet trajectory:**

The detection of metal transfer information is the most sophisticated method among our three procedures and returns most information. The neck shrinking detection provides a method of monitoring droplet transfer frequency. The droplet size detection indicates the transfer modes, welding current and arc stability. This algorithm is the one with most potential for further development in the future. However, the disadvantage of this method is also obvious: algorithm complexity, processing speed and mysterious relation with back-side welding pool profile.

Based on the results of this method, different operators should be used in different regulations to ensure satisfied detection results. Before detection, we have very little hint indicating which operator should be chosen. Although we already know that some particular operator is suitable for some particular regulation, there is still no guarantee that this particular operator is able to extract steady information from every image in that regulation due to the dynamic characteristic of MIG welding. As a matter of fact, there are still a certain mount of images that none of our operators is able to extract satisfying detection result from them. A further research and algorithm development is still required to improve detection quality and ensure most of the images can be extracted with satisfying results.

Processing speed is another issue for this method. Currently, the off-line processing speed is approximately 30-50 frames per second depending on the operator type and detection objective (neck shrinking, droplet size or droplet trajectory). Thus, using this algorithm on-line is nearly impossible right now considering its time-consuming operational period. Plus, it is still difficult to determine back-side profile basing on the information of droplet size and trajectory. As we mentioned earlier, the bypass current and back-side profile relationship is very mysterious which means that it is also difficult to establish a clear relationship between droplet size and back-side profile. Moreover, experimental data shows us that the back-side welding pool profile is relatively sensitive to the bypass current. Once full penetration achieved, a minor change in total bypass current such as 10A can cause obvious back-side profile change in width. Meanwhile, a 10A resulted change in droplet size is very small for our algorithm to detect and could mostly lost in filtering or de-noise.

**Back-side welding pool profile detection:**

The algorithm of back-side profile detection is the most reliable procedures. Its advantages are directness and processing speed. The back-side profile width is the most direct information to monitor full penetration in DB-GMAW. Also, the simplicity of the algorithm is efficient enough to bring this detection on-line.

To sum up, in this chapter, some knowledge of image processing technique and its mathematical expressions is introduced as a foundation of our approaches to the DB-GMAW image process. According to comparative results, appropriate operators and algorithms are selected successfully to obtain information of front and back side welding pool profile, neck shrinking, droplet size and trajectory. The three procedures demonstrate very attractive further research and development potential as well as good ability of technical support for full penetration monitoring.

# CHAPTER 7

## Nonlinear Modeling of DB-GMAW

In our previous chapters, DB-GMAW has demonstrated its ability to achieve full penetration on aluminum 6061 work piece. Different approaches of monitoring DB-GMAW full penetration through image processing technique are also developed to monitor the full penetration of DB-GMAW. In this chapter, we will discuss the significance of controlling DB-GMAW full penetration and related nonlinear modeling techniques.

### 7.1 Full penetration of DB-GMAW

Full penetration is a very common requirement in manufacturing applications in contact joint weld and groove joint weld， and it is usually one of basic requirements when welding a relative thin plate. A fully penetrated weld bead usually means that the bead holds equal strength compared with other area of un-faulted base metal. Please keep in mind that a fully penetrated weld bead does not necessary mean any priority over a partial penetrated weld bead. The desired penetration level always varies according to the application requirements. Plus, full penetration requirement is more common in aluminum welding since lots of aluminum base metal is relative thin plate compared to black metal work piece.

Aluminum is sometimes difficult to achieve full penetration by certain welding method due to its high reflectiveness [49] and low surface tension which makes the full penetration research of DB-GMAW on aluminum even more meaningful. The full penetration level of a groove weld bead usually depends on the shape and angle of the groove. For a non-grooved weld bead, a good full penetration level is showed in Figure 7-1.

In chapter 5.3, DB-GMAW has showed its ability to maintain the full penetration without burning through at a much higher current level than conventional GMAW due to the smaller electromagnetic force acting on the weld pool surface. In other words, DB-GMAW is able to increase the deposition rate because it can maintain full penetration at a much higher current level. Furthermore, a compromise on total welding current has to be made to adjust full penetration level in conventional GMAW which is not necessary in DB-GMAW. In DB-GMAW, we adjust bypass current value to achieve desired full penetration level while maintaining the total welding current unchanged so the deposition rate will not be compromised because of full penetration adjustment. Therefore, the DB-GMAW full penetration control has its advantages and potentials for many industrial applications.

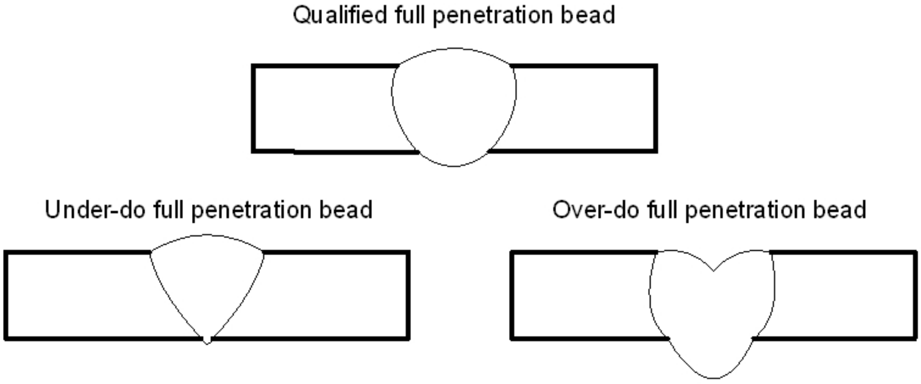

Figure 7-1, demonstration of different full penetration levels

This chapter discusses the modeling and validation procedure of DB-GMAW full penetration process. First of all, an effective method of monitoring full penetration of DB-GMAW should be constructed as a feedback of the system. We have already developed three image processing approaches which are front-side welding pool profile detection, droplet information detection and back-side welding pool profile detection. The advantages and disadvantages of these three detections have been discussed in earlier chapter. The droplet information detection is extremely helpful to analyze metal transfer. However, this algorithm is to complex to provide a good enough reliability. Furthermore, the long operating period of this detection makes on-line feedback extremely difficult to realize. In our procedure, we are using image from high speed camera which directly records the metal transfer process. There are also two other ways to research the metal transfer process: laser back-light system [20] and theoretical modeling [50]. Nevertheless, none of the three techniques has been adopted into on-line control due to the problem we mentioned before. Therefore, the droplet information detection will not be applied as feedback system of DB-GMAW. Compared with droplet information detection, front-side welding pool profile detection is an easier algorithm which had been adopted by some scholars as feedback of welding system. A seam-tracking aluminum GMAW process has been developed by Professor Yu Shi using front-side welding pool profile detection as on-line feedback [52]. However, front-side welding pool profile detection is very difficult to become the feedback of DB-GMAW full penetration modeling due to the mysterious relationship between front-side profile and back-side profile. In other words, the prediction of back-side profile basing on the front-side profile information is very inaccurate in DB-GMAW process. Therefore, we will not use the front-side profile detection as our feedback system. The back-side profile detection is the method which provides best calculation speed and most direct information about back-side welding pool profile. Thereby, we will adopt back-side profile detection as feedback system.

Plenty of scholars around the world have put enormous effort and dedication to understand the relationship between conventional GMAW penetration and its welding parameters. Early in the 1950s, Jackson and Shrubsall [52], as well as McGlone and Chadwick [53] investigated the causality of welding parameters on bead penetration and further developed mathematical model to predict weld bead penetration. Giedt and Tallerico studied the relationship between electron beam welding machine settings and weld bead penetration [54]. Metzbower bought this issue into laser welding in 1993 [55]. Kim, Basu and Siores also developed a linear mathematical model to predict GMAW penetration in 1996 [56]. In their models, a lot of parameters such as welding current, voltage, shielding gas flow rate and etc. were put into consideration which makes the model very complicated. Furthermore, although linear model structure is convenient and practical in control algorithm design, theoretically the penetration model is more likely to be a nonlinear model. Obviously, it is absolutely a disaster to consider too many factors in a practical case when the system is a nonlinear model. However, I wondered whether it is possible to build a nonlinear model after getting rid of some parameters (for example, making them constants).

Compared to conventional GMAW, DB-GMAW is even more complicated with more parameters to be put into consideration. Besides the welding current, voltage, gas flow rate and welding velocity, DB-GMAW also has bypass current and torch distances influencing the process. Thus, it is almost impossible to consider all these parameters in a mathematical model with good prediction accuracy.

Normally, once a process has achieved its stability and desired weld bead, we will fix some of the parameters such as shielding gas flow rate, wire to plate distance, welding voltage and etc. In experiments of chapter 5, full penetration bead has been achieved by DB-GMAW with parameters of Table-2. We also discover that even a small change in bypass current could result a significant change in back-side welding pool width.

In retrospect of Figure 5-8, we realized the fact that DB-GMAW full penetration is much more complex than conventional GMAW. It is also very obvious that DB-GMAW is a process with significant nonlinear characteristics. The advantages of nonlinear system modeling is that global mathematical model with good accuracy can be achieved. In our modeling process, some parameters are fixed to constant as demonstrated in Table-3. Throughout our data, we noticed that the Ex.5 in Table-2 provides a very good full penetration bead. After fixing these parameters in DB-GMAW, we make the total bypass current varies from 140A to 180A which means a single bypass current varies from 70A to 90A. Under this restriction, we will build the mathematical model using nonlinear system identification techniques.

Table 7-1, constant parameters for modeling experiments

| Constant parameters of modeling experiments: | |
|---|---|
| Wire type | 1.2 mm  ER 4047 |

Table 7-1, cont.

| | |
|---|---|
| Base material | Al6061 T6 thickness: 3.2mm |
| Shielding Gas (MIG) | Argon |
| Shielding Gas (Bypass) | Argon |
| Gas flow | 12 L/min |
| Welding speed | 112.5 cm/min |
| Wire feeding speed | 11.5m/min |
| Preset welding voltage | 21.5 V |
| Total welding current | 250A |

## 7.2 Nonlinear system identification

A nonlinear system is a system that contains nonlinear component where superposition principle does not applied anymore. Nonlinear control is developed to conquer the disadvantages of linear control method. As we all know, most actual system is nonlinear system indeed. However, we just use linear control method to control them because linear control method is earlier to realize and also sophisticated in theory. Usually, approximated linearization is applied to the system before developing linear control method. However, approximated linearization has its own limitations. An approximately linearized model could only predict the local behavior of the nonlinear system in the vicinity of the set point. Moreover, the dynamics of a nonlinear system are much richer than that of a linear system. There is some essentially nonlinear phenomenon that cannot be described or predicted by linear models. Nonlinear control could achieve global stability and global optimization if appropriate parameter nonlinear model is established [57].

Generally speaking, nonlinear control requires two steps of work. Step one is called modeling and identification of the system and step two is nonlinear control basing on the model. System identification is the process of building mathematical model of dynamical system basing on observed data from the system.

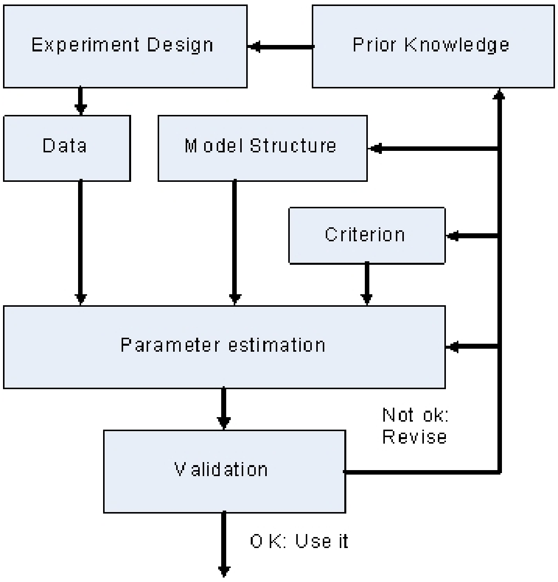

Figure 7-2, Procedure of system identification

The model structure identification is the real difficulty in model identification because there is no rule to follow. Experience and luck is both important here. Theoretically, there are several structures about SISO nonlinear dynamic models:

**The Volterra Series Model:**

For nonlinear system, it could be expressed as Eq.7-1 in discrete time case [57].

$$y(k) = h_0 + \sum_{i_r=0}^{k} h_1(i_1)u(k-i_1) + \sum_{i_1}^{k}\sum_{i_1}^{k} h_2(i_1,i_2)u(k-i_1)u(k-i_2) + \ldots \qquad \text{Eq.7-1}$$

$$h_n(\kappa_1,\ldots,\kappa_n) \quad n = 0,1,2\ldots\ldots$$

Eq.7-1 is called the Volterra weighting function series. The process is characterized by its Volterra kernels. Volterra weighting function series describe a system accurate mathematically. However, it is not a practical structure to use because it contains too many parameters.

**Block Oriented Models:**

Block oriented models include linear dynamic block and nonlinear static block

[57].

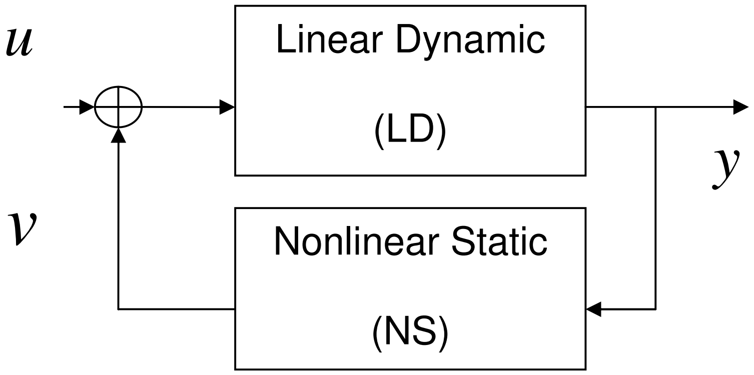

Figure 7-3, Block oriented models

The block oriented model can be further developed into several models:

**Simple Hammerstein Model:**

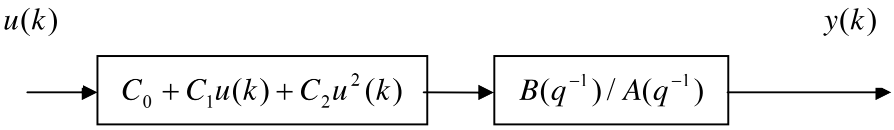

$\frac{B\ (q^{-1})}{A\ (q^{-1})}$ denotes to pulse transfer function.

**Simple Wiener Model:**

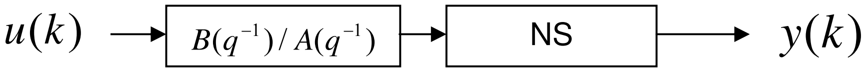

**Simple Wiener-Hammerstein Cascade Model:**

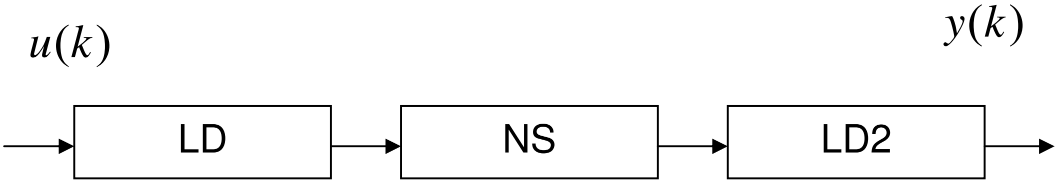

## The Generalized Hammerstein Model:

$$y(k+d) = C_0 + \frac{B_1(q^{-1})}{A_1(q^{-1})}u(k) + \frac{B_2(q^{-1})}{A(q^{-1})}u^2(k)\text{[57]} \qquad \text{Eq.7-2}$$

Eq.7-2 is a generalized Hammerstein model which only considers the influence from present input. Experience indicates that the inputs and output value from previous steps also have their contribution to present output in many applications. If we put these factors into consideration, the generalized Hammerstein model can be further developed into Eq.7-3:

$$y(k+d) = \phi^T(k)\theta \qquad \text{Eq.7-3}$$

Where

$$\phi^T(k) = [1, u(k), ..., u(k-nb_1), u^2(k), ..., u^2(k-nb_2), -y(k+d-1), ..., -y(k+d-n)]$$

$$\theta^T = [c_0 A_{(1)}, b_{10}, ..., b_{1nb_1}, b_{20}, ..., b_{2nb_2}, ..., a_1, ..., a_n]$$

$\theta^T$ is a linear matrix which includes all parameters of the nonlinear model. $\phi^T(k)$ is a matrix which includes all units of model polynomial [57].

All model structures introduced above is theoretical nonlinear model structure. Experience tells us that the actual model could be more complicated. When solving a real-world problem, the model polynomial usually includes units as $c_0, u(k), u^2(k), u(k) \bullet y(k), u^2(k) \bullet y^2(k)$. Also, it is very difficult to predict how many previous steps input and output should be included in the model. Normally, a model should be revised and redesigned many times before it could take actual effects.

Although the model structure is chosen mostly by experience, the parameters of the model could be tested to estimate how good the model is selected. In order to estimate the parameters of the model, a test signal should be designed and generated.

## Test signal for Parameter Estimation

For the identification of nonlinear systems, there are many kinds of test signals, such as step function, sine or multi-sine, chirp and Pseudo-Random

Multi-level Signal (PRMS for short). The general requirements for the test signals are: if a two level test signal is used, the experiments should be done in a number of working points; a multi-level test signal can be used for nonlinear system with the number of levels greater than the degree of the polynomial steady state characteristic of the process; PRMS has a wide range amplitude distribution with an auto-correlation function similar to white noise.

Usually, PRBS (Binary signal), PRTS (Ternary signal) and PRQS (Quinary signal) are commonly used PRMS in practical cases. A PRMS signal could be generated by multi-level shift registers.

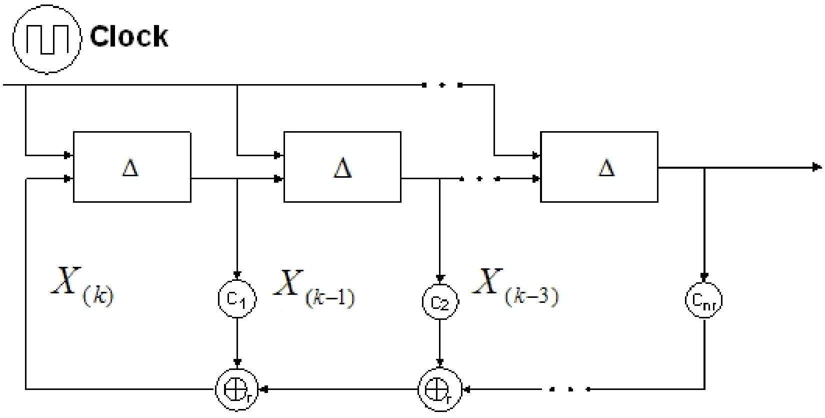

Figure 7-4, Multi-level shift register

For the former method, a shift register is built up from registers which store the information until new information is fed in. Every register except the first one receives the information from the previous one that is on their left. The transfer of the information happens periodically and synchronously. Each register may have $r$ levels like $0,1......r-1$. Then $r^{n_r}$ different states are imaginable.

The basic idea of generating PRMS is that the state of one register is considered as the test signal. This signal has $r$ levels with the most randomness if the shift register has all possible states in sequel. The degree of randomness increases very fast.

The shift register is a chain of delay operators. If the input to the first register is $x(k)$ then the output of the first register is $x(k-1)$. $x(k)$ can be determined by the following difference equation:

$$x(k) \equiv c_1 \otimes_r x(k-1) \oplus_r c_2 \otimes_r x(k-2) \oplus_r \ldots c_{n_r} \otimes_r x(k-n_r) \qquad \text{Eq.7-4}$$

The test signal will be mapped to practical input according to the real-world situation. The mapping method will be discussed later.

**Parameter Estimation:**

By assuming the model structure known, input signal is persistently exciting and output is noisy, parameter estimation could be performed. Although there are several different methods for option, least square method is a traditional way for parameter estimation.

Before the estimation, assume the experimental data are available, and listed as:

$$\{u(i), y(i), i = 1, 2, ..., n+N\}$$

Also, define $n$ as the maximum order of the backward shift operator polynomial with respect to the output $y(t)$, $m$ as the maximum order of the backward shift operator polynomial with respect to the input $u(t)$, and $N$ as the difference between the number of sampled data and $n$.

Define an error function in the form of

$$\begin{aligned} V &= \frac{1}{N}\sum_{k=n+1}^{n+N}(y(k)-\hat{y}(k\,|\,\theta))^2 \\ &= \frac{1}{N}\sum_{k=n+1}^{n+N}(y(k)-\varphi^T(k-n)\theta)^2 = \frac{1}{N}e_N^T e_N \end{aligned}$$

Where $e_N = y_N - \Phi_N\theta = \begin{bmatrix} e(n+1) \\ e(n+2) \\ \vdots \\ e(n+N) \end{bmatrix}$,

And $y_N = \begin{bmatrix} y(n+1) \\ y(n+2) \\ \vdots \\ y(n+N) \end{bmatrix}$

$$\Phi_N = \begin{bmatrix} -y(n) & \cdots -y(1) & u(n) & \cdots u(n+1-m) \\ -y(n+1) & \cdots -y(2) & u(n+1) & \cdots u(n+2-m) \\ \vdots & \cdots \vdots & \vdots & \cdots \vdots \\ -y(n+N-1) & \cdots -y(N) & u(n+N-1) & \cdots u(n+N-m) \end{bmatrix}$$

Then, since $V = \frac{1}{N}(y_N - \Phi_N\theta)^T(y_N - \Phi_N\theta)$

Take the derivative on both side with respect to $t$. And by making the derivative equal to zero, we can get the condition for the error to be the minimum value as:

$$\frac{\partial V}{\partial \theta} = -\frac{2}{N}\Phi_N^T(y_N - \Phi_N\theta) = 0$$

Hence, the estimated parameters are in the form of:

$$\hat{\theta}_N = (\Phi_N^T\Phi_N)^{-1}\Phi_N^T y_N \qquad \text{Eq.7-5}$$

So far, we have derived the expression equation from the tested data to the final estimated parameters.

**Validation**

The validation is the process to exam whether the model satisfies our requirements. By inputting the existing experimental data into the model, the simulated output could be calculated. The error between simulated results and actual experimental results would demonstrate whether the model needs revision. If the model passes through the validation, then it is ready to be used for feedback control.

### 7.3 Modeling DB-GMAW full penetration

There is no general method for the analysis and modeling on nonlinear models, such as the welding process in this dissertation. What we can do is to design as many models as possible and then find the one that fits the behavior of the original plant the best. After learning the basic knowledge of nonlinear modeling method in chapter 7.2, the content follows is actually a practical application of all the theoretical knowledge.

Before we started, let's review the experiment that we are going to model. The objective is to find out the relationship between bypass current and back-side welding pool profile width under the welding parameters showed in Table 7-1. Since the left bypass current is set equal to the right bypass current, we choose the value of a single bypass current as the system input. The system output is the back-side profile width in pixels. Thus, we construct a SISO (Single input single output) system. As we introduced before, the bypass current value is limited within the range of 70A and 90A.

In general, throughout this chapter, $u(k)$ stands for the system input which indicates bypass current value, while $y(k)$ as the system output is the width of the back-side weld bead in pixels.

### 7.3.1 Generation of test signals

For this practical problem, we choose Pseudo-Random Ternary Signal (PRTS) as our test signal. This is a test signal which is artificially generated with features that resemble to those of the Gaussian white noise, such as free distinct amplitude values. The sequence repeats itself after a certain period. The mean value of a sequence in a period is zero.

Commonly, there are two methods to generate the PRTS: by multi-level shift registers or by solving difference equation.

In this particular application, I choose the maximum length of the test signal to be $N_p = 26$ . Also, since this is a PRTS, the maximum length is $N_p = r^{n_r} - 1 = 3^{n_r} - 1 = 26$. Then, we can deduce that the number of shift register is $n_r = 3$, and choose the feedback coefficients as $c_1 = c_3 = -1$ and $c_2 = 1$, which makes the common difference equation as:

$$x(k) = (-1) \otimes_3 x(k-1) \oplus_3 1 \otimes_3 x(k-2) \oplus_3 (-1) \otimes_3 x(k-3) \qquad \text{Eq.7-6}$$

By choosing the appropriate initial value of the register, the overall length of the test signal will be available by repeatedly using the difference equation.

The test signal generated by the difference equation only has three levels as 0, 1 and 2 which meaning we need to convert these values into our desired input values. Our current value should change from 70A to 90A.

Mapping PRTS to centered signal with the amplitude of $U = \frac{(90-70)}{2} = 10$.

This can be done by the following mapping equations:

0→0

1→ $2U/(r-1) = 2 \times 10/(3-1) = 10$

2→ $-2U/(r-1) = -2 \times 10/(3-1) = -10$

Then add 80A to each of the signal value obtained. We chose initial value as $x_1 = x_2 = 0, x_3 = 1$.

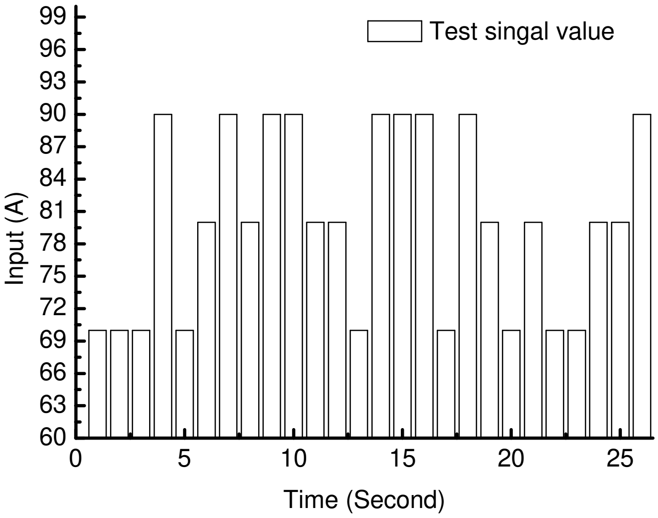

Figure 7-5, Plot of test signal values

In order to have better application of the test data, the sampling time should be chosen accordingly. The main consideration in choosing sample time is the time duration within the transients settles till 5%, which is denoted as $T_{95}$. The general requirement of sampling time is that $\Delta T / T_{95} \approx 0.05$. However, in this particular designed experiment, in order to get rid of the uncertainty in the transient stage, the whole test is designed after the system has entered the steady-state. In this context, the second important requirement of selecting the sampling time should be given. That is: the sampling time should be smaller than the smallest time constant $T_{\min}$ of the overall system in issue. Based on observation, I choose the sampling time to be 1 second, just in accordance to the specs above.

After several PRTS experiments, we can establish the single bypass current, total welding current and back-side welding profile width relationship as demonstrated in Figure 7-6.

Considering as GMAW process, there is inevitable noise with the input current which is not controllable. In later chapter, we will discuss some method to overcome the influence of noise.

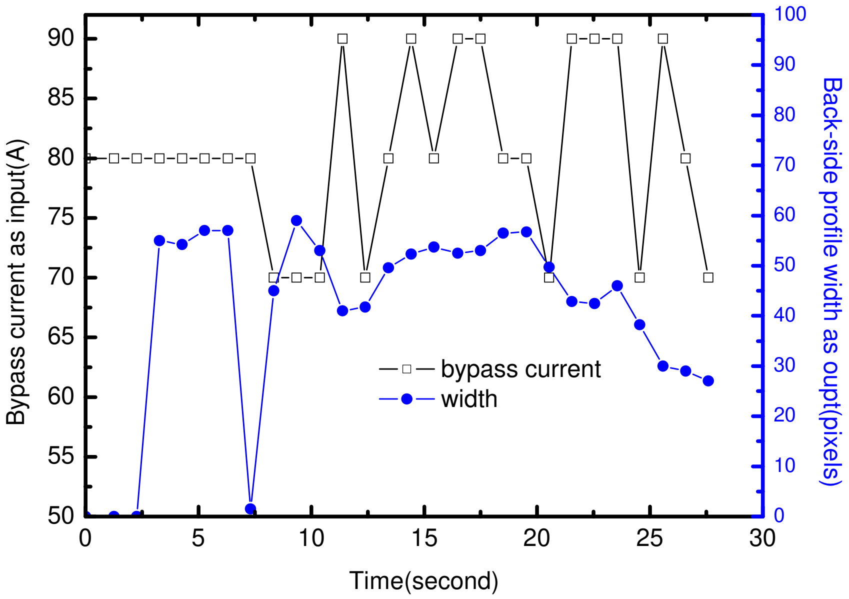

Figure 7-6, Bypass current and width waveform (PRTS)

### 7.3.2 Model validation

Model validation test is the process of determine whether the built model is adequate enough to represent the practical nonlinear system. Theoretically, there are many available models to choose from. However, there are several models commonly adopted in practical cases due to the consideration of easy establishment and controllability. The first commonly adopted model structure is called Generalized Hammerstein Model.

In various nonlinear system models, there is a type of model called Block Oriented Model. Generally, there are three categories of Block Oriented Model, named Hammerstein model, Wiener model and Wiener-Hammerstein model. The most frequently used model of such category is a modified one called Generalized Hammerstein model. Comparing with linear model, Hammerstein model has the term of the square of input, and the general expression is showed below:

$$y(k) = c_0 + \frac{B_1(q^{-1})}{A_1(q^{-1})} u(k) + \frac{B_2(q^{-1})}{A_2(q^{-1})} u^2(k)$$

Here, $A$ and $B$ are polynomials of the backward shift operator. However, this model in such form is nonlinear in parameter and thus hard to analyze and control. By introducing the common denominator:

$$A(q^{-1}) = A_1(q^{-1}) A_2(q^{-1})$$

Then, by multiplying this common denominator to both sides of the general expression, we get:

$$A(q^{-1}) y(k) = c_0 A(1) + A_2(q^{-1}) B_1(q^{-1}) u(k) + A_1(q^{-1}) B_2(q^{-1}) u^2(k)$$

Secondly, bilinear model is also very widely used basic model structure. For those models containing the square or cubic terms of the input $u(t)$, if the order of the corresponding terms are too high, the system usually becomes unstable due to significant error. Here, the bilinear model combines the input and output together to form a so-called bilinear term. The general form of the bilinear model is like:

$$A(q^{-1}) y(k) = c_0 + B(q^{-1}) u(k) + F(q^{-1}) u(k) y(k)$$

The two models given above are the most popular forms of nonlinear models. However, the practical system may have its own behavior, which may not fit these two models perfectly since they both have strict forms. In order to dig more models based on the two models above to better fit the system behavior, the combination of the fore-mentioned models is necessary.

There are many model validation methods and theorem. In this essay, two of those methods are given. The first way is probably the most easy-understood one: just plot estimated value and real value in the same coordination to see the error between them directly. Another method chosen here is to determine the effectiveness of each model by its relative mean square error (RMSE). This index has following form:

$$RMSE = \frac{\frac{1}{N}\sum_{k=1}^{N}[y(k) - \hat{y}(k)]^2}{\frac{1}{N}\sum_{k=1}^{N}[y(k) - \overline{y}(k)]^2} \qquad \text{Eq.7-7}$$

Where $\overline{y}(k)$ stands for the mean value of the output, and $\hat{y}(k)$ denotes the estimated value of output. Once the experimental data doesn’t change, the denominator of $RMSE$ will stay the same. Therefore, the smaller $RMSE$ means smaller the error of the model.

Experience indicates us that the current back-side profile width must have some relationship with previous output. So the first model structure we tested is:

$$\begin{aligned} y(k+3) &= c_0 - c_1 y(k+2) - c_2 y(k+1) - c_3 y(k) + b_1 u(k+2) + b_2 u(k+1) \\ &+ b_3 u(k) + d_1 u(k+2)^2 + d_2 u(k+1)^2 + d_3 u(k)^2 \end{aligned} \qquad \text{Eq.7-7}$$

By selecting a model structure like this, we assume that the output is influenced by three steps of previous output, three steps of previous input and three steps square value of previous input.

Considering the total 26 sampled data and the expression, we have $n = 3, m = 3, N = 23$. Thus, we have the related calculation matrix as:

$$y = \begin{bmatrix} y_{(4)} \\ y_{(5)} \\ \vdots \\ y_{(26)} \end{bmatrix}$$

$$\Phi_N = \begin{bmatrix} 1 & -y(3) & -y(2) & -y(1) & u(3) & u(2) & u(1) & u^2(3) & u^2(2) & u^2(1) \\ 1 & -y(4) & -y(3) & -y(2) & u(4) & u(3) & u(2) & u^2(4) & u^2(3) & u^2(2) \\ \vdots & \vdots & \vdots & \vdots & \vdots & \vdots & \vdots & \vdots & \vdots & \vdots \\ 1 & -y(25) & -y(24) & -y(23) & u(25) & u(24) & u(23) & u^2(25) & u^2(24) & u^2(23) \end{bmatrix}$$

By equation $\hat{\theta}_N = (\Phi_N^T \Phi_N)^{-1} \Phi_N^T y_N$, we can calculate the estimated parameters for this model. By substituting the experimental data into the matrix, we can calculate the estimation parameters matrix:

$$\hat{\theta}_N = \begin{bmatrix} -20.4589 \\ -0.8270 \\ 0.5087 \\ -0.1740 \\ -2.5279 \\ -1.1307 \\ 4.6156 \\ 0.0154 \\ 0.0090 \\ -0.0294 \end{bmatrix}$$

With the estimation parameter matrix, we can use the same input matrix to calculate simulated outputs with this model. The simulated outputs waveform and actual experimental data outputs are showed in Figure 7-7.

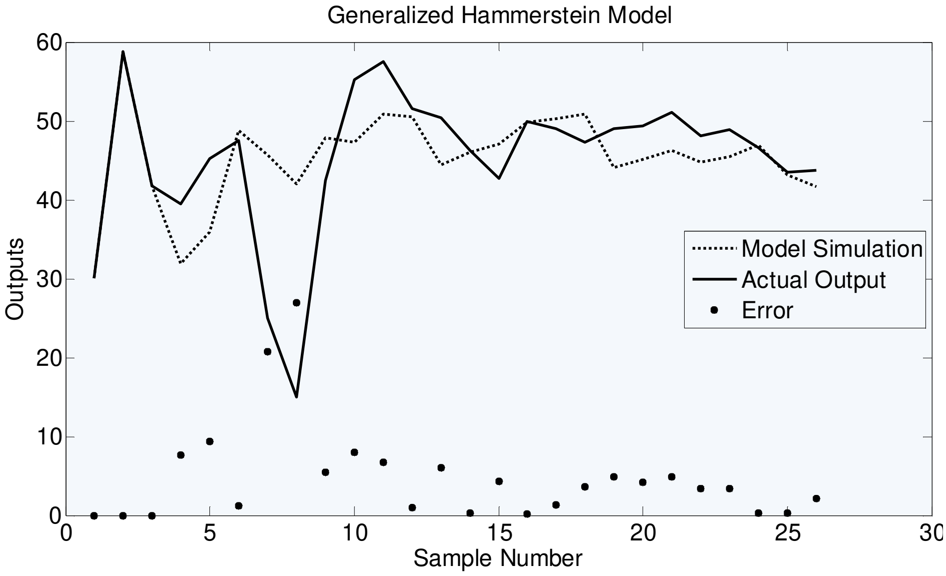

Figure 7-7, Simulation and actual output waveforms (Hammerstein)

The $RMSE$ calculated is 0.8290. Considering the inevitable disturbance and noise in any GMAW process, the $RMSE$ value is acceptable.

By observing the estimation parameter matrix, it is noticeable that the parameters involved with $u^2(k+2)$, $u^2(k+1)$, $u^2(k)$ are actually relatively small. It means that these three terms don't affect the output significantly. Moreover, these three nonlinear terms are very complicated in actual control algorithm which could cause serious problems. Thus, it is possible and benefic for us to search a simpler model structure such as bilinear model structure.

The bilinear model structure we choose follows Eq.7-8:

$$y(k+3) = c_0 - c_1 y(k+2) - c_2 y(k+1) + b_2 u(k+1) + b_3 u(k) + d_0 u(k) \bullet y(k) \qquad \text{Eq.7-8}$$

This model structure is simpler than the one demonstrated in Eq.7-7. The term $u(k) \bullet y(k)$ is adopted to represent the nonlinearity of the process in stead of $u^2(k+2)$, $u^2(k+1)$, $u^2(k)$. Plus, we take out terms as $u(k+2)$ and $y(k)$ to make the model structure even simpler. Since $u(k+2)$ and $y(k)$ are also relatively less significant than other similar terms. The related calculation matrix can be rewritten into:

$$y = \begin{bmatrix} y_{(4)} \\ y_{(5)} \\ \vdots \\ y_{(26)} \end{bmatrix}$$

$$\Phi_N = \begin{bmatrix} 1 & -y(3) & -y(2) & u(2) & u(1) & u(1)*y(1) \\ 1 & -y(4) & -y(3) & u(3) & u(2) & u(2)*y(2) \\ \vdots & \vdots & \vdots & \vdots & \vdots & \vdots \\ 1 & -y(25) & -y(24) & u(24) & u(23) & u(23)*y(23) \end{bmatrix}$$

By using $\hat{\theta}_N = (\Phi_N^T \Phi_N)^{-1} \Phi_N^T y_N$, we can calculate the estimation parameter matrix:

$$\hat{\theta}_N = \begin{bmatrix} 94.6489 \\ -0.3638 \\ 0.0347 \\ -0.3929 \\ -0.2911 \\ -0.0014 \end{bmatrix}$$

With the new model and new estimation parameter matrix, we can evaluate our new model structure.

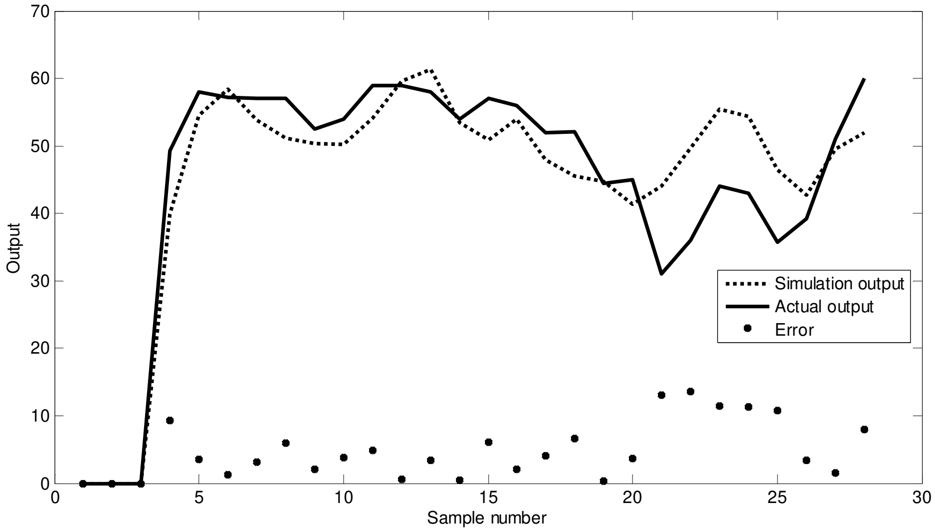

Figure 7-8, Simulation and actual output waveforms (Bilinear)

The *RMSE* for this bilinear model structure is 0.2657 which is obviously better than the General Hammerstein model.

Step response is a common way for model structure validation besides *RMSE* .

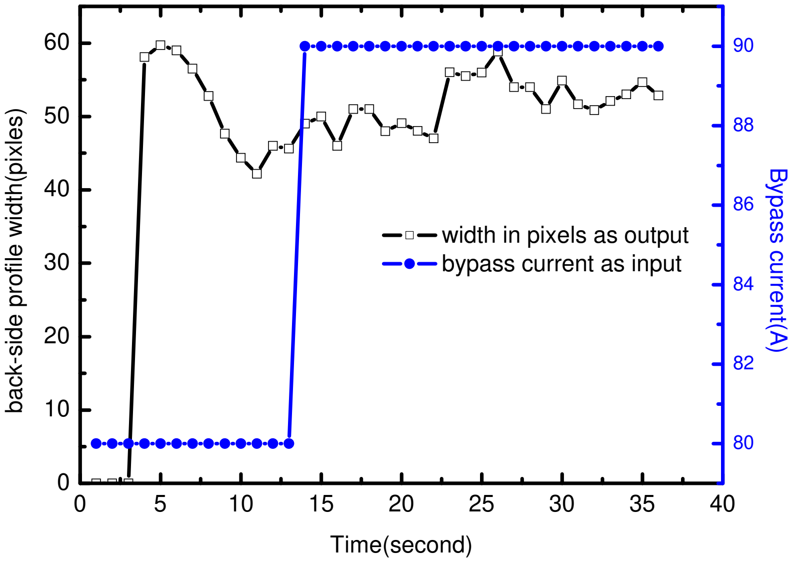

Figure 7-9, Input and output waveforms of system step response

Since we already have a model with parameters, by putting the step response input into the model, the step response simulated by the model is calculated. The result of comparison between simulation and actual data of step response is demonstrated in Figure 7-10.

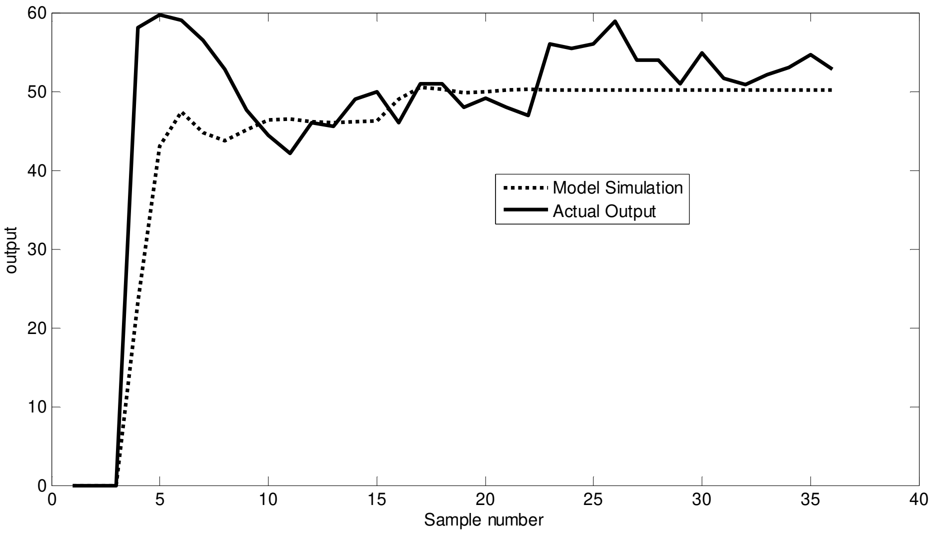

Figure 7-10 Simulation and actual output of step response for bilinear model

Figure 7-10 shows a good result for the bilinear model in step response simulation. In our model, there is no term describing the influence of noise and disturbance of the process, and that is the reason the actual output oscillation is not reflected in the simulation.

The stability of GMAW process is naturally much worse than GTAW due to its characteristics. For a GTAW process, the welding current and voltage can be fixed as stable as a constant. However, a 5-10% disturbance or noise in welding current and voltage during GMAW process is always common and inevitable due to the unique characteristic of GMAW process. In Figure 7-6 and Figure 7-9, the bypass current waveform is constructed by our input signal to the welding machine. With the influence of noise, the actual current collected by the current sensor is showed in Figure 7-11 and Figure 7-12.

Technically, we can include a term to simulate the noise influence of the process. However, it is very likely that the accuracy of the model won't be improved evidently by doing this. First of all, it is very difficult to identify whether the noise is a white noise or a color noise. Secondly, it is also very difficult to estimate the related parameter of the noise.

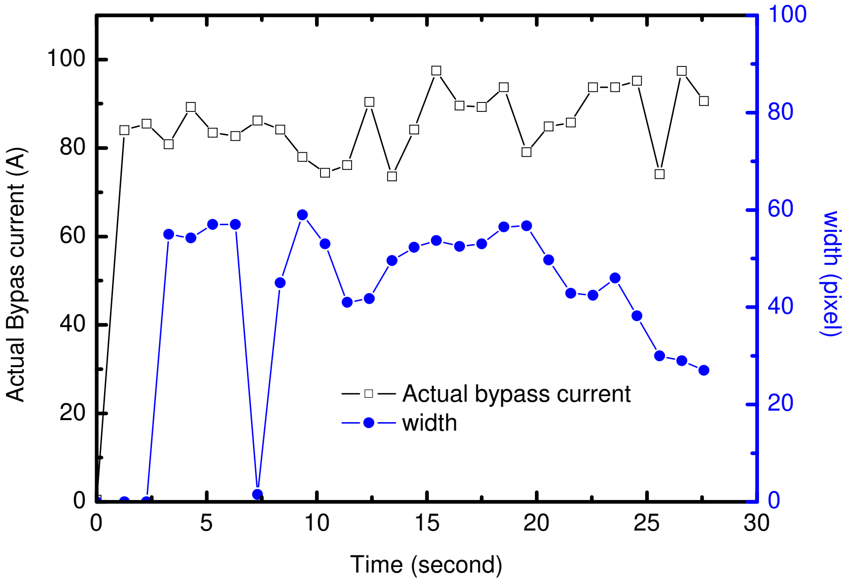

Figure 7-11, Actual PRTS current and width output

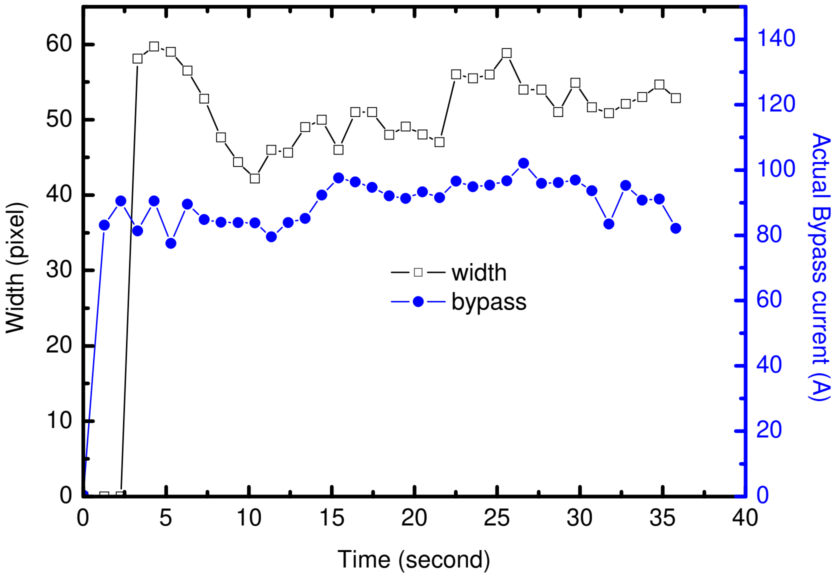

Figure 7-12, Actual step response bypass current and width output

Exclusive of current disturbance, there are many other factors influencing the output such as slight torch distance difference and radiation condition which are also difficult to be reflected in the model construction. However, a small difference between these conditions can cause significant alteration of the output result.

Based on the fact that the parameters of model might change themselves due to the influences from other uncontrollable factors, we will develop our control algorithm using adaptive control technique. The details of control algorithm design will be discussed in next chapter.

# CHAPTER 8

## Robust adaptive nonlinear control of full penetration on DB-GMAW

In this chapter, the procedure of control algorithm design of full penetration on DB-GMAW is discussed. First of all, the common techniques of control on welding process are introduced. We will cover the basic knowledge of adaptive control, predictive control and robust boundedness. Secondly, details of nonlinear control algorithm designing on our process would be revealed.

### 8.1 Control of full penetration on DB-GMAW

The full penetration process is a non-minimum phase plant with large and variable model order, large and variable delays and variable model parameters [59]. Due to this fact, adaptive control is widely adopted in welding process control including both GTAW process [60] and GMAW process [61].

In previous chapter, the procedure of system parameter estimation using least squares and regression models has been introduced. We use that technique to establish our bilinear model of DB-GMAW. For a dynamic system such as DB-GMAW, the parameters of the model vary from time to time. As a result, On-line determination of process parameters is a key element in adaptive control [58]. A recursive parameter estimator appears explicitly as a component of a self-tuning regulator. Parameter estimation also occurs implicitly in a model-reference adaptive controller [58].

In adaptive controllers, the observations are obtained sequentially in real time. It is then desirable to make the computations recursively to save computation time. Computation of the least-squares estimate can be arranged in such a way that the results obtained at time $t-1$ can be used to get the estimates at time $t$. The solution in Eq.7-5 to the least-squares problem will be rewritten in a recursive form. Let $\hat{\theta}(t-1)$ denote the least square estimate based on $t-1$ measurements. Assume that the matrix $\Phi^T\Phi$ is nonsingular for all $t$. Now, define [58]:

$$y(i) = \varphi_1(i)\theta_1^0 + \varphi_2(i)\theta_2^0 + \cdots + \varphi_n(i)\theta_n^0 = \varphi^T(i)\theta^0$$

Where $\varphi^T(i) = (\varphi_1(i) \quad \varphi_2(i) \quad \cdots \quad \varphi_n(i))$

And $\theta^0 = (\theta_1^0 \quad \theta_2^0 \quad \cdots \quad \theta_n^0)$

Thus, $\Phi(t) = \begin{pmatrix} \varphi^T(1) \\ \vdots \\ \varphi^T(t) \end{pmatrix}$

Now, we can define $P(t)$ as:

$$P(t) = (\Phi^T(t)\Phi(t))^{-1} = (\sum_{i=1}^{t} \varphi(i)\varphi^T(i))^{-1} \qquad \text{Eq.8-1}$$

So that:

$$\begin{aligned} P(t)^{-1} &= \Phi^T(t)\Phi(t) = \sum_{i=1}^{t} \varphi(i)\varphi^T(i) \\ &= \sum_{i=1}^{t-1} \varphi(i)\varphi^T(i) + \varphi(t)\varphi^T(t) = P^{-1}(t-1) + \varphi(t)\varphi^T(t) \end{aligned} \qquad \text{Eq.8-2}$$

The least-squares estimate $\hat{\theta}(t)$ can be written as:

$$\hat{\theta}(t) = P(t)(\sum_{i=1}^{t} \varphi(i)y(i)) = P(t)(\sum_{i=1}^{t-1} \varphi(i)y(i) + \varphi(t)y(t)) \qquad \text{Eq.8-3}$$

From Eq.8-2 and Eq.8-3, we know that:

$$\sum_{i}^{t-1} \varphi(i)y(i) = P^{-1}(t-1)\hat{\theta}(t-1) = P^{-1}(t)\hat{\theta}(t-1) - \varphi(t)\varphi^T(t)\hat{\theta}(t-1) \qquad \text{Eq.8-4}$$

The estimate at time $t$ can now be written as:

$$\begin{aligned} \hat{\theta}(t) &= \hat{\theta}(t-1) - P(t)\varphi(t)\varphi^T(t)\hat{\theta}(t-1) + P(t)\varphi(t)y(t) \\ &= \hat{\theta}(t-1) + P(t)\varphi(t)(y(t) - \varphi^T(t)\hat{\theta}(t-1)) \\ &= \hat{\theta}(t-1) + K(t)\varepsilon(t) \end{aligned} \qquad \text{Eq.8-5}$$

Where $K(t) = P(t)\varphi(t)$

$$\varepsilon(t) = y(t) - \varphi^T(t)\hat{\theta}(t-1)$$

The residual $\varepsilon(t)$ can be interpreted as the error in predicting the signal $y(t)$ one step ahead based on the estimate $\hat{\theta}(t-1)$ [58].

For nonsingular square matrices $A, C$ and $C^{-1} + DA^{-1}B$, we know that $A + BCD$ is invertible, plus:

$$(A + BCD)^{-1} = A^{-1} - A^{-1}B(C^{-1} + DA^{-1}B)^{-1}DA^{-1} \qquad \text{Eq.8-6}$$

The proof of above equation will not be detailed here. Proof can be found at Page 50 in Ref. 58.

By combining Eq.8-1, 8-2 and 8-6, we know that:

$$\begin{aligned} P(t) &= (\Phi^T(t)\Phi(t))^{-1} = (\Phi^T(t-1)\Phi(t-1) + \varphi(t)\varphi^T(t))^{-1} \\ &= (P(t-1)^{-1} + \varphi(t)\varphi^T(t))^{-1} \\ &= P(t-1) - P(t-1)\varphi(t)(I + \varphi^T(t)P(t-1)\varphi(t)^{-1}\varphi^T(t))P(t-1) \end{aligned} \qquad \text{Eq.8-7}$$

Finally, we have recursive least-squares estimation (RLS). Assume that the matrix $\Phi(t)$ has full rank, that is, $\Phi^T(t)\Phi(t)$ is nonsingular, for all $t \geq t_0$. Given $\hat{\theta}(t_0)$ and $P(t_0) = (\Phi^T(t_0)\Phi(t_0))^{-1}$, the least–squares estimate $\hat{\theta}(t)$ then satisfies the recursive equations

$$\begin{aligned} \hat{\theta}(t) &= \hat{\theta}(t-1) + K(t)(y(t) - \varphi^T(t)\hat{\theta}(t-1)) \\ K(t) &= P(t)\varphi(t) = P(t-1)\varphi(t)(I + \varphi^T(t)P(t-1)\varphi(t))^{-1} \\ P(t) &= P(t-1) - P(t-1)\varphi(t)(I + \varphi^T(t)P(t-1)\varphi(t))^{-1}\varphi^T(t)P(t-1) \\ &= (I - K(t)\varphi^T(t))P(t-1) \end{aligned} \qquad \text{Eq.8-8}$$

### 8.2 Control algorithm design

Assuming at moment $k$, the actual output $y(k)$ is collected by the feedback system. We will assume the initial $\hat{\theta}(1)$ is an all one matrix. So at moment $k$,

$$\varphi^T(k) = \begin{bmatrix} 1 & u(k-2) & u(k-3) & u(k-3)y(k-3) & -y(k-1) & -y(k-2) \end{bmatrix}$$

And $\varepsilon(k) = y(k) - \varphi^T(k)\hat{\theta}(k-1)$

According to Eq.8-8, we can calculate $\hat{\theta}(k)$. After obtaining $\hat{\theta}(k)$, we can make an one step prediction about $\hat{y}_p(k+1)$ if we assume the input doesn't change.

Recall the model structure demonstrated in Eq.7-8, we know that:

$$\begin{aligned}\hat{y}_p(k+1) &= \hat{\theta}_1(k) + \hat{\theta}_2(k)u(k-1) + \hat{\theta}_3(k)u(k-2) + \hat{\theta}_4(k)u(k-2)y(k-2) \\ &- \hat{\theta}_5(k)y(k) - \hat{\theta}_6(k)y(k-1)\end{aligned} \qquad \text{Eq.8-9}$$

Assume that:

$$u(k-1) = -\frac{\hat{\theta}_3(k)}{\hat{\theta}_2(k)}u(k-2) - \frac{\hat{\theta}_4(k)}{\hat{\theta}_2(k)}u(k-2)y(k-2) - \frac{\hat{\theta}_1(k)}{\hat{\theta}_2(k)} + \nu(k-1) \qquad \text{Eq.8-10}$$

Substitute Eq.8-10 into Eq.8-9, we have:

$$\hat{y}_p(k+1) = -\hat{\theta}_5(k)y(k) - \hat{\theta}_5(k)y(k-1) + \hat{\theta}_2(k)\nu(k-1) \qquad \text{Eq.8-11}$$

Assume our desired output is $\omega$, our goal is to find out a value for $y(k+2)=\omega$. In other words, we need to find out a $\nu(k)$ to do that. From Eq.8-10, we can develop that:

$$\begin{aligned}\nu(k) &= \frac{1}{\hat{\theta}_2(k)}(\omega + \hat{\theta}_5(k)\hat{y}_p(k+1) + \hat{\theta}_6(k)y(k)) \\ &= u(k) + \frac{\hat{\theta}_3(k)}{\hat{\theta}_2(k)}u(k-1) + \frac{\hat{\theta}_4(k)}{\hat{\theta}_2(k)}u(k-1)y(k-1) + \frac{\hat{\theta}_1(k)}{\hat{\theta}_2(k)}\end{aligned} \qquad \text{Eq.8-12}$$

Thus, the next input $u(k)$ can be calculated by Eq.8-13:

$$\begin{aligned}u(k) &= \frac{1}{\hat{\theta}_2(k)}(\omega - \hat{\theta}_1(k) - \hat{\theta}_3(k)u(k-1) - \hat{\theta}_4(k)u(k-1)y(k-1) \\ &+ \hat{\theta}_5(k)\hat{y}_p(k+1) + \hat{\theta}_6(k)y(k))\end{aligned} \qquad \text{Eq.8-13}$$

Another important idea of our control design is to use the parameter projection algorithm in the online estimation. The basic idea of parameter projection algorithm can be indicated in Eq.8-14 [63]:

$$\hat{\theta}(t) = P\left\{\hat{\theta}(t-1) + \frac{\phi(t-1)e(t)}{1+\phi^T(t-1)\phi(t-1)}\right\} \qquad \text{Eq.8-14}$$

Where $\hat{\theta}(t)$ denotes the estimate of $\theta_*$ at $t$ and $P$

represents the projection operator necessary to ensure

$\hat{\theta}(t) \in \wp \forall t$. $e(t)$ is the prediction error defined as

$$e(t) = y(t) - \phi^T(t-1)\hat{\theta}(t-1)$$

Considering our practical restriction of output value, $u(k)$ needs to be bounded within 70-90A. Thus, if the calculated $u(k)$ is larger than 90A, it is forced to equal to 90A; if the calculated $u(k)$ is smaller than70, it is forced to equal to 70A. Eq.8-14 performs such projection for our control algorithm. In 1992, Changyun Wen and David, Hill had indicated that such projection operation doesn't change the stability of the system [63].

The constant parameters of control experiments also follow Table 7-1. The basic structure of control experimental system is showed in Figure 8-1. Plus, the structure of control algorithm is showed in Figure 8-2.

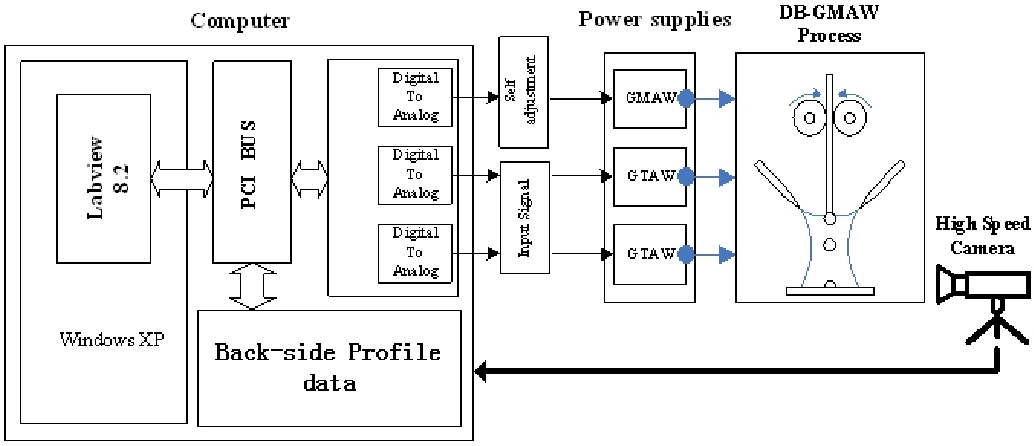

Figure 8-1, Structure of control experimental system

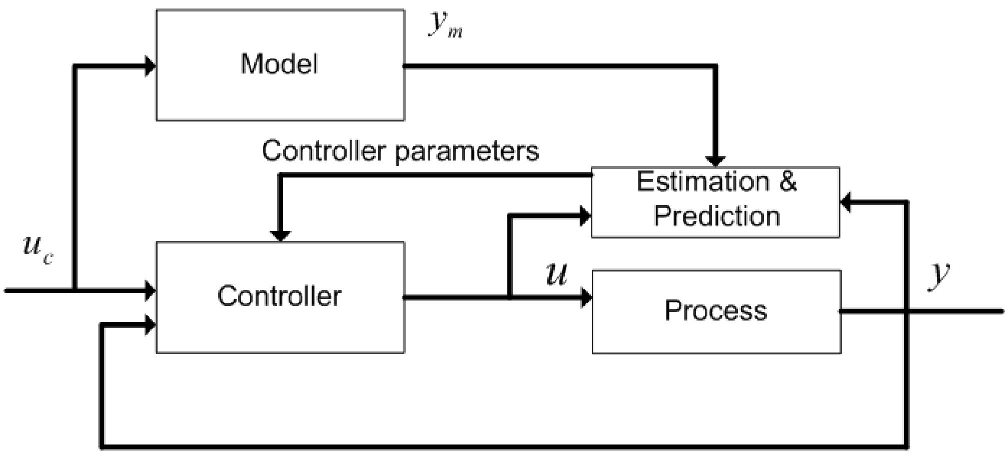

Figure 8-2, Structure of control algorithm

The simulation result of our control algorithm is showed in Figure 8-3, the desired output value $\omega$ is set as 45 pixels.

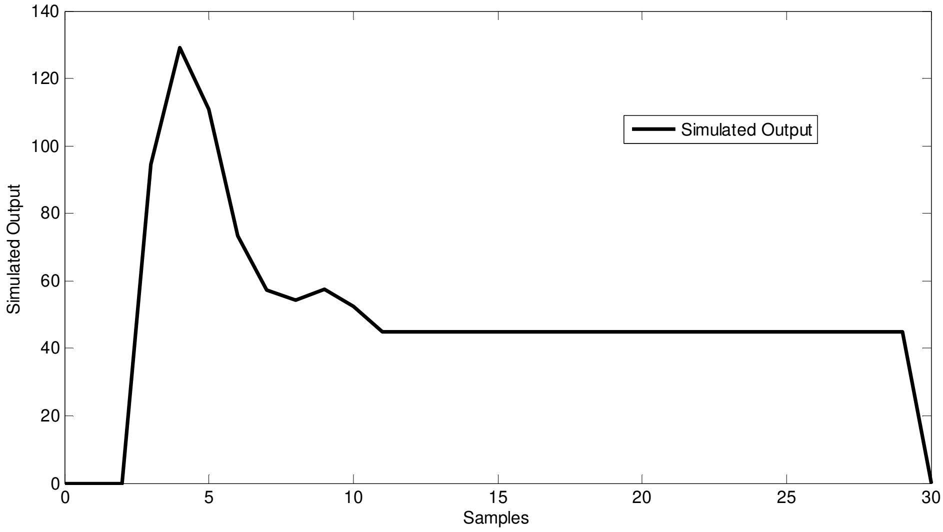

Figure 8-3, Simulation result of control algorithm

After Matlab Simulation, we use the control algorithm to test real-time control of DB-GMAW process. Figure 8-4 shows the control result of this algorithm. The preset reference value of Figure 8-4 is also 45 pixels.

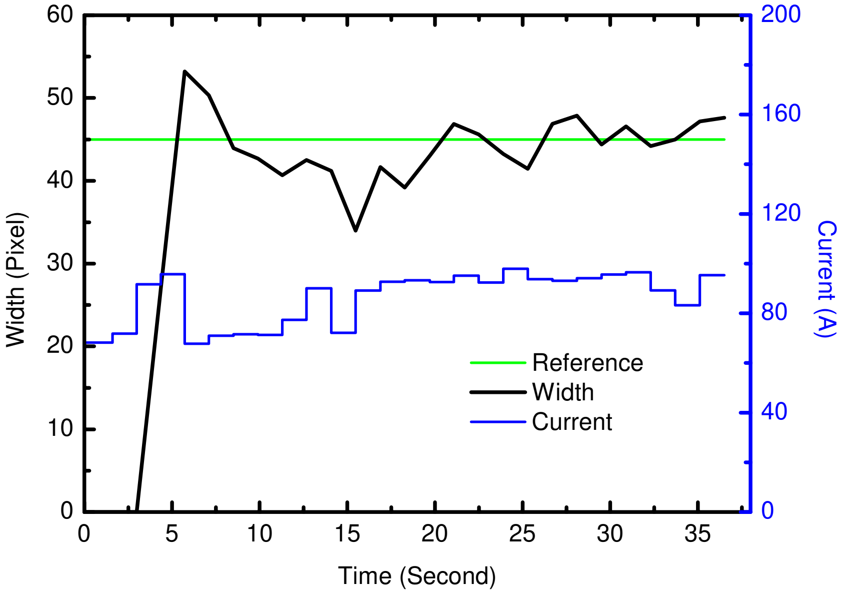

Figure 8-4, On-line control result of DB-GMAW process

From Figure 8-4, we can tell that it takes approximately 15-18 steps for the process to approach to the reference value and get steady. This observation agrees with the simulation result showed in Figure 8-3.

We also test the robustness of our control algorithm. According to our current welding speed and work piece geography, the approximate time of one weld process is 40 second. The data demonstrated in Figure 8-4 is also collected under this welding speed. To test the robustness of the control algorithm, I change the welding speed from 40 second a circle to 37 second a circle during the process. Figure 8-5 shows the data of our test.

In Figure 8-5, after the process approaches stable around 17 seconds, the welding speed is changed to 37 second a circle. After the occurrence of this disturbance, the width of back-side profile goes unstable first and then to zero which means that full penetration is not achieved at that moment. Full penetration was achieved again around 12 steps after the disturbance. Unfortunately, the experiment is not long enough to see the process approaching stable again after disturbance. However, the robustness test demonstrates the control algorithm's ability to cope with disturbance.

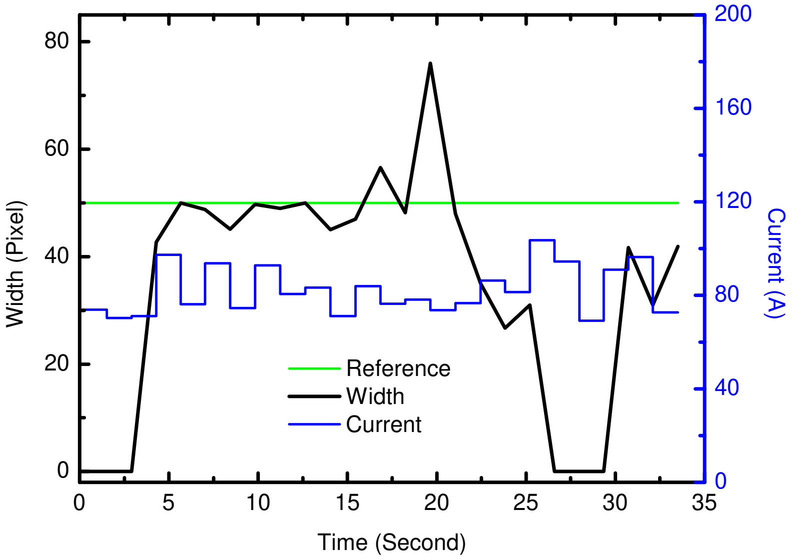

Figure 8-5, Control result of robustness test

Figure 8-6 shows an open loop process of DB-GMAW. In the experiment of Figure 8-6, the input is set as a constant of 80A. As we can see, when the input is constant, the back-side profile width can not stabilize itself at a certain level. Thus, the nonlinear adaptive control is benefic to stable the penetration level.

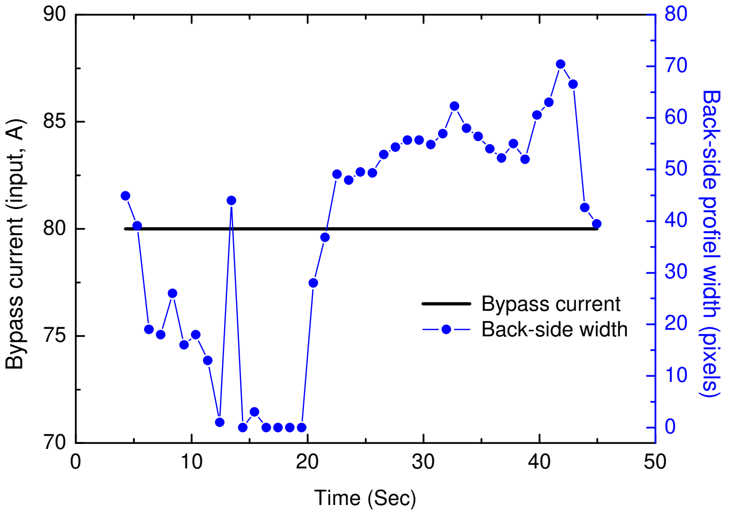

Figure 8-6, Open loop penetration of DB-GMAW (80A)

### 8.3 Chapter conclusion

In this chapter, the control algorithm is designed for DB-GMAW full penetration control via nonlinear adaptive control techniques. Stimulation results are compared with actual output for verification. Robustness of the control system is also tested. We can draw several conclusions based on our design activity:

1. Adaptive control technique is very essential in welding process control due to the Characteristics of typical GMAW. The complicated physical process of GMAW process makes it very difficult to establish a precise model for penetration prediction. The parameters of the model will not stay constant which means online parameter estimation is very important technique to be adopted.
2. The control algorithm design in this chapter is benefic to stabilize penetration level of DB-GMAW. The stimulation result verifies the feasibility to the algorithm. The actual output demonstrated that the penetration can be maintained within desired level.

## CHAPTER 9

## Conclusion and Future Work

### 9.1 Conclusion

Welding processes are widely used in many manufacturing areas, such as automotive, aerospace and shipbuilding industries. As one of the most widely adopted light metal, aluminum plays essential role in many manufacturing areas, such as automotive, aerospace and shipbuilding industry. GMAW is the most important aluminum industrial joining method. Any improvement of aluminum GMAW process has the ability and potential to bring significant benefit to related industries.

In this dissertation, the author developed a novel GMAW of aluminum which is believed to have the potential of producing lower base metal heat input and better efficiency than traditional aluminum GMAW. The basic structure of this dissertation can be divided into four parts: Process construction (Chapter.1, Chapter.2 and Chapter.3); Physical characteristic analysis (Chatper.4 and Chapter. 5); Image processing of process (Chatper.6); Modeling and Control design of process (Chapter.7, Chapter.8 and Chapter.9). In process construction, we basically introduced the background information of the research and the working theory of DB-GMAW. The advantages of DB-GMAW are revealed and the physical construction of DB-GMAW is established. In physical characteristic analysis, we theoretically analyzed metal transfer and base metal heat input of DB-GMAW. Plus, we verified our theoretical analysis via experiments. In image processing of process, we develop different procedures of image processing method for DB-GMAW to obtain an appropriate feedback design. Finally, in Modeling and Control design of process, we introduced the knowledge of nonlinear modeling technique and control theory. We established a nonlinear model of DB-GMAW and adopted this model into simulation and control design.

The main achievement and contribution of the dissertation can be summarized as follow:

1. Proposed a novel GMAW process to improve efficiency and stability of traditional GMAW of aluminum. The new GMAW, DB-GMAW, uses two GTAW systems as bypasses to reduce base metal heat input without compromising welding quality and efficiency.
2. Established a GMAW platform following proposed method. During construction, a series of experiments are performed to ensure the validity and stability of process. The parameters selected after experiments are sufficient to provide a stable DB-GMAW, which give a very helpful guide for further system development.
3. Research the physical characteristics of DB-GMAW both theoretically and experimentally. The unique characteristics of DB-GMAW is explained by previous theoretical work and verified by designed experiments, which is meaningful for further research.
4. Design an appropriate image processing approach for DB-GMAW. This research developed three different approaches for DB-GMAW image processing and compared their advantages and disadvantages. These different algorithms can be helpful for further research of DB-GMAW.
5. Design a nonlinear modeling and control algorithm for DB-GMAW. By using PRTS test signal, we test the system model with several different model structures. Based on the model, a nonlinear control algorithm is developed. The control algorithm shows that although welding process is a very complicated multi-physics process, an appropriate control design can still improve the stability of the process.

### 9.2 Future work

The main objective of the research is to establish a novel GMAW process which has the ability to reduce base metal heat input and increase efficiency and stability. To ensure the reliability and exploit the industrial potential of DB-GMAW, more work in different aspects can be done to improve the design and control of DB-GMAW, which includes:

1. Substitute the GTAW bypasses with GMAW bypasses: It is a significant

way to improve productivity by replacing GTAW bypasses with GMAW bypasses. With a relative smaller welding current, the productivity can be even tripled by doing that. In the beginning of the chapter, we have already introduced Consumable DE-GMAW which could provide obvious improvement of productivity. By adding another GMAW bypass, we can further develop Consumable Double Electrode GMAW into Consumable Triple Electrode GMAW. The feasibility of triple Electrode GMAW has been tested by DB-GMAW process. In build up welding or resurfacing welding, high productivity with low base metal heat input is essential for manufacturing efficiency and quality control.

2. Improve the image processing algorithm: In the dissertation, we applied different image processing techniques to DB-GMAW. For practical reason, the final selected method is back-side profile monitoring. However, there are many advantages of front-side profile detection and droplet information detection, especially droplet information detection. The droplet information detection provides lots of information about the profile and process. Although it is still very difficult to determine an exact control decision making through droplet information detection, the potential of this detection is very huge. We believe that the droplet information detection can be an excellent welding processing analytical application once a better understanding and faster algorithm is developed.
3. Control algorithm design: Although some initial stage work of modeling and control has been accomplished in this dissertation, the research of control design for DB-GMAW still requires plenty of further work. First of all, the sampling rate of image processing is currently slow. In the future, a c language based platform should be developed for a faster image processing rate which can improve the model accuracy significantly. As a complicated process, DB-GMAW can be easily developed into a MIMO (Multi-input multi-output) nonlinear system. Currently, we fixed many system parameters to construct a SISO system. In the future, we can

develop a new adaptive control algorithm for the MIMO process. A MIMO nonlinear model is very benefic to further understanding and control of DB-GMAW since a MIMO nonlinear model has the wider capability to indicate system behaviors. Adaptive control algorithm for the MIMO system means better system stability.

# REFERENCE

[1] O'Brien, R. L., "Welding handbook: Welding processes".2 [M], Eighth Edition. Miami, FL, American Welding Society, 1991.

[2] Song, T. H., "Welding handbook: Welding methods and equipments".1 [M], Second Edition. Beijing, P R China, Chinese Welding Society, 2001.

[3] Li, K. H., Chen, J. S. and Zhang, Y. M., "Double-electrode GMAW process and control" [J] , Welding Journal, 86(8)-231s-237s, 2007.

[4] Li, K. H. and Zhang, Y. M., "Metal transfer in double-electrode gas metal arc welding" [J], Journal of Manufacturing Science and Engineering-Transaction of the ASME, 129(6): 991-999, 2007.

[5] Lincoln Electric Co, "The procedure handbook of welding". [M], 12th Edition, Cleveland, Ohio, Lincoln Electric Co, 1973.

[6] Liu, X. P., Li, K. H., Zhang, Y. M. and Johnson, Q. M., "Dual Bypass GMAW of Aluminum" [J]. Transactions of NAMRI/SME, Vol.35: 335-341, 2007.

[7] Cary, H. B. and Scott, C. H., "Modern Welding Technology" [M]. Upper Saddle River, NJ, Pearson Education, 2005.

[8] Serope, K. and Schmid, S. R. "Manufacturing and Engineering and Technology" [M]. Prentice Hall, 2001.

[9] Althouse, A. D., Turnquist, C. H., Bowditch, W. A. and Bowditch, K. E. "Modern Welding" [M]. South Holland, ILL: The Goodheart – Willcox Company, Inc., 1984.

[10] Fennander, H., Kyrki, V., Fellman, A., Saleminen, A. and Kälviäinen, H. “Visual measurement and tracking in laser hybrid welding” [J]. Machine Vision and Applications, s00138-007-0111-1, 2007.

[11] Schubert, E. “Process Stability of Automated Gas Metal Arc Welding of Aluminum” [M]. Springer Berlin/Heidelberg, Vol299, 2004.

[12] Ueyama, T., Ohnawa, T., Tanak, M. and Nakata, K. “Effects of torch configuration and welding current on weld bead formation in high speed tandem pulsed gas metal arc welding of steel sheets” [J]. Science and Technology of Welding & Joining, Vol10: 750-759, 2005.

[13] Lin, S. B., Gang, T., Yang, C. L. and Cui, H. B. “An initial study on welding procedure using tandem MIG welding of high strength aluminum alloy” [J]. China Welding, Vol2, 2004.

[14] Li, K. H. and Zhang, Y. M. “Consumable Double-Electrode GMAW Part 1: The Process,” Welding Journal, 87(1): 11s-17s, 2008.

[15] http://en.wikipedia.org/wiki/Electric_arc.

[16] Song, T. H., “Welding handbook: Welding methods and equipments”.2 [M], Second Edition. Beijing, P R China, Chinese Welding Society, 2001.

[17] Klas, W., “Welding processes handbook.” [M], New York: CRC Press LLC. 2003.

[18] Ed, C. “Gas Metal Arc & Flux Cored Welding Parameters”. [M], Chicago: Weldtrain. 1991.

[19] Heald, P. R., Madigan, R B., Siewert, T. A and Liu, S. “Mapping the droplet transfer modes for an ER100S-1 GMAW electrode”. [J], Welding Journal, Vol.73: 38s-44s, 1994.

[20] Fan, H. G. and Kovacevic, R. “Droplet formation, Detachment, and Impingement on the molten pool in Gas Metal Arc Welding”. [J], Metallurgical and Materials Transactions B, 30 (4): 791-801, 1999.

[21] Waszink, J. H. and Graat, L. H J. “Experimental investigation of the forces acting on a drop of weld metal”. [J], Welding Journal, 62(4): 108-116, 1983.

[22] Allum, C. J. “Metal transfer in arc welding as a varicose instability. Ⅰ. Varicose instabilities in a current-carrying liquid cylinder with surface charge”. [J], Journal of Physics D: Appl. Phys, 18 (7):1431-1446, 1985.

[23] Allum, C. J. “Metal transfer in arc welding as a varicose instability. Ⅱ. Development of model for arc welding”. [J], Journal of Physics D: Appl. Phys, 18 (7):1447-1468, 1985.

[24] Hu, J. and Tsai, H. J. “Droplet acceleration in the arc”. [M], Innovative algorithms and techniques in Automation, Industrial Electronics and Telecommunications, PP: 211-217, 2007.

[25] Celina, M. S and Scotti, A. “The influence of double pulse on porosity formation in aluminum GMAW”. [M], Journal of Material Processing Technology, 171(Feb): 366-372, 2006.

[26] Praveen, P., Yarlagadda, P. K. D.V and Kangb, M. J. “Advancements in pulse gas metal arc welding”. [J], Journal of Material Processing Technology, 164-165(May): 1113-1119, 2005.

[27] Lancaster, J. F. “The physics of welding”. [M], Oxford, England, Pergamon Press.

[28] Shibata, K., Sakamoto, H. I. “Laser-MIG hybrid welding of aluminum alloys”. [J]. Welding in the World, 2006, 50(1-2): 28-34.

[29] Appel, L., Serve, M., Baum, L., and Cramer, H. “High-quality and economically viable coating by means of tandem gas-shielded metal-arc welding”. [J]. Welding Research Abroad, 2003, 41(1): 18-23.

[30] Morehead, T. “Automatic multi-wire GMAW multiplies productivity”. [J]. Welding Journal, 2003, 82(6):40-43.

[31] Merklein, M., and Geiger, M. “New materials and production technologies for innovative lightweight constructions”. Journal of Materials Processing Technology, 2002, 45(5): 532-536.

[32] Joseph, C., and Benedyk, K. “Light metals in automotive applications”. Light metal age, 2000, 10(2): 34-35.

[33] Kim, Y. S., and Eagar, T. W. “Analysis of metal transfer in gas metal arc welding”. Welding Journal, 1993, 72 (6):269-277.

[34] Wang, G., Huang, P, G., and Zhang Y M. “Numerical analysis of metal transfer in gas metal arc welding under modified pulsed current conditions”. Metallurgical and Materials Transactions B, 2004, 35B (8):857-866.

[35] Lin, Q., Li, X., and Simpson, S. W. “Metal transfer measurement in gas metal arc welding”. Journal of Physics D, 2001, 4(3):347-353.

[36] Tong, H. Ueyama, T., Nakata, K., and Ushio, M. “High speed welding of

aluminum alloy sheets using laser assisted alternating current pulsed metal inert gas process". [J]. Science and Technology of Welding and Joining, 2003, 8(3):229-234.

[37] Hoyaux, M. H. "Arc physics". [M]. Springer-verlag, New York. 1968.

[38] Tsai, M. C., and Kou S. "Electromagnetic-Force-Induced Convection in Weld Pools with a Free Surface". Welding Journal, 1990, 69(6):P241s-246s.

[39] Lin, M.L., and Eagar, T. W. "Influence of arc pressure on weld pool geometry". Welding Journal, 1985, 64(6):163s-169s.

[40] Rokhlin, S. I., and Guu, A. C. "A Study of Arc Force, Pool Depression, and Weld Penetration during Gas Tungsten Arc Welding". Welding Journal, 1993, 72(8):P381s-390s.

[41] Tsai, M. C., and Kou, S. "Electromagnetic-Force-Induced Convection in Weld Pools With a Free Surface". Welding Journal, 1990, 69(6): P241s-246s.

[42] Ushio, M., and Wu, C. S. "Mathematical modeling of three-dimensional heat and fluid flow in a moving gas metal arc weld pool". [J], Metallurgical and Materials Transactions B, 1997, 28(3): 509-516.

[43] Pan, J. L. "Fundamental and Practical Approaches to the Reliability of Welded Structure". [J], Welding arc control system, 4th Int. Symp. Of JWS, 1982, Vol. Ⅰ, pp.23-28.

[44] Pan, J. L., "Welding arc control system". [M], Chinese J. of Mech. Eng., 1983, No.1 pp.1-8.

[45] Gonzalez, R, C. and Woods, R, E., "Digital Image processing". [M], second

edition. Publishing House of Electronics Industry, Beijing, 2002.

[46] Wang, Z, Z. and Zhang, Y, M., “Image processing algorithm for automated monitoring of metal transfer in double-electrode GMAW”. [J]. Measurement science & technology, 2007, Vol. 18:2048-2058.

[47] Bicknell, A., Smith, J. C., and Lucas, J. “Arc voltage sensor for monitoring of penetration in TIG welds”. [J]. Science, Measurement & Technology, 1994, Vol. 141: 513-520.

[48] Zhang, M. X., Wu, C.S., Li, K. H., and Zhang, Y. M. “FEA based prediction of weld dimension in new DE-GMAW process”. [J]. Transactions of the China welding Institution. 2007, Vol. 28:33-39.

[49] Hirose, A., Kobayashi, K. F., and Todaka, H. “$CO_2$ laser beam welding of 6061-T6 aluminum alloy thin plate”. [J]. Metallurgical and Materials Transactions A, 1997, Vol. 28: 2657-2662.

[50] Wang, Z., Huang, P. G., and Zhang, Y. M. “Numerical analysis of metal transfer in gas metal arc welding”. [J]. Metallurgical and Materials Transactions B, 2003, Vol. 34: 345-353.

[51] Shi, Y., Fan, D., Li, J. J., and Chen, J. H. “Vision-based control system for aluminum alloy MIG welding pool width”. [J]. 2007, Transactions of the China welding institution. Vol. 28: 9-12.

[52] Jackson, C. E., and Shrubsall, A. E. “Control penetration and melting rate with welding technique”. [J]. 1953, Welding Journal, 32(4): 172s-179s.

[53] McGlone, J. C., and Chadwick, D. B. “The submerged arc butt welding of mild steel Part 2: The prediction of weld bead geometry from the procedure

parameters". [J]. 1978, Welding Institute Report. 80/1978/PE.

[54] Giedt, W. H., and Tallerico, L, N. "Prediction of electron beam depth of penetration". [J]. 1988, Welding Journal, 67(12): 299s-305s.

[55] Metzbower, E. A. "Penetration depth in laser beam welding". [J]. 1993, Welding Journal, 72(8): 403s-407s.

[56] Kim, I. S., Basu, A., and Siores, E. "Mathematical models for control of weld bead penetration in the GMAW process". [J]. 1996, International Journal of advanced Manufacturing Technology, Vol. 12: 393-401.

[57] Haber, R., and Keviczky, L. "Nonlinear system identification- Input-Output Modeling approach: Vol. 1: Nonlinear System Parameter Identification". [M]. 1999, Kluwer Academic Publisher.

[58] Astrom, K. J., and Wittenmark, B. "Adaptive Control", 2nd edition. [M]. 2006, Pearson Education, Inc.

[59] Zhang, Y. M., Walcott, B. L., and Wu, L. "Adaptive predictive decoupling control of full penetration process in GTAW". [J]. 1992, Control application, Vol. 2: 938-943.

[60] Suzuki, A., Hardt, D. E., and Valavani, L. "Application of Adaptive Control Theory to On-line GTA Weld Geometry Regulation". [J]. 1991, Journal of Dynamic Systems, Measurement and Control. Vol. 113: 93-103.

[61] Ozcelik, S., Moore, K. L., and Naidu, S. D. "Application of MIMO direct adaptive control to gas metal arc welding". 1998, Transactions of American control conference, Vol. 3: 1762-1766.

[62] Rossiter, J. A. “Model-Based Predictive Control” [M]. 2003, CRC Press LLC.

[63] Wen, C. Y., and Hill, D. J. “Global Boundedness of Discrete-time Adaptive control Just Using Estimator Projection”. [J]. 1992, Automatica, Vol. 28. No.6: pp1143-1157

# VITA

Xiaopei Liu was born on August 1st, 1981 in Harbin, Heilongjiang, China.

EDUCATION:

| | |
|---|---|
| University of Bristol, Bristol, United Kingdom<br>College of Engineering<br>M.S. in Engineering Management | 10/2005 |
| Tsinghua University, Beijing, China<br>Department of Electrical Engineering<br>B.S. in Electrical Engineering | 07/2004 |

PUBLICATIONS:

Journal papers:

[1]. Shi, Y., Liu, X., Zhang, Y., and Johnson, M. Analysis of Metal Transfer and Correlated Influences in Dual Bypass GMAW of Aluminum [J].Welding Journal, 2008, Vol.87: 229s-236s.

[2]. Liu, X., Li, K., Zhang, Y., and Johnson, M. Dual Bypass GMAW of Aluminum [J]. Transactions of NAMRI/SME, 2007, Vol.35:P335-341.

[3]. Liu, X., Shi, Y., Zhang, Y., and Johnson, M. Influence of DB-GMAW on Welding Base Metal Heat Input and Full penetration. (Submitted to publication)

Conference papers:

[1]. Liu, X., Shi, Y., Johnson, M. and Zhang, Y. Dual Bypass GMAW of Aluminum Rings. Transaction of FABTECH International & AWS Welding Show, 2007,

PP: 157-158.

Xiaopei Liu

09/23/2008